

# TECH SERIES

## The Solid Rocket Motor - Part 4 Departures from Ideal Performance for Conical Nozzles and Bell Nozzles, Straight-Cut Throats and Rounded Throats

by Charles E. Rogers

### Introduction

This article is part of a continuing series in *High Power Rocketry* on the solid propellant rocket motor. In this series solid propellant selection and characterization, internal ballistics and grain design, and solid rocket motor performance analysis and prediction will be covered in extensive detail. Previous installments of this series were published in the following issues of *High Power Rocketry* magazine; *Performance Analysis of the Ideal Rocket Motor* (Part "0" of the series), in the Jan 1997 issue (Ref. 1); Parts 1 and 2, *Solid Propellant Selection and Characterization*, in the February (A) 2001 and February (B) 2001 issues (Ref. 2); and Part 3, *Solid Propellant Grain Design and Internal Ballistics*, in the October/November 2002 issue (Ref. 3).

In what was in retrospect Part "0" of this series, *Performance Analysis of the Ideal Rocket Motor*, the derivations of the equations for the theoretical ideal performance of a rocket nozzle and rocket motor were presented. In Parts 1 and 2 of this series, *Solid Propellant Selection and Characterization*, the methods and equations for the theoretical specific impulse for solid propellants based on theoretical ideal performance were presented. In this installment of the series departures from ideal performance will be presented. Losses from the ideal thrust coefficient to the actual thrust coefficient for nozzles on solid rocket motors, liquid rocket engines, and hybrid rocket motors will be covered. Methods for quantifying the losses from the theoretical specific impulse to the delivered specific impulse for solid rocket motors and hybrid rocket motors will be covered. Losses from ideal performance will be presented for conical nozzles and bell nozzles, straight-cut throats and rounded throats.

Of particular interest is that for the first time for high power and experimental/amateur rocket motors the thrust coefficient losses from straight-cut throats on conical nozzles will be quantified, both from historical professional solid rocket motor data

and recent experimental static firing data. With a better understanding of the thrust coefficient losses from straight-cut throats, it will be shown how to optimize the design of straight-cut throats to maximize performance. As will be shown, simple design modifications have the potential to increase the thrust, total impulse and specific impulse of most high power solid rocket motors, and probably almost all experimental/amateur solid rocket motors by 3.5% to 8%, a significant across-the-board increase in performance for two entire classes of rocket motors.

While this article is part of a series on solid rocket motors, and the specific results presented are for solid rocket motors, the methods and equations that will be presented for determining the thrust coefficient for conical nozzles, bell nozzles, and rounded throats are applicable to solid rocket motors, liquid rocket engines, or hybrid rocket motors. While the overall design optimization lessons-learned for straight-cut throats are probably applicable for experimental/amateur liquid rocket engines, the specific straight-cut throat thrust coefficient results are applicable only to solid rocket motors and hybrid rocket motors. The methods presented for determining the losses from the theoretical specific impulse to the delivered specific impulse are only applicable to solid rocket motors and hybrid rocket motors, different techniques are used for liquid rocket engines.

The present author would like to give special thanks to Gary Rosenfield of AeroTech, Inc. and RCS Rocket Motor Components, Inc., for providing selected AeroTech nozzles drawings from the RCS Resource Library Compact Disk (CD) (Ref. 4), Anthony Cesaroni and Mike Dennett from Cesaroni Technology Incorporated (CTI) for providing motor thrust and chamber pressure test data including propellant geometry data and detailed nozzle drawings, Derek Deville from Environmental Aerosciences Corporation (EAC) for providing motor thrust and chamber pressure test data including propellant geometry data and detailed nozzle drawings, and Dr. Trong Bui from the NASA Dryden Flight Research Center for performing corrections to chamber pressure time history data using a MATLAB computer program.

Copyright ©2004 by Charles E. Rogers. All rights reserved. Published with permission.



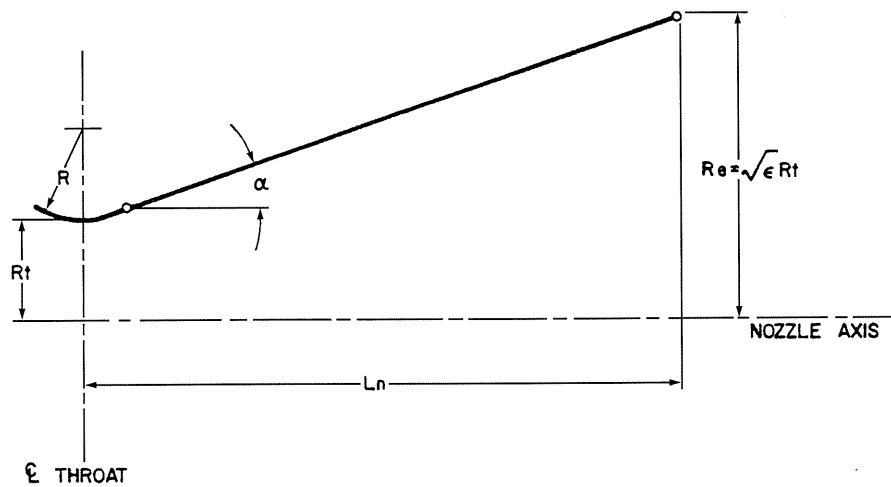


**Figure 3 — Typical Design for a Conical Nozzle with a Rounded Throat.**

facture, and ease of using a single nozzle "blank" for multiple motors with different throat areas. A single mold can be used to make injection-molded phenolic nozzle "blanks," or with automated machining graphite nozzle "blanks" can be machined in large numbers. Then each nozzle throat can be drilled to a specific throat area to tailor the nozzle for different rocket motors. These throats are called "straight-cut" throats from the action of the vertical drilling with a drill bit used to open up the throat area.

Many high power and experimental/amateur rocketeers use equations for thrust coefficient and specific impulse either not taking into account losses from ideal performance, or using typical losses from ideal performance representative of rounded throats. Clearly straight-cut throats will cause additional losses in thrust coefficient and specific impulse. One area that will be focused on in this installment of *The Solid Rocket Motor* series will be to quantify these additional losses, and to see if the design of straight-cut throats can be optimized to reduce thrust coefficient and specific impulse losses.

### Thrust Coefficient and Specific Impulse

Two parameters will be of interest in calculating the losses for, and optimizing the design of straight-cut throats; the thrust coefficient and specific impulse. The nozzle thrust coefficient is defined as the thrust divided by the product of the chamber pressure and the nozzle throat area.

$$C_F \equiv \frac{F}{p_c A_{th}} \quad (1)$$

$$F = C_F A_{th} p_c \quad (2)$$

Where:

$$A_{th} = \text{nozzle throat area, m}^2 \text{ (in}^2\text{)}$$

$$C_F = \text{thrust coefficient, dimensionless}$$

$$F = \text{thrust, N (lb)}$$

$$p_c = \text{chamber pressure, Pa (lb/in}^2\text{)}$$

The specific impulse of the rocket motor is the thrust of the motor divided by the propellant flow rate.

In SI Units:

$$I_{sp} = \frac{F}{\dot{m} g_0} \quad (3a)$$

Where:

$$F = \text{thrust, N}$$

$$g_0 = \text{acceleration due to gravity at sea level, } 9.8066 \text{ m/s}^2 \text{ (32.174 ft/sec}^2\text{)}$$

$$I_{sp} = \text{specific impulse, N-sec/kg (sec)}$$

$$\dot{m} = \text{propellant mass flow rate, kg/sec}$$

In English Units:

$$I_{sp} = \frac{F}{\dot{w}} \quad (3b)$$

Where:

$$F = \text{thrust, lb}$$

$$I_{sp} = \text{specific impulse, lbf-sec/lbm (sec)}$$

$$\dot{w} = \text{propellant flow rate, lb/sec}$$

As will be seen, the thrust coefficient and specific impulse are interrelated. If a nozzle produces a

higher thrust by having a higher thrust coefficient for a particular propellant flow rate and chamber pressure, the specific impulse of the rocket motor will also be increased.

### Characteristic Velocity ( $c^*$ )

Another parameter of interest for understanding losses in specific impulse from combustion losses upstream of the nozzle throat is the characteristic velocity ( $c^*$ ). The characteristic velocity is defined by Eq. (4).

$$c^* \equiv \frac{p_c A_{th}}{\dot{m}} \quad (4)$$

Where:

$c^*$  = characteristic velocity, m/sec (ft/sec)

In Ref. 1 a theoretical expression for characteristic velocity is derived showing that the characteristic velocity is a function of the combustion conditions and the ratio of specific heats.

$$c^* = \left[ \frac{1}{\gamma} \left( \frac{\gamma + 1}{2} \right)^{\frac{\gamma+1}{\gamma-1}} \frac{RT_c}{\bar{M}} \right]^{\frac{1}{2}} \quad (5)$$

Where:

$\bar{M}$  = average molecular weight of combustion gases, kg/mol (lb/mole)

$R$  = universal gas constant, 8314.3 J/mole - °K (1545 ft-lb/mole - °R)

$T_c$  = adiabatic equilibrium flame temperature, °K (°R)

$\gamma$  = ratio of specific heats, dimensionless

With the characteristic velocity based on how much chamber pressure is generated for a given throat area by a given mass flow from combustion (Eq. (4)), and additionally by inspection of Eq. (5), it becomes clear that the characteristic velocity depends primarily on the combustion conditions, and therefore is a relative measure of the efficiency of combustion.

Combining Eq. (4), the definition of the characteristic velocity ( $c^*$ ), with Eqs. (1) and (2), the definition of the thrust coefficient ( $C_F$ ), results in Eq. (6), the thrust of the rocket motor as a function of mass flow, characteristic velocity, and thrust coefficient.

$$F = \dot{m} c^* C_F \quad (6)$$

Eq. (7), from Ref. 5, gives the rocket motor specific impulse as a function of the characteristic velocity

and the thrust coefficient.

$$I_{sp} = (c^* C_F) / g_0 \quad (7)$$

Eqs. (4)-(7) provide insight into how combustion losses in the motor upstream of the nozzle throat, and thrust coefficient losses in the nozzle, lower the thrust and specific impulse of the motor. Suppose there are losses upstream of the nozzle throat due to inefficient combustion. From Eq. (5), with losses in the fundamental combustion process, such as reduction in the adiabatic equilibrium flame temperature ( $T_c$ , the combustion temperature), we would expect to see a reduction in the characteristic velocity. From Eq. (4), the loss in characteristic velocity would result in a reduction in chamber pressure for a given mass flow through the motor. A reduction in chamber pressure will reduce the thrust, thus a lower characteristic velocity will result in a reduced thrust (Eq. (6)). A reduced thrust, for the same mass flow (propellant flow), results in a reduced specific impulse. Thus the lower characteristic velocity will result in a reduced specific impulse (Eq. (7)), as we would expect because the reduction in characteristic velocity was caused by inefficient combustion, which would of course lower the specific impulse.

If efficient combustion is occurring in the motor, the motor will have a high characteristic velocity. The motor will be producing a high chamber pressure for a given propellant mass flow (Eq. (4)). But what if the nozzle is inefficiently expanding the products of combustion, which creates the thrust? Then there will be a reduction in the nozzle thrust coefficient. A loss in thrust coefficient causes a direct loss in thrust (Eq. (6)). For a given propellant mass flow, creating a given chamber pressure, if nozzle thrust coefficient losses reduce the motor thrust, there will be a loss in specific impulse (Eq. (7)).

As will be seen, losses in specific impulse due to departures from ideal performance will be broken down into losses in the fundamental combustion process upstream of the nozzle throat (characteristic velocity,  $c^*$  losses) and losses in the expansion of the combustion products through the nozzle (thrust coefficient losses).

### The Ideal Thrust Coefficient

To determine the thrust coefficient for the nozzle of a rocket motor the ideal thrust coefficient is calculated first. Corrections are then made to the ideal thrust coefficient to take into account departures from the ideal performance assumptions used to derive the ideal thrust coefficient equation.

The derivation of the ideal thrust coefficient equa-

tion was presented in, what was in retrospect Part "0" of this series, the article *Performance Analysis of the Ideal Rocket Motor* published in the January 1997 issue of *High Power Rocketry* (Ref. 1). Note that there are small differences in the nomenclature used in the equations in Ref. 1 and the equations in this article. The nomenclature used in this article is consistent with the nomenclature used in the rest of *The Solid Rocket Motor* series of articles.

Note that the derivation of the ideal thrust coefficient equation presented in Ref. 1 is based on a control volume drawn around a liquid rocket engine thrust chamber and nozzle. The assumption is made in the derivation that the stream thrust from injecting the propellants into the combustion chamber is zero, due to the velocity of the propellant flow into the chamber being much lower than the nozzle exhaust velocity. This same assumption can be made for a hybrid rocket motor. This assumption is exactly correct for a solid rocket motor, as no propellant is injected at all into the motor, the propellant is cast into the motor case. With the stream thrust into the combustion chamber being zero, the stream thrust at the nozzle exit remains, which with the pressure differential acting on the exit area of the motor results in the classic equation for the thrust of a rocket (Eq. (8)).

$$F = \dot{m}V_e + (p_e - p_\infty)A_e \quad (8)$$

Where:

- $A_e$  = exit area, m<sup>2</sup> (in<sup>2</sup>)
- $\dot{m}$  = mass flow rate of propellant, kg/sec (slugs/sec)
- $p_e$  = nozzle exit pressure, Pa (lb/in<sup>2</sup>)
- $p_\infty$  = atmospheric pressure, Pa (lb/in<sup>2</sup>)
- $V_e$  = nozzle exhaust velocity, m/sec (ft/sec)

The ideal thrust coefficient equation is derived from Eq. (8), based on an ideal perfect gas analysis for the flow through the rocket motor nozzle. The derivation is presented in Ref. 1, resulting in the ideal thrust coefficient equation (Eq. (9)).

$$C_F^0 = \sqrt{\frac{2\gamma^2}{\gamma-1} \left(\frac{2}{\gamma+1}\right)^{\frac{\gamma+1}{\gamma-1}} \left[1 - \left(\frac{p_e}{p_c}\right)^{\frac{\gamma-1}{\gamma}}\right]} + \left(\frac{p_e - p_\infty}{p_c}\right) \varepsilon \quad (9)$$

$$\varepsilon = \frac{A_e}{A_{th}} \quad (10)$$

Where:

- $C_F^0$  = ideal thrust coefficient, dimensionless
- $\varepsilon$  = nozzle expansion area ratio, dimensionless

In the derivation in Ref. 1 of the ideal thrust coefficient equation (Eq. (9)), the characteristic velocity ( $c^*$ ) equation (Eq. (4)), and the nozzle expansion area ratio equation as a function of the nozzle exit pressure to chamber pressure ratio (which will be subsequently presented as Eq. (11)), it is assumed that the ratio of specific heats is constant, and thus a single value for the ratio of specific heats is used in Eqs. (4), (9), and (11). When several values for the ratio of specific heats are available (typically for the chamber, throat, and nozzle exit), since the constant ratio of specific heats assumed in the derivation in Ref. 1 is for the expansion from the motor chamber to the nozzle exit, the average of the chamber and nozzle exit ratio of specific heats values should be used. In particular the present author prefers to use the average of the chamber value and the nozzle exit value, with the nozzle exit value based on equilibrium flow.

Many students at engineering universities, engineers in industry performing general rocket calculations, and high power and experimental/amateur rocketeers use Eq. (9), with a divergence correction added, as the equation for the thrust coefficient,  $C_F$ . The present author prefers to more accurately describe the thrust coefficient from Eq. (9) as the ideal thrust coefficient,  $C_F^0$ , i.e., the ideal thrust coefficient with no departures from ideal performance included, consistent with the nomenclature used in NASA SP-8076 (Ref. 6, portions reprinted in Ref. 3), NASA SP-8039 (Ref. 7), and NASA SP-8064 (Ref. 8, portions reprinted in Ref. 2).

Based on Eq. (9) the ideal thrust coefficient as a function of the chamber pressure to atmospheric pressure ratio and the nozzle expansion area ratio, for two typical ratios of specific heats, is plotted in Figures 4 and 5. Note in Figures 4 and 5 that for all nozzles the ideal thrust coefficient increases as the atmospheric pressure decreases, and that at any atmospheric pressure the maximum ideal thrust coefficient for a given chamber pressure is produced when the nozzle is ideally expanded, i.e. the nozzle exit pressure equals the atmospheric pressure.

The nozzle exit pressure to chamber pressure ratio ( $p_e/p_c$ ) that is required for Eq. (9) is a function of the nozzle expansion area ratio and the ratio of specific heats for the gas flow through the nozzle.

$$\frac{A_e}{A_{th}} = \frac{\left(\frac{\gamma-1}{2}\right)^{\frac{1}{2}} \left(\frac{2}{\gamma+1}\right)^{\frac{\gamma+1}{2(\gamma-1)}}}{\left(\frac{p_e}{p_c}\right)^{\frac{1}{\gamma}} \left[1 - \left(\frac{p_e}{p_c}\right)^{\frac{\gamma-1}{\gamma}}\right]^{\frac{1}{2}}} \quad (11)$$

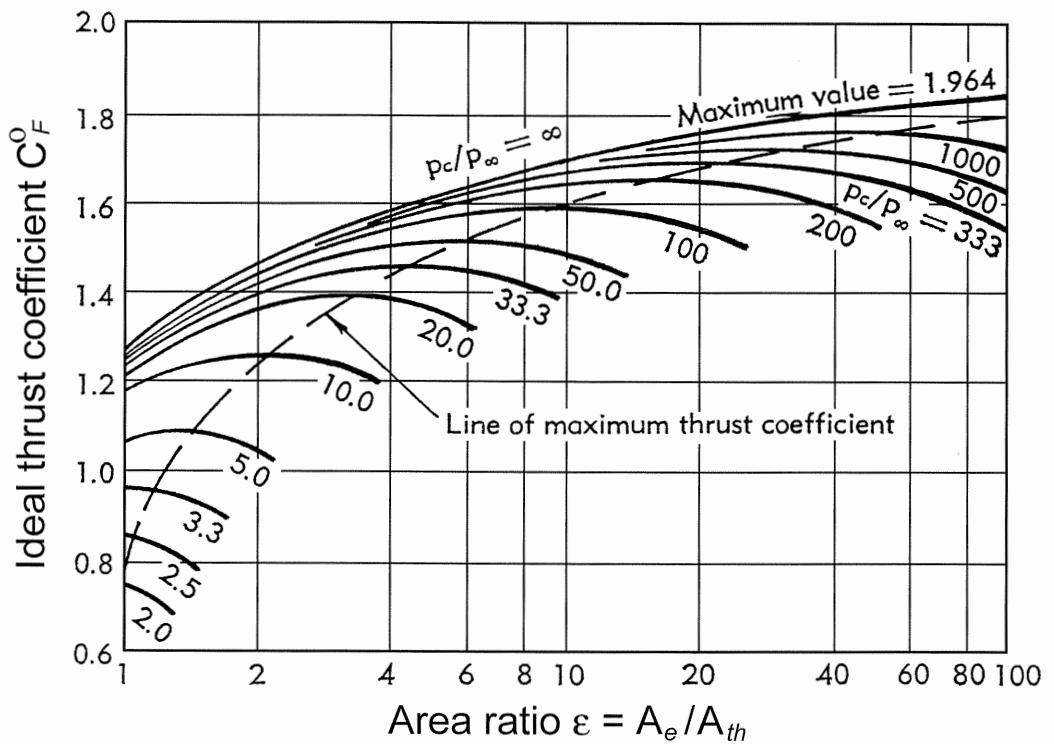


**Figure 4 — Variation of Ideal Thrust Coefficient with Nozzle Expansion Area Ratio and Pressure Ratio  $p_c/p_\infty$  for  $\gamma = 1.2$ .**

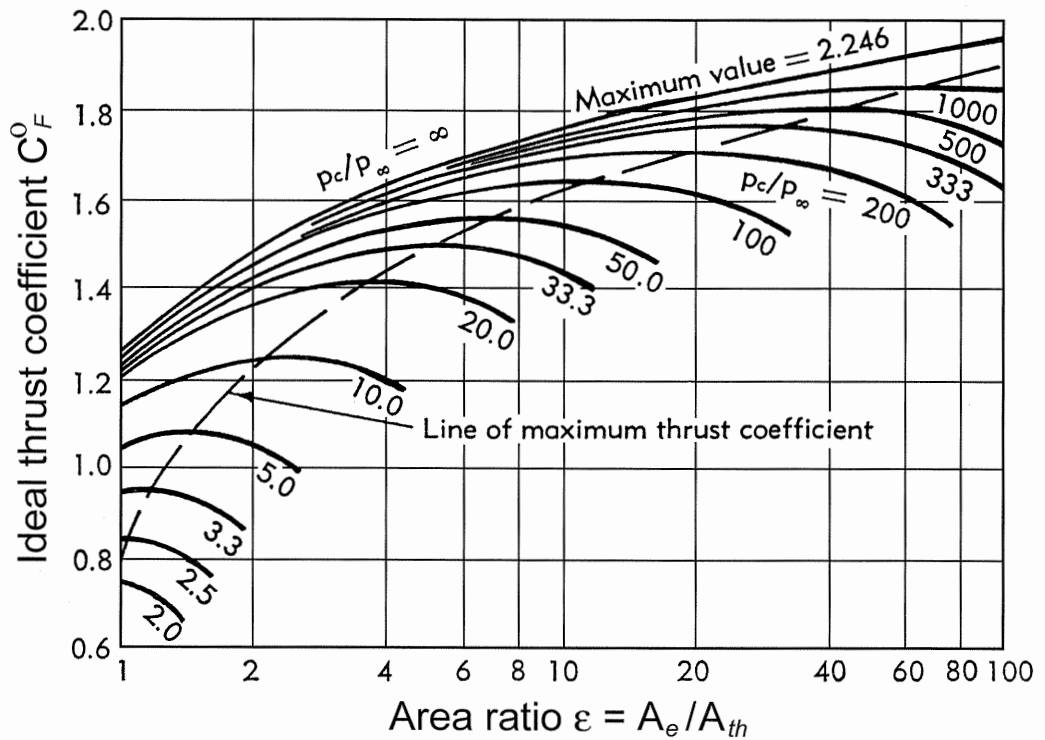


**Figure 5 — Variation of Ideal Thrust Coefficient with Nozzle Expansion Area Ratio and Pressure Ratio  $p_c/p_\infty$  for  $\gamma = 1.3$ .**

Based on Eq. (11) the nozzle expansion area ratio as a function of the chamber pressure to exit pressure ratio (the inverse of  $p_e/p_c$ ), for several ratios of specific heats, is plotted in Figure 6. Note in Figure 6 that as the expansion area ratio of the nozzle is increased the chamber pressure to exit pressure ratio increases, meaning that for a given chamber pressure the nozzle exit pressure will decrease.

If the desired nozzle exit pressure to chamber pressure ratio is known, and the nozzle expansion area ratio for that exit pressure to chamber pressure ratio needs to be determined, the exit pressure to chamber pressure ratio can simply be entered into Eq. (11) to determine the nozzle expansion area ratio. The more common situation is that the nozzle expansion area ratio is known, and it is the nozzle exit pressure to chamber pressure ratio that needs to be determined. Data for the chamber pressure to exit pressure ratio (the inverse of the exit pressure to chamber pressure ratio) can be read off Figure 6, but for computer simulations a numerical solution of

Eq. (11) is required. Given the nozzle expansion area ratio, Eq. (11) must be solved using an iterative numerical method to determine the exit pressure to chamber pressure ratio. The present author recommends the Newton-Raphson numerical method, although the half-interval method or other simple iterative methods can be used. Or for simplified calculations using a calculator, the data can be read off the plot in Figure 6.

The fact that the maximum ideal thrust coefficient for a given chamber pressure is achieved when the nozzle is ideally expanded is discussed in Ref. 1, and can be derived theoretically by substituting Eq. (11) into Eq. (9), and then taking the derivative of the resulting equation with respect to exit pressure. The derivative is equal to zero when the exit pressure is equal to the atmospheric pressure, in this case indicating a maximum value of the function (rather than a minimum value), the maximum value of the ideal thrust coefficient.

Note that while  $C_F^0$  (Eq. (9)) is called the "ideal"

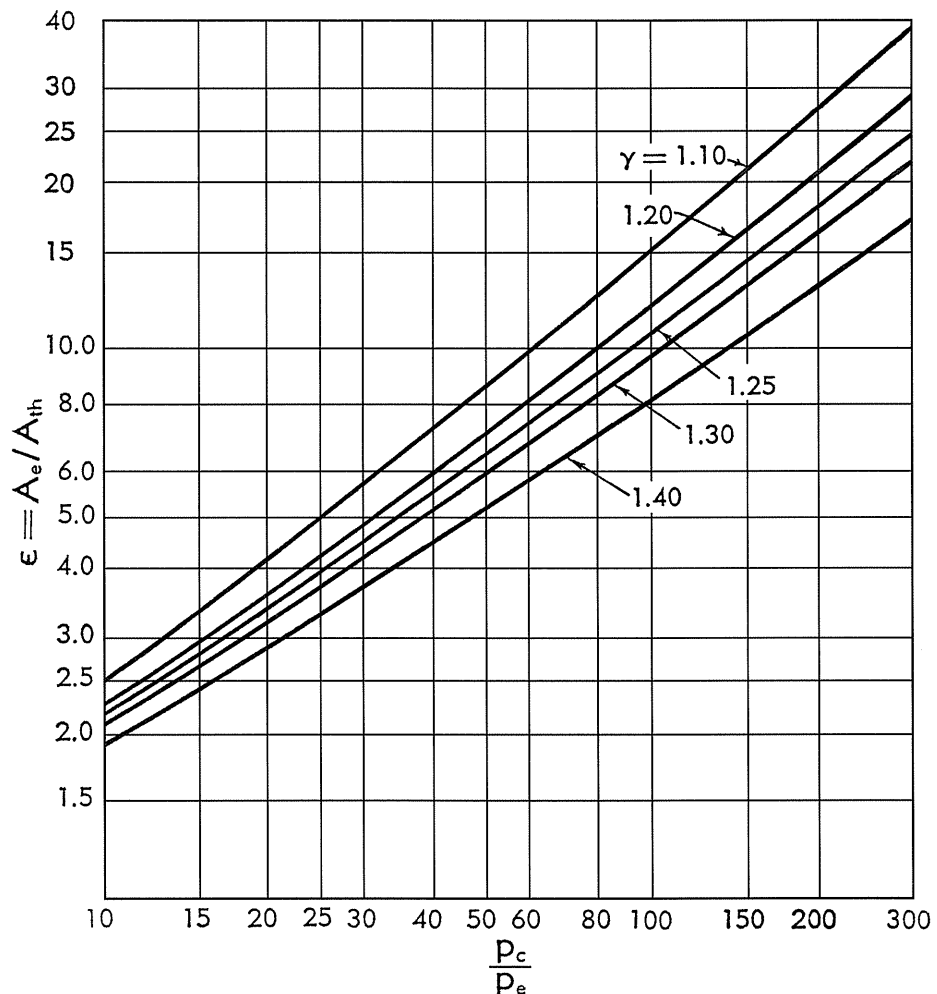


Figure 6 — Variation of Nozzle Expansion Area Ratio with Chamber Pressure to Exit Pressure Ratio ( $p_c/p_e$ ).

thrust coefficient, it is called "ideal" because it is based on an ideal performance analysis, with no losses from ideal performance. The truly "optimum" or "ideal" nozzle is an ideally expanded nozzle (nozzle exit pressure equals atmospheric pressure,  $p_e = p_\infty$ ), because this will produce the maximum thrust coefficient at the atmospheric pressure for which the nozzle is ideally expanded. This poses an interesting question; are underexpansion and overexpansion losses considered to be departures from ideal performance? The answer is no. Based on the ideal rocket motor performance analysis from Ref. 1, Eq. (9) gives the ideal performance of the nozzle given the chamber pressure, nozzle area ratio and atmospheric pressure, including the effect of nozzle underexpansion or overexpansion. While there are several corrections to the ideal performance from Eq. (9) which will be covered in detail in this article, there are no corrections required for underexpansion or overexpansion, because the effect of underexpansion or overexpansion is already included in Eq. (9).

Note that after the derivation of Eqs. (8), (9), and (11) (presented in Ref. 1) is complete, with the results plotted in Figures 4-6, the only gas property required for the flow through the nozzle is the ratio of specific heats. The exit pressure to chamber pressure ratio for the nozzle (a function of the nozzle expansion area ratio) and the ideal thrust coefficient are both independent of the combustion temperature and the molecular weight of the gases making up the nozzle flow. For most solid propellants, liquid rocket engine fuel and oxidizer combinations, and hybrid rocket motor fuel and oxidizer combinations the ratio of specific heats for the flow through the nozzle is typically between 1.2 and 1.3, the values used for Figures 4 and 5, and which are included with additional ratio of specific heat values in Figure 6. (Although for some propellants the ratio of specific heats can be as low as 1.13.)

Again it's important to note that based on the control volume analysis used to derive the equation for the thrust of a rocket (Eq. (8)), and the ideal perfect gas analysis used to derive the ideal thrust coefficient equation and associated equations (Eqs. (9)-(11)), that Eqs. (8)-(11) are valid for solid rocket motors, liquid rocket engines, and hybrid rocket motors. It's also important to note that Eqs. (8)-(11), and the data presented in Figures 4-6, are valid for both conical nozzles and bell nozzles. There are however important differences in the divergence correction to ideal performance for conical nozzles and bell nozzles, which will be presented later in this article. There are no divergence losses and no throat losses included in Eqs. (8)-(11) and Figures 4-6, the equations and data presented assume no divergence losses and a "perfect" throat with no losses.

Despite being based on an ideal perfect gas analy-

sis, the ideal thrust coefficient equation (Eq. (9)) can be accurate to within 1% to 5% for solid rocket motors, liquid rocket engines and hybrid rocket motors with rounded throats, and can be accurate to within 1% to 3% for nozzles with rounded throats when a non-ideal correction for nozzle divergence angle is included. As will be seen though, for nozzles with straight-cut throats the ideal thrust coefficient equation can be in error up to 9.5% due to high, unaccounted for losses.

To reduce the errors in the thrust coefficient predicted by the ideal thrust coefficient equation the effects of departures from ideal performance will be considered, and quantified for both rounded throats and straight-cut throats, conical nozzles and bell nozzles.

### Theoretical Specific Impulse

The counterpart to the ideal thrust coefficient is the theoretical specific impulse. From NASA SP-8064 (Ref. 8, reprinted in Ref. 2) and other references, the theoretical specific impulse is determined using Eq. (12).

$$I_{sp}^o = \frac{1}{g_0} \left\{ \frac{2R\gamma}{\gamma-1} \frac{T_c}{M} \left[ 1 - \left( \frac{P_e}{P_c} \right)^{\frac{\gamma-1}{\gamma}} \right] \right\}^{\frac{1}{2}} \quad (12)$$

Where:

$$I_{sp}^o = \text{theoretical specific impulse,} \\ \text{N-sec/kg (sec), lbf-sec/lbm (sec)}$$

The theoretical specific impulse is calculated assuming ideal expansion ( $p_e = p_\infty$ ), with no divergence losses or other losses associated with departures from ideal performance.

For the theoretical specific impulse there are three options for calculating chamber and exhaust composition and performance; frozen flow, equilibrium flow, and chemical kinetics. Frozen flow provides the lowest performance, equilibrium flow the highest performance, with the chemical kinetics-based performance lying between frozen and equilibrium. Equilibrium flow is also known as shifting equilibrium, because while chemical reactions are assumed to occur instantaneously under equilibrium conditions, the equilibrium values are continuously changing as the flow pressures and temperatures vary through the combustion chamber and nozzle. While including chemical kinetics provides the most accurate calculation of theoretical performance, it is very numerically intensive. With the much simpler calculations for equilibrium flow versus including chemical kinetics, and with equilibrium flow provid-

ing an upper bound for the theoretical performance of the propellant, it is customary in the solid rocket motor industry to calculate the theoretical specific impulse,  $I_{sp}^0$ , based on equilibrium flow.

The JANNAF Thermochemical Equilibrium Code, the NASA Lewis Code, and the Air Force Chemical Equilibrium Specific Impulse Code (AFCESIC, also known as the United States Air Force [USAF] ISP Code) are three of the computer programs in use in the solid rocket motor industry for calculation of  $I_{sp}^0$ . The PROPEP program based on the Naval Weapons Center PEP program, documented in Ref. 9, is widely used in the model rocket and high power rocket industries, and by experimental/amateur rocketeers.

Many high power and experimental/amateur rocketeers run programs such as PROPEP, and assume that the theoretical specific impulse predicted by the program for their propellant will be the specific impulse delivered by their rocket motors using the propellant. This will not be the case, with losses from the theoretical performance the actual specific impulse of the rocket motors will be less. It's important to quantify these losses from the theoretical performance, which will be covered in a later section.

### Actual Thrust Coefficient and Delivered Specific Impulse

It's important to note that beyond the ideal thrust coefficient and the theoretical specific impulse, what we're really interested in is predictions for the actual thrust coefficient and the delivered specific impulse for the nozzle and motor.

$C_{F,act}$  = actual thrust coefficient, including all nozzle losses, dimensionless

$I_{spd}$  = delivered specific impulse,  
N-sec/kg (sec), lbf-sec/lbm (sec)

The actual thrust coefficient ( $C_{F,act}$ ) is also referred to as the "measured" thrust coefficient, the actual thrust coefficient which would be measured based on test data. The delivered specific impulse ( $I_{spd}$ ) is the actual (delivered) specific impulse of the motor, based on the motor total impulse and propellant weight. It is the actual specific impulse the motor would deliver when fired on a thrust stand.

While the ideal thrust coefficient and theoretical specific impulse are theoretical values, the actual thrust coefficient and the delivered specific impulse represent the actual performance of the nozzle and motor, including all departures from ideal performance and all real-world losses.

The procedure used is to start with the theoretical (ideal) prediction for the thrust coefficient (the ideal thrust coefficient,  $C_{F}^0$ ) and the theoretical (ideal) prediction for the specific impulse (the theoretical specific impulse,  $I_{sp}^0$ ), and make corrections for non-ideal performance to arrive at predictions for the actual thrust coefficient and the delivered specific impulse.

### Nozzle Divergence Correction Factor, $C_F$ Efficiency Factor, and the Momentum and Pressure Differential Components of Thrust

One of the primary corrections to the ideal thrust coefficient is the effect of nozzle divergence. For conical nozzles, the classic equation for the divergence correction factor (Eq. (13)) is used (from NASA SP-8076, also Refs. 1, 5, 10, 11, and many other references).

$$\lambda = \frac{1}{2} (1 + \cos \alpha) \quad (13)$$

Where:

$\alpha$  = nozzle divergence half angle, deg

$\lambda$  = nozzle divergence correction factor, dimensionless

The geometry definition for the nozzle divergence half angle ( $\alpha$ ) for conical nozzles was presented in Figure 5.

For bell nozzles, the divergence correction factor is determined using Eq. (14) (from NASA SP-8076 [pages 23-24 of Ref. 3], original reference Ref. 12).

$$\lambda = \frac{1}{2} \left[ 1 + \cos \left( \frac{\alpha + \theta_{ex}}{2} \right) \right] \quad (14)$$

Where:

$\theta_{ex}$  = nozzle exit plane lip angle, deg

The geometry definitions for bell nozzles for the nozzle divergence half angle ( $\alpha$ ) and the nozzle exit plane lip angle ( $\theta_{ex}$ ) will be presented in Figure 7.

Returning to the equation for the thrust of a rocket (Eq. (8)), we can see that the thrust of a rocket is made up of a momentum component ( $\dot{m} V_e$ ) and a pressure differential component,  $(p_e - p_\infty) A_e$ .

$$\text{Eq. (8): } F = \underbrace{\dot{m} V_e}_{\substack{\uparrow \\ \text{Momentum} \\ \text{Component}}} + \underbrace{(p_e - p_\infty) A_e}_{\substack{\uparrow \\ \text{Pressure} \\ \text{Differential} \\ \text{Component}}}$$

As noted previously, many students at engineer-

ing universities, engineers in industry performing general rocket calculations, calculations done by high power and experimental/amateur rocketeers, and in many of the references and course material used at engineering universities, the nozzle divergence correction factor ( $\lambda$ ) is simply applied to the ideal thrust coefficient to determine the actual thrust coefficient.

$$C_{F,act} = \lambda C_F^0$$

This has the effect of applying the divergence correction factor to both the momentum component and the pressure differential component.

$$F = \lambda [ \dot{m} V_e + (p_e - p_\infty) A_e ]$$

$$F = \lambda \dot{m} V_e + \lambda (p_e - p_\infty) A_e$$

The divergence correction factor should clearly be applied to the momentum component, but should it be applied to the pressure differential component also? Additionally, we can group the remaining thrust coefficient losses from the ideal thrust coefficient into a  $C_F$  efficiency factor term ( $\eta_F$ ). Should this  $C_F$  efficiency factor be applied to the momentum component only, or to both the momentum component and the pressure differential component?

Note that the divergence correction factor equation for conical nozzles (Eq. (13)), and the divergence correction factor equation for bell nozzles (Eq. (14)), are valid for when the divergence correction factor is applied only to the momentum component of Eq. (8) (which will be subsequently described as the NASA SP Method), or when the divergence correction factor is applied to both the momentum component and the pressure differential component of Eq. (8) (which will be subsequently described as the Standard Method).

Depending on how the divergence correction factor and the  $C_F$  efficiency factor are applied, there are three different methods for correcting the ideal thrust coefficient to the final actual thrust coefficient for the rocket motor nozzle.

### Sutton Performance Correction Factor Method

In Sutton, *Rocket Propulsion Elements* (Ref. 5) a method using performance correction factors is presented for correcting the ideal thrust and ideal thrust coefficient to the actual thrust and actual thrust coefficient. On pages 90-91 of Ref. 5, an empirical thrust correction factor is defined which is equal to the ratio of the actual thrust to the ideal thrust.

$$\zeta_F = F_a / F_i \quad (15)$$

$$F_a = \zeta_F F_i \quad (16)$$

Where:

$$F_a = \text{actual thrust, N (lb)}$$

$$F_i = \text{ideal thrust, N (lb)}$$

$$\zeta_F = \text{thrust correction factor, dimensionless}$$

The thrust correction factor can also be applied directly to the thrust coefficient. From Ref. 5:

$$F_a = \zeta_F C_F p_c A_{th} \quad (17)$$

Note that from Ref. 5 the thrust coefficient in Eq. (17) is the ideal thrust coefficient. The present author will now substitute in nomenclature consistent with the other thrust coefficient equations presented in this article for the final equation, Eq. (18).

$$F_a = \zeta_F C_F^0 p_c A_{th} \quad (18)$$

Note that from Ref. 5 the thrust correction factor is equal to the product of the velocity correction factor and the discharge correction factor.

$$\zeta_F = \zeta_v \zeta_d \quad (19)$$

Where:

$$\zeta_d = \text{discharge correction factor, dimensionless}$$

$$\zeta_v = \text{velocity correction factor, dimensionless}$$

From Ref. 5; the velocity correction factor is approximately equal to the ratio of the actual specific impulse to the theoretical (ideal) specific impulse, and thus can be used to correct the theoretical specific impulse to the actual specific impulse. Using nomenclature consistent with the rest of this article:

$$\zeta_v = I_{spd} / I_{sp}^0 \quad (20)$$

$$I_{spd} = \zeta_v I_{sp}^0 \quad (21)$$

The discharge correction factor is defined as the ratio of the actual mass flow rate through the nozzle to the ideal mass flow rate.

$$\zeta_d = (\dot{m}_a / \dot{m}_i) \quad (22)$$

Where:

$$\dot{m}_a = \text{actual mass flow rate through nozzle, kg/sec (lbm/sec)}$$

$\dot{m}_i$  = ideal mass flow rate through nozzle,  
kg/sec (lbm/sec)

Interestingly, from Ref. 5, the value of the discharge correction factor is usually larger than 1 (1.0 to 1.15); i.e. the actual flow through the nozzle is larger than the theoretical (ideal) flow, due to (1) the molecular weight of the gasses increases slightly flowing through the nozzle, increasing the gas density, (2) heat transfer into the nozzle walls, decreasing the temperature of the flow in the nozzle, increasing its density, (3) changes in the specific heat ratio and other gas properties compared to the ideal analysis, and (4) incomplete combustion, which increases the density of the exhaust gasses.

While the discharge correction factor corrects the mass flow through the nozzle, and the velocity correction factor corrects the exhaust velocity (but based on a energy conversion efficiency, see Ref. 5), by multiplying the ideal thrust coefficient by the thrust correction factor (the product of the velocity correction factor and the discharge correction factor), the net effect of the Sutton Performance Correction Method is that both the momentum component and the pressure differential component from Eq. (8) are multiplied by the thrust correction factor ( $\zeta_F$ ). Thus the Sutton Performance Correction Method fits into the method category where both the momentum component and the pressure differential component from Eq. (8) are multiplied by the same correction factor(s), which captures the divergence correction and the correction for other thrust coefficient losses, although in a different form using a single thrust correction factor ( $\zeta_F$ ) as described by the equations above.

### The NASA SP Method

In the NASA SP Method presented in NASA SP-8076 (Ref. 6, reprinted in Ref. 3) and NASA SP-8039 (Ref. 7), the divergence correction factor and a nozzle  $C_F$  efficiency factor are applied to only the momentum component in the rocket thrust equation (Eq. (8)), resulting in the following equations for thrust coefficient and thrust.

$$C_{F,act} = \lambda \eta_F \left( C_{F,vac}^o - \frac{P_e}{P_c} \varepsilon \right) + \left( \frac{P_e - P_\infty}{P_c} \right) \varepsilon \quad (23)$$

$$F = \lambda \eta_F (P_c A_{th} C_{F,vac}^o - P_e A_e) + (P_e - P_\infty) A_e \quad (24) = P_c A_{th} C_{F,act}$$

Where:

$C_{F,vac}^o$  = ideal thrust coefficient (Eq. (9)), with  $p_\infty = 0$  (vacuum), dimensionless

$\eta_F$  =  $C_F$  efficiency factor, dimensionless

From Section 2.1.1.2.1 of NASA SP-8076 (pages 18-19 of Ref. 3), the deliverable motor efficiency ( $\eta_\mu$ ) is defined such that

$$I_{spd} = \eta_\mu I_{spd}^o \quad (25)$$

Where:

$\eta_\mu$  = deliverable motor efficiency, dimensionless

$I_{spd}^o$  = theoretical delivered specific impulse, N-sec/kg (sec), lbf-sec/lbm (sec)

Note from the glossary section of NASA SP-8076 (pages 56-57 of Ref. 3), the delivered specific impulse ( $I_{spd}$ ) and the theoretical delivered specific impulse ( $I_{spd}^o$ ) are both based on a particular chamber pressure, atmospheric pressure, nozzle expansion area ratio and nozzle divergence half angle.

$I_{spd}$  = measured (delivered) propellant specific impulse, N-sec/kg (lbf-sec/lbm) (ratio of  $I_{tot}$  to propellant weight, corresponding to  $\bar{p}_c$ ,  $\varepsilon$ ,  $p_\infty$ , and  $\alpha$  [nozzle half angle] of the motor [ref. 12])

$I_{spd}^o$  = theoretical delivered propellant specific impulse, N-sec/kg (lbf-sec/lbm) (theoretical  $I_{sp}$  corresponding to particular values of  $\bar{p}_c$ ,  $\varepsilon$ ,  $p_\infty$  and  $\alpha$  [ref.12])

Where:

$I_{tot}$  = total impulse, N-sec (lb-sec), (total integral of thrust-time)

$\bar{p}_c$  = average chamber pressure, Pa (lb/in<sup>2</sup>)

Therefore, while divergence losses are included in the theoretical delivered specific impulse and the delivered specific impulse, the additional thrust coefficient losses captured by the  $C_F$  efficiency factor

( $\eta_F$ ) are not included in the theoretical delivered specific impulse. Thus, as noted in NASA SP-8076 (pages 18-19 of Ref. 3), the deliverable motor efficiency ( $\eta_\mu$ ) is approximately equal to the product of the  $c^*$  efficiency factor ( $\eta_\theta$ ) and the  $C_F$  efficiency factor ( $\eta_F$ ). It is "approximately equal to" due to the complexities of the NASA SP Method thrust coefficient and thrust equations, Eqs. (23) and (24).

$$\eta_\mu \approx \eta_\theta \eta_F \quad (26)$$

Where:

$$\eta_\theta = c^* \text{ efficiency factor, dimensionless}$$

The present author proposes, based on equations from Section 2.1.1.2.1 and Section 2.1.2.2 of NASA SP-8076 (pages 18-19 and pages 23-24 of Ref. 3), the definitions of theoretical specific impulse and delivered specific impulse, and Eqs. (25) and (26) above, that the delivered specific impulse can be determined from the theoretical specific impulse using Eq. (27).

$$I_{spd} = \frac{C_{F,act}}{(C^0_F)_{p_e = p_\infty}} \eta_\theta I^0_{sp} \quad (27)$$

The ratio of the actual thrust coefficient to the ideal thrust coefficient with ideal expansion is used in Eq. (27) because with the complex equation for the actual thrust coefficient (Eq. (23)), there is no simple way to directly include the nozzle losses from ideal performance ( $\lambda, \eta_F$ ) in Eq. (27).

### The Standard Method

In many of the references and much of the course material used for undergraduate and graduate engineering courses, engineers in industry performing general rocket calculations, and calculations performed by high power and experimental/amateur rocketeers, to determine the actual thrust coefficient the ideal thrust coefficient is simply multiplied by the nozzle divergence correction factor ( $\lambda$ ).

$$C_{F,act} = \lambda C^0_F$$

The present author proposes what will be called the Standard Method, where the product of the ideal thrust coefficient and the nozzle divergence correction factor is simply multiplied by the  $C_F$  efficiency factor ( $\eta_F$ ).

$$C_{F,act} = \lambda \eta_F C^0_F \quad (28)$$

This has the effect of applying the divergence cor-

rection factor and the  $C_F$  efficiency factor to both the momentum component and the pressure differential component in the equation for the thrust of a rocket (Eq. (8)).

$$F = \lambda \eta_F [\dot{m} V_e + (p_e - p_\infty) A_e]$$

As was done in the NASA SP Method, based on NASA SP-8076 the deliverable motor efficiency ( $\eta_\mu$ ) is defined such that

$$I_{spd} = \eta_\mu I^0_{spd}$$

As in the NASA SP Method, while divergence losses are included in the theoretical delivered specific impulse ( $I^0_{spd}$ ) and the delivered specific impulse ( $I_{spd}$ ), the additional thrust coefficient losses captured by the  $C_F$  efficiency factor are not included in the theoretical delivered specific impulse.

A difference in the Standard Method relative to the NASA SP Method is that rather than having the product of the  $c^*$  efficiency factor ( $\eta_\theta$ ) and the  $C_F$  efficiency factor ( $\eta_F$ ) being approximately equal to the deliverable motor efficiency ( $\eta_\mu$ ), the product of the  $c^*$  efficiency factor and the  $C_F$  efficiency factor are exactly equal to the deliverable motor efficiency.

$$\eta_\mu = \eta_\theta \eta_F \quad (29)$$

Including underexpansion or overexpansion effects, the equation for the delivered specific impulse from the theoretical specific impulse remains the same as used in the NASA SP Method.

$$I_{spd} = \frac{C_{F,act}}{(C^0_F)_{p_e = p_\infty}} \eta_\theta I^0_{sp} \quad (30)$$

If ideal expansion ( $p_e = p_\infty$ ) is assumed for  $C_{F,act}$ , then

$$\frac{(C_{F,act})_{p_e = p_\infty}}{(C^0_F)_{p_e = p_\infty}} = \frac{\lambda \eta_F (C^0_F)_{p_e = p_\infty}}{(C^0_F)_{p_e = p_\infty}} = \lambda \eta_F$$

Eq. (30), the delivered specific impulse equation, then reduces to:

$$I_{spd} = \lambda \eta_F \eta_\theta I^0_{sp} \quad (31)$$

Assuming ideal expansion ( $p_e = p_\infty$ ).

Approximate (nearly exact) for close to ideal expansion.

The Standard Method equations, including equations for the divergence correction factor ( $\lambda$ ) for conical nozzles and for bell nozzles, are presented in Figure 7.

**The Standard Method for Actual Thrust Coefficient  
and Delivered Specific Impulse**

$$F = C_{F,act} A_{th} p_c \quad \text{Eq. (1), Eq. (2)}$$

$$C_F^o = \sqrt{\frac{2\gamma^2}{\gamma-1} \left(\frac{2}{\gamma+1}\right)^{\frac{\gamma+1}{\gamma-1}} \left[1 - \left(\frac{P_e}{P_c}\right)^{\frac{\gamma-1}{\gamma}}\right]} + \left(\frac{P_e - P_\infty}{P_c}\right) \varepsilon \quad \text{Eq. (9)}$$

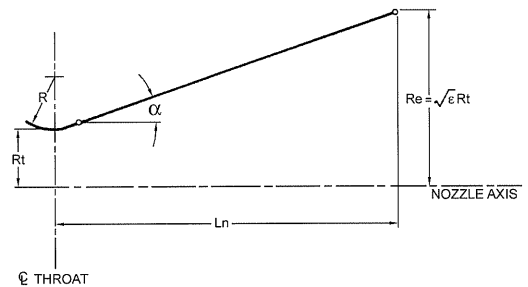
$$\varepsilon = \frac{A_e}{A_{th}}$$

$$C_{F,act} = \lambda \eta_F C_F^o \quad \text{Eq. (28)}$$

$$I_{spd} = \lambda \eta_F \eta_\theta I_{sp}^o \quad \text{Eq. (31)}$$

For Conical Nozzle:

$$\lambda = \frac{1}{2} (1 + \cos \alpha) \quad \text{Eq. (13)}$$



For Bell Nozzle:

$$\lambda = \frac{1}{2} \left[1 + \cos \left(\frac{\alpha + \theta_{ex}}{2}\right)\right] \quad \text{Eq. (14)}$$

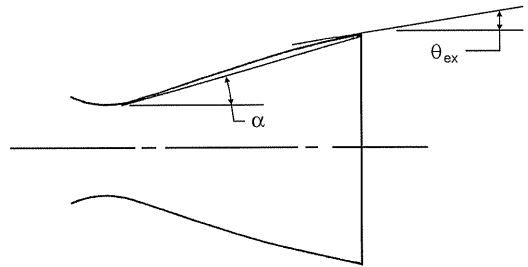


**Figure 7 — The Standard Method for Actual Thrust Coefficient  
and Delivered Specific Impulse.**

**Recommended Method —  
The Standard Method**

The present author recommends that the Standard Method be used for correcting the ideal thrust coefficient and the theoretical specific impulse to the actual thrust coefficient and the delivered specific impulse. The rationale for recommending the Standard Method will be presented in this section.

First, from a contrary view, Section 2.1.3.2.2 of NASA SP-8039 recommends that the divergence cor-

rection should only be applied to the momentum component of the rocket motor thrust (the NASA SP Method). Similar arguments can be made that throat losses captured using the  $C_F$  efficiency factor, especially losses from straight-cut throats, will have a larger effect on the momentum component than on the pressure differential component of the equation for rocket thrust, and thus applying the  $C_F$  efficiency factor to the momentum component only may be more accurate (the NASA SP Method).

The only differences between the Standard Method and the NASA SP Method arise from

$D_{th} = 0.75\text{in}$   
 $p_c = 500\text{ psia}$   
 $p_\infty = 14.69\text{ psia}$

Based on basic equation for rocket thrust (Eq. (8)).  
 No divergence correction or  $C_F$  efficiency factor correction.  
 Nozzle Half Angle ( $\alpha$ ) = 0 deg  
 $\lambda = 1.0$   
 $\eta_F = 1.0$   
 $\gamma = 1.2$

	$\epsilon = 3.0$	$\epsilon = 4.0$	$\epsilon = 5.0$	$\epsilon = 5.31$ (ideal expansion)	$\epsilon = 6.0$	$\epsilon = 7.0$	$\epsilon = 8.0$
$D_e$ (in)	1.2991	1.5	1.6771	1.7283	1.8371	1.9843	2.1213
$p_e / p_c$	0.06562	0.04344	0.03188	0.02937	0.02484	0.02016	0.01688
Thrust (total) (lb)	323.78	329.04	330.77	330.85	330.49	328.94	326.52
Pressure Differential Component (lb)	24.02	12.42	2.76	0.0	-6.02	-14.26	-22.09
-Percent of Total Thrust	7.4%	3.8%	0.8%	0%	-1.8%	-4.3%	-6.8%
Momentum Component (lb)	299.76	316.62	328.01	330.85	336.51	343.20	348.61
-Percent of Total Thrust	92.6%	96.2%	99.2%	100%	101.8%	104.3%	106.8%

$D_e$  = nozzle exit diameter  
 $D_{th}$  = nozzle throat diameter

**Table 1 — Percentage of the Total Thrust for a Typical Large High Power Rocket Motor from the Momentum Component and the Pressure Differential Component of the Rocket Thrust Equation (Eq. (8)).**

whether to apply the divergence correction factor and the  $C_F$  efficiency factor to either both the momentum component and the pressure differential component in the thrust equation, or to the momentum component only. If the motor nozzle is ideally expanded ( $p_e = p_\infty$ ), then there is no pressure differential component, and as can be seen in Eqs. (23)-(31) the NASA SP Method equations reduce to the Standard Method equations; i.e., for ideal expansion, the two methods produce identical results.

With the Standard Method and the NASA SP Method identical for ideal expansion, for nozzles that are nearly, or close to ideally expanded, the two methods will be very close. Table 1 shows the percentage of total thrust from the momentum component and the pressure differential component from the rocket thrust equation (Eq. (8)) for a typical

large high power rocket motor nozzle. Table 1 was constructed using the basic equation for rocket thrust (Eq. (8)), with no nozzle divergence (nozzle divergence half angle  $\alpha = 0$  deg), and with the divergence correction factor  $\lambda = 1.0$ , and the  $C_F$  efficiency factor  $\eta_F = 1.0$ .

Note in Table 1 that when the nozzle is ideally expanded, the pressure differential component is of course zero. Also note in Table 1 that for expansion ratios greater than the expansion ratio for ideal expansion the pressure differential component is negative, it subtracts from the total thrust. Thus the percentage of the total thrust that is the momentum component goes over 100%, since it is making up for the negative thrust from the pressure differential term.

As can be seen from Table 1, when the nozzle is close to ideally expanded, or even somewhat off

from ideal expansion, the majority of the thrust from the nozzle is from the momentum component. With the portion of the thrust from the pressure differential component being relatively small, the error from applying or not applying the divergence correction factor and the  $C_F$  efficiency factor corrections to the pressure differential component will be small. Thus for nozzles that are close, or relatively close to ideal expansion, there is little difference between the two methods.

In Section 2.1.3.2.2 of NASA SP-8039 (Ref. 7), and on pages 359-361 of *Mechanics and Thermodynamics of Propulsion* by Hill and Peterson (Ref. 11), derivations based on a point-source flow assumption are presented to determine where to apply the divergence correction factor ( $\lambda$ ). The point-source flow geometry used in the derivations presented in NASA SP-8039 and *Mechanics and Thermodynamics of Propulsion* is presented in Figure 8. From *Mechanics and Thermodynamics of Propulsion* the equation for the thrust of the nozzle in Figure 8 is Eq. (32).

$$F = \dot{m}u_e \frac{1 + \cos \alpha}{2} + (p_e - p_\infty)A_e \quad (32)$$

Where:

$$u_e = \text{nozzle exhaust velocity, m/sec (ft/sec)}$$

Note from Eq. (32) that when the conventional nozzle exit area ( $A_e$ ) is used the conical nozzle divergence correction factor (see Eq. (13)) is applied only to the momentum component of the nozzle thrust. The spherical exit area of the nozzle ( $A'_e$ ), which results from the point-source flow assumption shown in Figure 8, can be determined from the conventional nozzle exit area using Eq. (33).

$$A'_e = [2/(1 + \cos \alpha)]A_e \quad (33)$$

Where:

$$A'_e = \text{nozzle spherical exit area, m}^2 \text{ (in}^2\text{)}$$

Note that Eq. (33) can be used to substitute area

$A'_e$  in place of area  $A_e$  in Eq. (32), resulting in Eq. (34), the nozzle thrust equation based on the spherical nozzle exit area  $A'_e$ .

$$F = \frac{1 + \cos \alpha}{2} [\dot{m}u_e + (p_e - p_\infty)A'_e] \quad (34)$$

Note from Eq. (34) that when the nozzle thrust equation is based on the spherical nozzle exit area  $A'_e$ , the nozzle divergence correction factor is applied to both the momentum component and the pressure differential component of the nozzle thrust.

Clearly for conical nozzles with typical divergence half angles there is very little difference between the conventional nozzle exit area  $A_e$  and the spherical exit area  $A'_e$ . Thus there will be very little difference between applying the nozzle divergence correction factor to both the momentum component and the pressure differential component of thrust (using the spherical exit area  $A'_e$ ) or applying the nozzle divergence correction factor to the momentum component of thrust only (using the conventional exit area  $A_e$ ).

While using a different technique in applying correction factors, fundamentally the Sutton Performance Correction Method multiplies the ideal thrust coefficient by a single correction factor, the thrust correction factor ( $\zeta_F$ ). Thus the Sutton Performance Correction Method shares the primary trait with the present author-proposed Standard Method of not applying a correction factor to the momentum component only, but applying a correction factor to both the momentum component and the pressure differential component by simply multiplying the ideal thrust coefficient by a correction factor.

In the opinion of the present author, the concept used in the NASA SP Method and the Standard Method of breaking down the losses into thrust coefficient losses and  $c^*$  efficiency losses is a more powerful concept and much more useable for high power and experimental/amateur rocketeers, than the concept used in the Sutton Performance

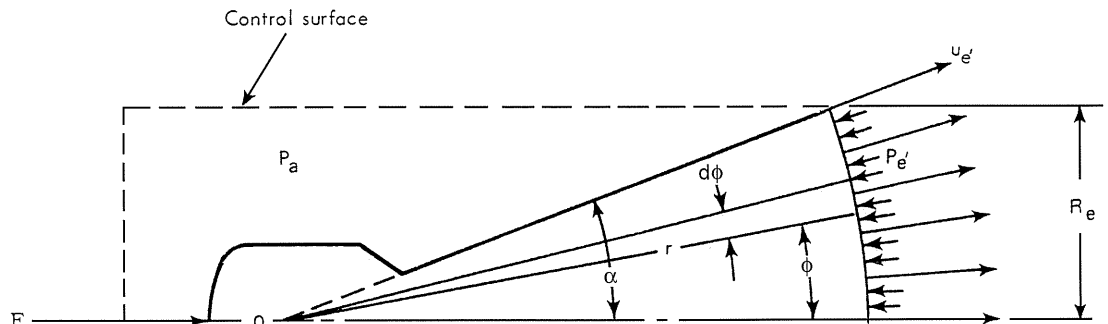


Figure 8 — Spherically Symmetric Nozzle Flow Based On Point-Source Flow Assumption.

Correction Method of a velocity correction factor and a discharge correction factor. The present author prefers that the thrust coefficient corrections be applied to both the momentum component and the pressure differential component (the Standard Method), rather than just to the momentum component (the NASA SP Method).

The present author proposes that the discharge correction factor from the Sutton Performance Correction Method will be very difficult for high power and experimental/amateur rocketeers to quantify from nozzle test data. While the Sutton thrust correction factor could be used directly, the divergence correction factor is buried within it. The present author prefers to separate out the divergence correction factor, since it is easy to calculate and has accepted values, leaving the "all other thrust coefficient losses" in the  $C_F$  efficiency factor term.

Finally, the present author recommends that the Standard Method be used primarily because of the widespread use by engineering students, engineers in industry performing general rocket calculations, and high power and experimental/amateur rocketeers, of the technique of simply multiplying the ideal thrust coefficient ( $C_F^0$ ) by the nozzle divergence correction factor ( $\lambda$ ) to determine the actual thrust coefficient ( $C_{F,act}$ ).

$$C_{F,act} = \lambda C_F^0 \quad (35)$$

To the present author's knowledge at the time of

the writing of this article, with the exception of some internal-use computer programs by the present author, every solid rocket motor, hybrid rocket motor, and liquid rocket engine computer program, software, spreadsheet, performance charts, etc., for predicting performance and calculating thrust from chamber pressure used by model, high power, and experimental/amateur rocketeers uses Eq. (35). All of these computer programs, software packages, spreadsheets, performance charts, etc., can be easily updated to the Standard Method proposed by the present author by simply multiplying the ideal thrust coefficient and the divergence correction factor with the  $C_F$  efficiency factor ( $\eta_F$ ), i.e., by using Eq. (28).

$$\text{Eq. (28):} \quad C_{F,act} = \lambda \eta_F C_F^0$$

Representative values for the  $C_F$  efficiency factor ( $\eta_F$ ) for straight-cut throats and rounded throats will be presented later in this article.

Additionally, the PROPEP program that is widely used by high power rocketeers and experimental/amateur rocketeers, the JANNAF Thermochemical Equilibrium Code, the NASA Lewis Code, and the USAF ISP Code all produce results for the theoretical specific impulse,  $I_{sp}^0$ . Using Eq. (31) the delivered specific impulse ( $I_{spd}$ ) can be determined from the theoretical specific impulse from the above programs based on representative or calculated values for the divergence correction factor ( $\lambda$ ), the  $C_F$  efficiency factor ( $\eta_F$ ), and the  $c^*$  efficiency factor ( $\eta_\theta$ ).

- SkyAngle™ Classic:**  
Compact, strong, and easy to track. The original spinning design that redefined rocket recovery. 8 sizes for mid/high power.
- SkyAngle™ Classic II:**  
A beefed-up version of the Classic. Extra tough. The best made even better.
- SkyAngle CERT-3™:**  
3 parachutes for projects in the 16 - 130 pound range plus a heavy-duty drogue. These models really live up to their name!
- SkyAngle Deployment FreeBag™:**  
Easy-to-use Aramid deployment sleeves. 4 sizes to fit virtually any HP chute out there.
- SkyAngle Recovery Components:**  
Swivels, Streamers, Harness Straps, Shock Cords, Chute Protectors, & Delta Links.
- SkyAngle Logo Merchandise:**  
Caps, shirts, bags, coffee mugs and more!

**When you're ready for the best, you're ready for SkyAngle.**

SkyAngle recovery devices perform like no other. Just ask anyone who deploys them.

Professionally tested for accurate capacity, every SkyAngle parachute is expertly crafted in the USA and comes with a lifetime warranty.

Innovative design. Rugged materials. Quality construction. Just a few more reasons why SkyAngle products are preferred for high power recovery.

So get ready for the best. Get SkyAngle and discover for yourself:

**Rocket Recovery Redefined...**



The b2 Rocketry Company

**678•454•2613**

[www.b2rocketry.com](http://www.b2rocketry.com)

$$\text{Eq. (31): } I_{spd} = \lambda \eta_F \eta_\theta I_{sp}^0$$

Providing high power rocketeers and experimental/amateur rocketeers for the first time with a method for determining the delivered specific impulse from the theoretical specific impulse obtained from PROPEP-type programs.

### Specific Impulse Losses — Characteristic Velocity Losses, Thrust Coefficient Losses, and the Variation of the $c^*$ Efficiency Factor with Motor Size

The Standard Method equation used to determine the delivered specific impulse from the theoretical specific impulse (Eq. (31)), illustrates some important concepts in terms of departures from ideal performance. Specific impulse losses from ideal performance are due to (1) fluid flow losses including two-phase flow in which particles fail to achieve kinetic and thermal equilibrium, (2) combustion inefficiency, (3) heat losses to the motor hardware, and (4) boundary layer losses in the nozzle. The losses from ideal performance for specific impulse can be broken up into two types; (1) losses upstream of the nozzle throat characterized by  $c^*$  (characteristic velocity) combustion losses represented by the  $c^*$  efficiency factor ( $\eta_\theta$ ), and (2) losses in the nozzle from inefficient expansion of the gas in the nozzle characterized by thrust coefficient losses represented by the divergence correction ( $\lambda$ ) (divergence losses, which are easy to separate out and quantify) and the  $C_F$  efficiency factor ( $\eta_F$ ) (all of the other thrust coefficient losses).

$$\text{Eq. (31): } I_{spd} = \lambda \eta_F \eta_\theta I_{sp}^0$$

In other words, if a motor is delivering a low specific impulse, the motor development engineer would look for two possible sources; either the nozzle isn't functioning as efficiently as desired (the nozzle thrust coefficient is low, likely source a low  $C_F$  efficiency factor), or there are combustion losses ( $c^*$  losses) upstream of the nozzle throat (a low  $c^*$  efficiency factor). Two-phase flow losses, heat

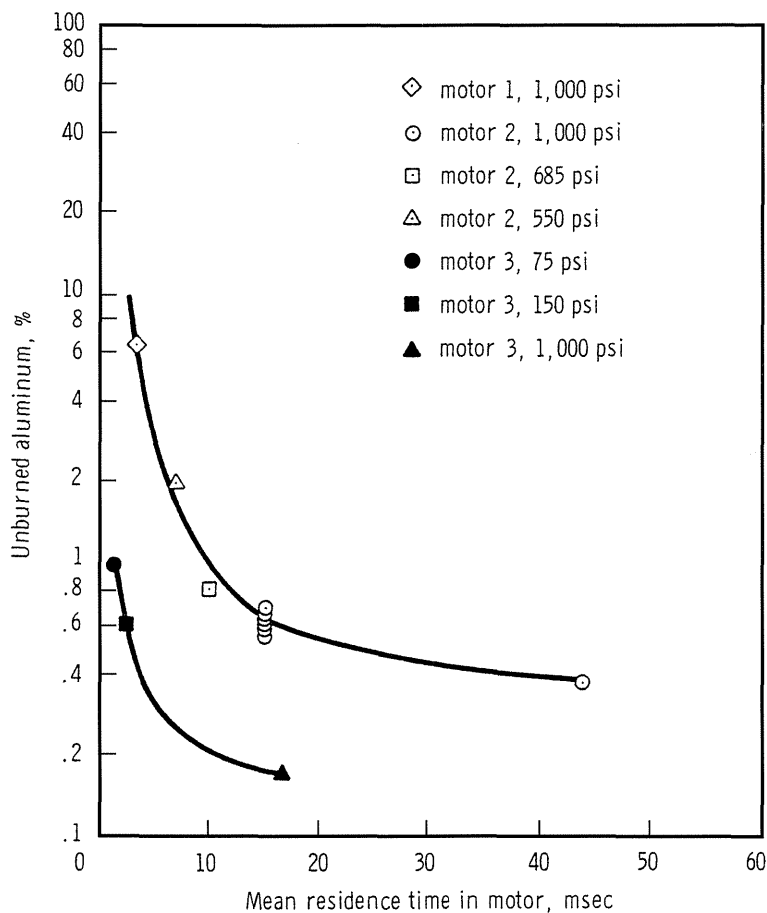


**Figure 9 — Effect of Residence Time on Completeness of Metal Combustion.**

transfer into the nozzle structure, and boundary layer losses can lower the thrust coefficient (lower the  $C_F$  efficiency factor). Combustion inefficiency, internal two-phase flow losses, and heat transfer into the motor structure can lower the  $c^*$  efficiency factor. A low residence time in the motor for metalized (typically aluminum) propellants can result in unburned metal exiting the motor, as shown in Figure 9 from NASA SP-8064 (page 52 of Ref. 2, original reference Ref. 13) showing unburned aluminum as a function of residence time for an aluminized propellant. Unburned metal is lost energy from combustion, resulting in combustion inefficiency, lowering the  $c^*$  efficiency factor.

Figure 10, from NASA SP-8064 (page 52 of Ref. 2, original reference Ref. 14), presents  $I_{sp}$  efficiency (in percent) versus motor residence time for an aluminized propellant (Al-PBAN) (Footnote 1). Note that when comparing with Figure 9, when the residence time is increased, less of the aluminum is unburned, and the motor delivers a higher specific impulse efficiency. Note also from the individual

Footnote 1 — Al = aluminum; PBAN = polybutadiene-acrylic acid-acrylonitrile terpolymer

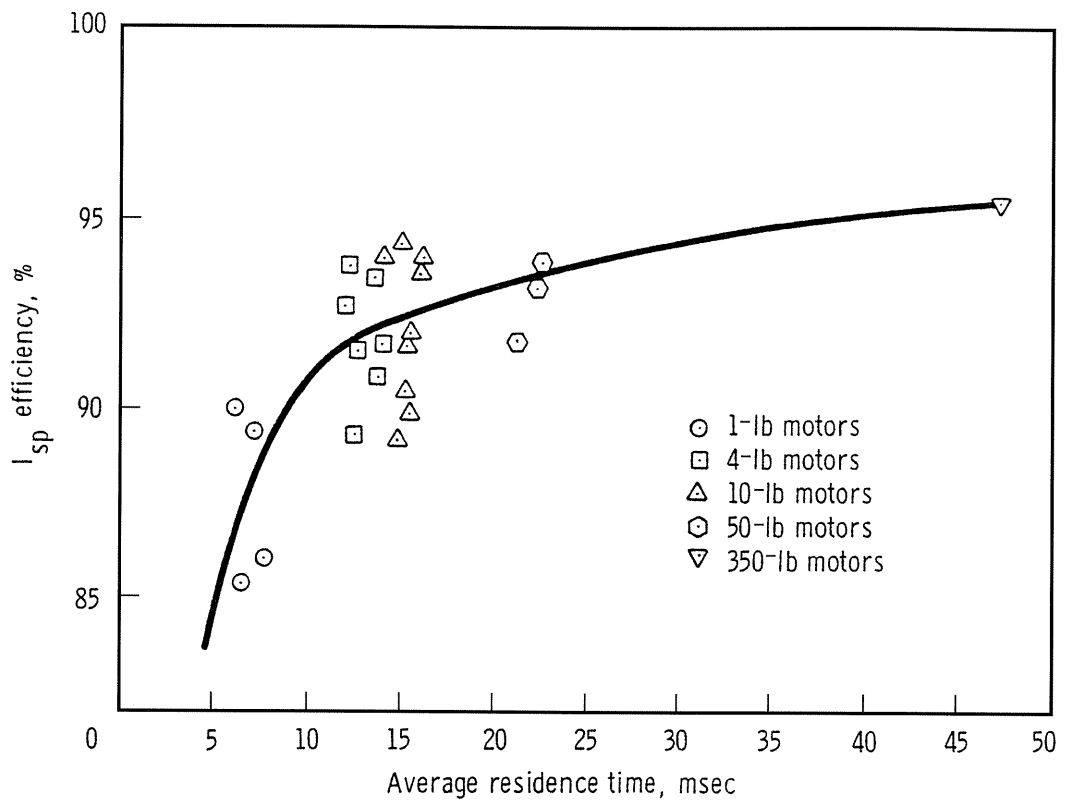


**Figure 10 — Effect of Residence Time on  $I_{sp}$  Efficiency in an Al-PBAN Propellant.**

data points in Figure 10 that larger motors generally have longer residence times due to generally having longer cores. Larger motors also have lower heat losses and boundary layer losses. One can conclude therefore that in general, larger motors are more efficient than smaller motors, and will have higher values of the  $c^*$  efficiency factor. One can see this from the data presented in Figure 10. If the data was plotted versus motor propellant weight rather than motor residence time; the 1 lb propellant weight motors have an average  $I_{sp}$  efficiency of approximately 87.5% ( $\eta_0 \approx 0.875$ ), the 10 lb propellant weight motors have an average  $I_{sp}$  efficiency of approximately 92% ( $\eta_0 \approx 0.92$ ), the 50 lb propellant weight motors have an average  $I_{sp}$  efficiency approaching 92.5% ( $\eta_0 \approx 0.925$ ), and the 350 lb propellant weight motors have an average  $I_{sp}$  efficiency of approximately 95% ( $\eta_0 \approx 0.95$ ).

While non-metallized propellants will not have the problem of unburned metal for short residence times shown in Figure 9, or the kinetic portion of two-phase flow losses, small motors will still have thermal equilibrium losses, combustion inefficiency losses, and heat losses that on a percentage basis will be higher than for large motors, and will show the same basic trend of increasing  $I_{sp}$  efficiency with motor size seen in Figure 10.

Note the low  $I_{sp}$  efficiency values for 1 lb propellant weight motors in Figure 10, and the trend line indicating even lower  $I_{sp}$  efficiency for motors with less than 1 lb of propellant. It's clear from Figure 10 that for composite aluminized (or metallized) propellant high power rocket motors and model rocket motors with propellant weights under 1 lb that losses from the theoretical specific impulse predicted by PROPEP-type programs can be 15% or more. Experimental/amateur rocketeers making motors with aluminized (or metallized) propellant also need to be aware of losses from the theoretical specific impulse predicted by PROPEP-type programs of approximately 12.5% for 1 lb propellant weight motors, 8% for 10 lb propellant weight motors, 7.5% for 50 lb propellant weight motors, and 5% for 350 lb or greater propellant weight motors (based on the  $I_{sp}$  efficiency and  $\eta_0$  values from Figure 10 and the previous paragraphs), when their propellant is installed in an actual motor. Rather than delivering a theoretical specific impulse for the propellant, it delivers the actual delivered specific impulse for the motor.

Normally in propellant characterization tests the experimental/amateur rocketeer characterizes the  $K_n$  (propellant burning surface area divided by throat area) versus chamber pressure, burn rate versus

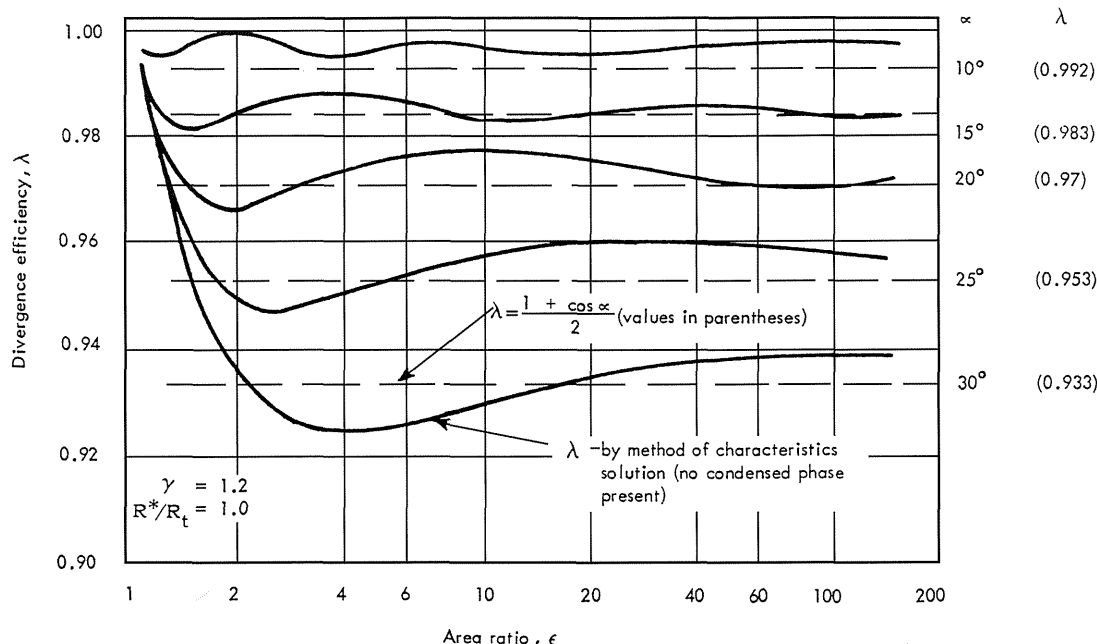


**Figure 11 — Divergence Efficiency for Conical Nozzles.**

chamber pressure, and erosive burning characteristics of their propellant. The present author recommends that as an additional "characterization" of their propellant, that experimental/amateur rocketeers track delivered specific impulse as a percentage (0-100%) of the theoretical specific impulse, and  $c^*$  efficiency factor ( $\eta_0$ ), both as a function of motor size. This will allow the experimental/amateur rocketeer to make more accurate predictions for motor performance as motor size is increased from 1 lb propellant weight to 50 lb propellant weight, to even up to 350+ lb propellant weight, with a continuing increase in delivered specific impulse and  $c^*$  efficiency factor as the motor size is increased.

#### Comparison of the Conical Nozzle Divergence Correction Factor Equation with the Method of Characteristics

Figure 11 from NASA SP-8039 (Ref. 7, original reference Ref. 15) shows a comparison of the nozzle divergence correction factor ( $\lambda$ ) (labeled as divergence efficiency in Figure 11) predicted using the conical nozzle divergence correction factor equation (Eq. (13)) for a series of conical nozzles with different divergence half angles, compared with predictions using the Method of Characteristics, the primary nozzle design method used in the professional liquid rocket engine and solid rocket motor industries. As can be seen from Figure 11, despite the simplified form of Eq. (13) it compares quite well with the much more sophisticated Method of Characteristics method.

#### Applicability to Hybrid Rocket Motors and Liquid Rocket Engines

The previous sections on determining the delivered specific impulse from the theoretical specific impulse obtained from codes such as the JANNAF Thermochemical Equilibrium Code, the NASA Lewis Code, the Air Force Chemical Equilibrium Specific Impulse Code (the USAF ISP Code), and the PROPEP program, presented techniques specifically tailored to solid rocket motors. The present author proposes that with similar thermal equilibrium losses, combustion inefficiency losses, heat losses to the motor hardware, and for metallized fuel two-phase flow losses, that hybrid rocket motors can be modeled using similar techniques, i.e., the Standard Method delivered specific impulse equation, Eq. (31). One difference is the combustion efficiency losses included in the  $c^*$  efficiency factor ( $\eta_0$ ) will also be a function of the mixing efficiency of the hybrid liquid oxidizer and the solid fuel. A hybrid rocket motor with an oxidizer injector with a high mixing efficiency will have a higher  $c^*$  efficiency factor, independent of motor size.

The delivered specific impulse material presented in previous sections is not applicable to liquid rocket engines. Different JANNAF techniques are used for the specific impulse of liquid rocket engines.

## **$C_F$ Efficiency Factor for Straight-Cut Throats and Rounded Throats - Historical Thiokol Solid Rocket Motor Data**

$C_F$  efficiency factor ( $\eta_F$ ) data for historical Thiokol solid rocket motors from Ref. 16 is presented in Figure 12. The historical Thiokol solid rocket motor data from Ref. 16 was of interest, because the data provided for each motor included the actual thrust coefficient ( $C_{F,act}$ ) based on actual static test data, and the predicted ideal thrust coefficient ( $C_F^0$ ) calculated using Eq. (9). The nozzle geometry data provided for each motor also allowed the nozzle divergence correction factor ( $\lambda$ ) to be determined. Thus from the Thiokol data from Ref. 16, the  $C_F$  efficiency factor can be determined from Eq. (28),

$$\text{Eq. (28):} \quad C_{F,act} = \lambda \eta_F C_F^0$$

resulting in Eq. (36).

$$\eta_F = \frac{C_{F,act}}{\lambda C_F^0} \quad (36)$$

The actual thrust coefficient, ideal thrust coefficient, divergence correction factor and the  $C_F$  efficiency factor for selected Thiokol solid rocket motors from Ref. 16 is presented in Figure 12. Note that all of the Thiokol solid rocket motors included in Ref. 16 were reviewed; the data in Figure 12 is for all of

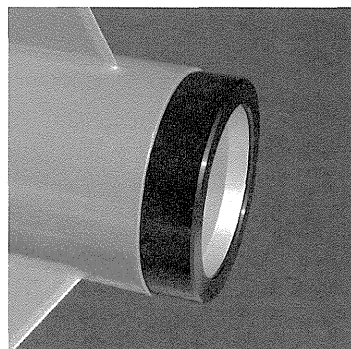
the motors with conical nozzles and straight-cut or rounded throats where sufficient details of the nozzle geometry was presented. A detailed cut-away drawing for each motor showing details of the nozzle geometry is also included in Figure 12. For motors with straight-cut throats the throat straight-cut section Length-to-Diameter (L/D) ratio is listed. Additionally, since there are thrust coefficient losses from two-phase flow effects which would be dependent on whether the propellant was metallized or not, and larger motors have lower thrust coefficient losses from heat losses into the nozzle structure and boundary layer losses in the nozzle; the motor length, propellant weight, and the percentage metallization of the propellant are also presented in Figure 12.

## **Experimental Measurement of Thrust Coefficient, Chamber Pressure, and $C_F$ Efficiency Factor**

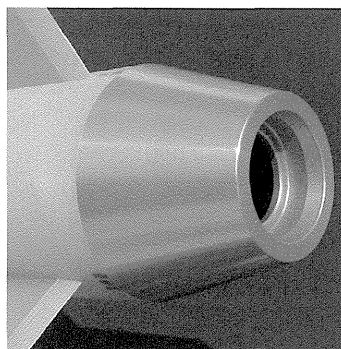
In addition to the historical Thiokol solid rocket motor data from Ref. 16, experimental data from static tests of high power solid rocket motors was analyzed to provide additional data on measured (actual) thrust coefficients and  $C_F$  efficiency factors. The high power solid rocket motor experimental data was also intended to provide a comparison of typical thrust coefficients and  $C_F$  efficiency factors

## **AERO PACK INTERNATIONAL**

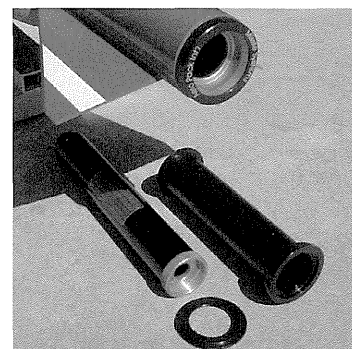
- |  |  |
|--|--|
| <ul style="list-style-type: none"> <li>» Quick-Change Motor Retainers</li> <li>» Quick-Change Tailcone Retainers</li> <li>» Quick-Change Motor Adapters</li> <li>» 30 inch Drogue/Pilot Chutes</li> <li>» Stainless Ball Bearing Swivels</li> <li>» Laser Engraving Service</li> <li>» Ultimate Rocketry Hats</li> </ul> | <ul style="list-style-type: none"> <li>29 thru 98mm precision machined and anodized 6061-T6 &lt;&lt;</li> <li>38mm to 3.0", 54mm to 3.0", 54mm to 3.9", 75 mm to 3.9" &lt;&lt;</li> <li>29-38mm, 38-54mm, 54-75mm, 64-75mm, 75-98 mm &lt;&lt;</li> <li>Bright orange rip-stop nylon X-form, tubular nylon lines &lt;&lt;</li> <li>Stainless steel, 500lb rating, 3/4" welded stainless rings &lt;&lt;</li> <li>Personalized identification, TRA / NAR no, phone no. &lt;&lt;</li> <li>Cotton duck, embroidered, large flap for neck &amp; ears &lt;&lt;</li> </ul> |
|--|--|



RA54 Retainer w/AeroTech motor



TRA5439 Tailcone Retainer w/AeroTech motor



A3854 Adapter w/AeroTech motors

sales@aerpack.net

<http://aerpack.net>

phone: 858.566.2900

## Historical Thiokol Solid Rocket Motor Data (Ref. 16)

**Actual Thrust Coefficient ( $C_{F,act}$ )**

**Ideal Thrust Coefficient ( $C_F^0$ )**

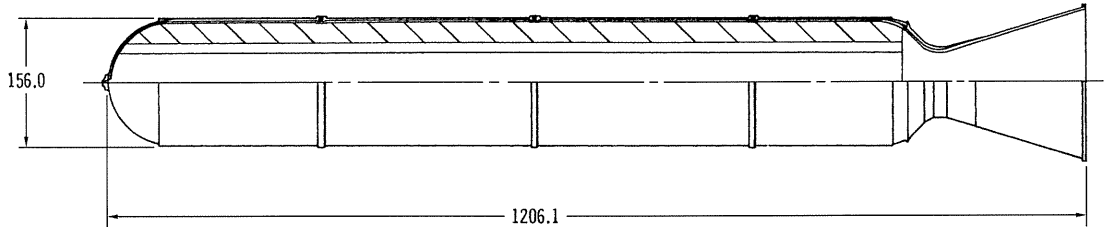
**Nozzle Divergence Correction Factor ( $\lambda$ )**

**$C_F$  Efficiency Factor ( $\eta_F$ )**

Application of the  $C_F$  efficiency factor ( $\eta_F$ ) and the divergence correction factor ( $\lambda$ ) based on the Standard Method:

$$C_{F,act} = \lambda \eta_F C_F^0$$

All dimensions in inches.

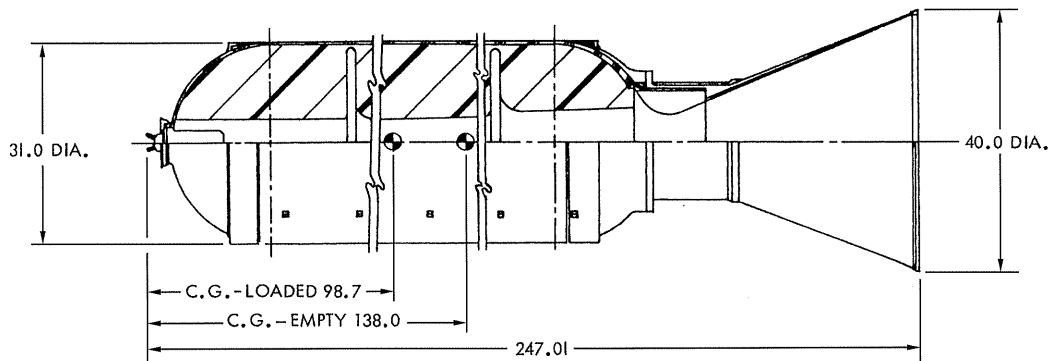


**TA-M-1 156-inch Booster**

Length = 1206.1 in  
 Prop Wt = 798,074 lb  
 $\rho_c$  (avg) = 668 psia (Note 5)  
 Composite AP/AL  
 16% AL  
 $\gamma$  (chamber) = NA  
 $\gamma$  (nozzle exit) = 1.18

Conical Divergent Section  
 Half Angle = 17.5 deg  
 Expansion Ratio = 7.12  
 Rounded Throat

Nozzle Performance (Sea Level):  
 Theoretical  $C_F$ :  $C_F^0 = 1.49$  (Note 1)  
 Actual (Measured)  $C_F$ :  $C_{F,act} = 1.46$  (Note 2)  
 Divergence Correction:  $\lambda = 0.97686$  (Note 3)  
 Nozzle  $C_F$  Correction:  $\eta_F = 1.003$  (Note 4)



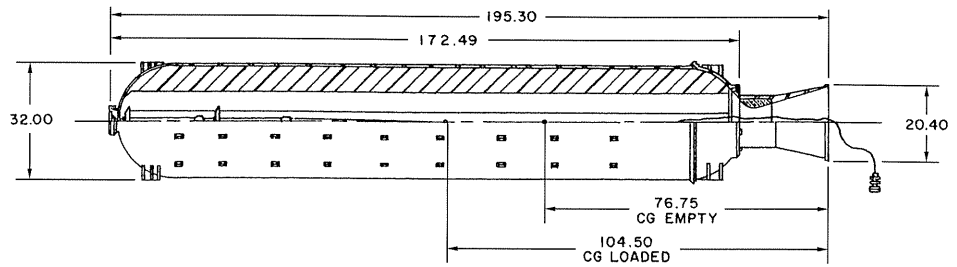
**TX-354-3 Castor II**

Length = 247.01 in  
 Prop Wt = 8,220 lb  
 $\rho_c$  (avg) = 640 psia  
 PBAA/AP/AL  
 20% AL  
 $\gamma$  (chamber) = NA  
 $\gamma$  (nozzle exit) = 1.16

Conical Divergent Section  
 Half Angle = 22.62 deg  
 Expansion Ratio = 21.22  
 Rounded Throat

Nozzle Performance (Vacuum):  
 Theoretical  $C_F$ :  $C_F^0 = 1.86$   
 Actual (Measured)  $C_F$ :  $C_{F,act} = 1.77$   
 Divergence Correction:  $\lambda = 0.96154$   
 Nozzle  $C_F$  Correction:  $\eta_F = 0.990$

**Figure 12 — Historical Thiokol Solid Rocket Motor Data (Ref. 16); Actual Thrust Coefficient ( $C_{F,act}$ ), Ideal Thrust Coefficient ( $C_F^0$ ), Nozzle Divergence Correction Factor ( $\lambda$ ), and  $C_F$  Efficiency Factor ( $\eta_F$ ).**

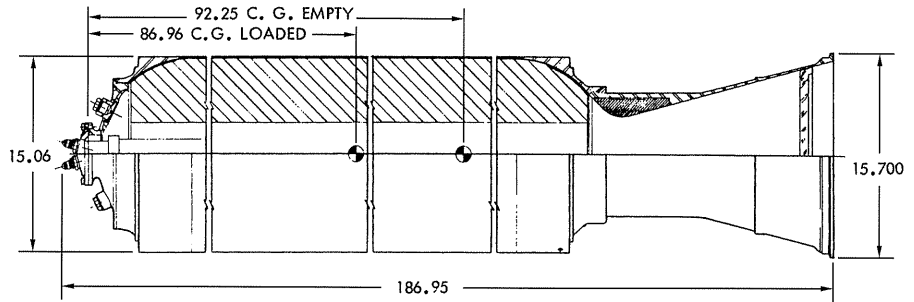


**TX-12 Sergeant**

Length = 195.3 in  
 Prop Wt = 5,925 lb  
 $\rho_c$  (avg) = 527 psia  
 63% AP, binder and fuel not specified  
 $\gamma$  (chamber) = 1.26  
 $\gamma$  (nozzle exit) = NA

Conical Divergent Section  
 Half Angle = 15.0 deg  
 Expansion Ratio = 5.37  
 Rounded Throat

Nozzle Performance (Sea Level):  
 Theoretical  $C_F$ :  $C_F^0 = 1.46$   
 Actual (Measured)  $C_F$ :  $C_{F,act} = 1.37$   
 Divergence Correction:  $\lambda = 0.98296$   
 Nozzle  $C_F$  Correction:  $\eta_F = 0.955$

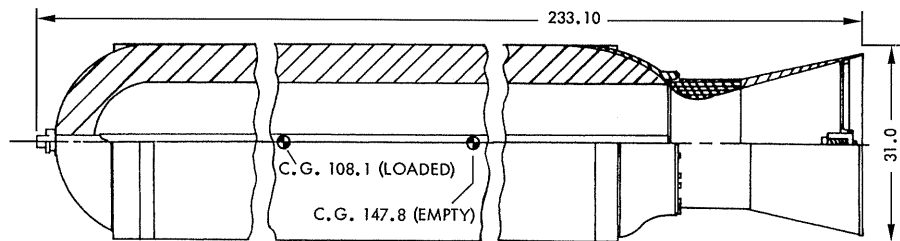


**TX-77-10**

Length = 186.95 in  
 Prop Wt = 1,200 lb  
 $\rho_c$  (avg) = 1,150 psia  
 Polysulfide/AP/AL  
 2% AL  
 $\gamma$  (chamber) = NA  
 $\gamma$  (nozzle exit) = 1.22

Conical Divergent Section  
 Half Angle = 15.0 deg  
 Expansion Ratio = 6.04  
 Rounded Throat

Nozzle Performance (Sea Level):  
 Theoretical  $C_F$ :  $C_F^0 = 1.58$   
 Actual (Measured)  $C_F$ :  $C_{F,act} = 1.47$   
 Divergence Correction:  $\lambda = 0.98296$   
 Nozzle  $C_F$  Correction:  $\eta_F = 0.947$



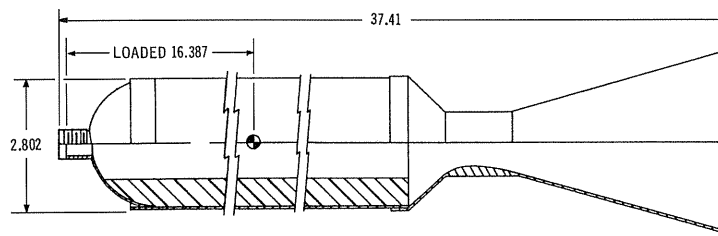
**TX-33-39 Scout**

Length = 233.10 in  
 Prop Wt = 7,313 lb  
 $\rho_c$  (avg) = 512 psia  
 PBAA/AP/AL  
 14% AL  
 $\gamma$  (chamber) = NA  
 $\gamma$  (nozzle exit) = 1.16

Conical Divergent Section  
 Half Angle = 15.0 deg  
 Expansion Ratio = 5.87  
 Rounded Throat

Nozzle Performance (Sea Level):  
 Theoretical  $C_F$ :  $C_F^0 = 1.49$   
 Actual (Measured)  $C_F$ :  $C_{F,act} = 1.38$   
 Divergence Correction:  $\lambda = 0.98296$   
 Nozzle  $C_F$  Correction:  $\eta_F = 0.942$

**Figure 12 (continued)**

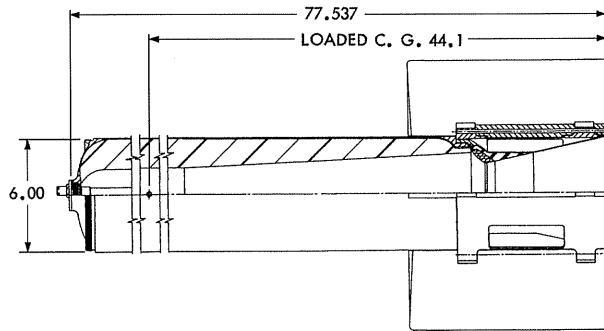


**TX-M-330-0 Arbalist**

Length = 37.41 in  
 Prop Wt = 7.518 lb  
 $\rho_c$  (avg) = 1,500 psia  
 MAPO/AP/AL  
 16% AL  
 $\gamma$  (chamber) = NA  
 $\gamma$  (nozzle exit) = 1.14

Conical Divergent Section  
 Half Angle = 15.0 deg  
 Expansion Ratio = 5.24  
 Rounded Throat

Nozzle Performance (Sea Level):  
 Theoretical  $C_F$ :  $C_F^0 = 1.61$   
 Actual (Measured)  $C_F$ :  $C_{F,act} = 1.42$   
 Divergence Correction:  $\lambda = 0.98296$   
 Nozzle  $C_F$  Correction:  $\eta_F = 0.897$

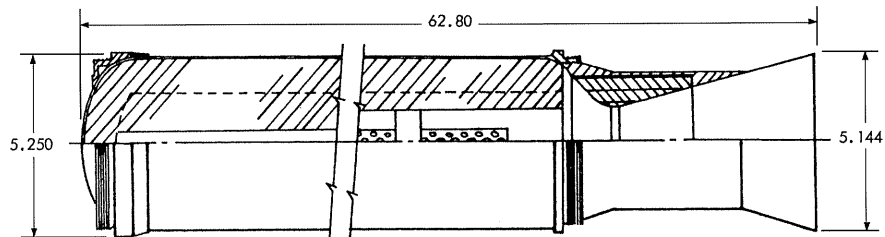


**TE-M-483 Zap Motor**

Length = 77.537 in  
 Prop Wt = 84.70 lb  
 $\rho_c$  (avg) = 2,014 psia  
 Composite/AP/AL  
 10% AL  
 $\gamma$  (chamber) = 1.164  
 $\gamma$  (nozzle exit) = 1.2

Conical Divergent Section  
 Half Angle = 12.0 deg  
 Expansion Ratio = 3.51  
 Straight-Cut Throat  
 Throat L/D = 0.037  
 Rounded Entrance

Nozzle Performance (Sea Level):  
 Theoretical  $C_F$ :  $C_F^0 = 1.56$   
 Actual (Measured)  $C_F$ :  $C_{F,act} = 1.46$   
 Divergence Correction:  $\lambda = 0.98907$   
 Nozzle  $C_F$  Correction:  $\eta_F = 0.946$



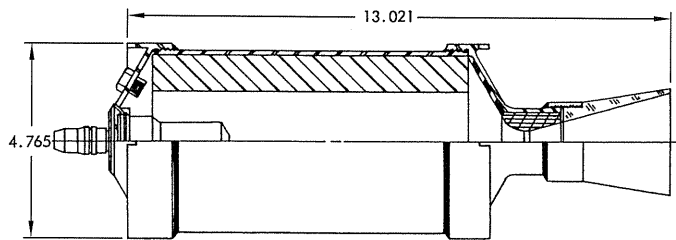
**TE-M-146 Cherokee**

Length = 62.80 in  
 Prop Wt = 52.12 lb  
 $\rho_c$  (avg) = 1,775 psia  
 Polysulfide/AP/AL  
 2% AL  
 $\gamma$  (chamber) = 1.178  
 $\gamma$  (nozzle exit) = 1.185

Conical Divergent Section  
 Half Angle = 15.0 deg  
 Expansion Ratio = 5.89  
 Straight-Cut Throat  
 Throat L/D = 0.118  
 Rounded Entrance

Nozzle Performance (Sea Level):  
 Theoretical  $C_F$ :  $C_F^0 = 1.63$   
 Actual (Measured)  $C_F$ :  $C_{F,act} = 1.58$   
 Divergence Correction:  $\lambda = 0.98296$   
 Nozzle  $C_F$  Correction:  $\eta_F = 0.986$

**Figure 12 (continued)**

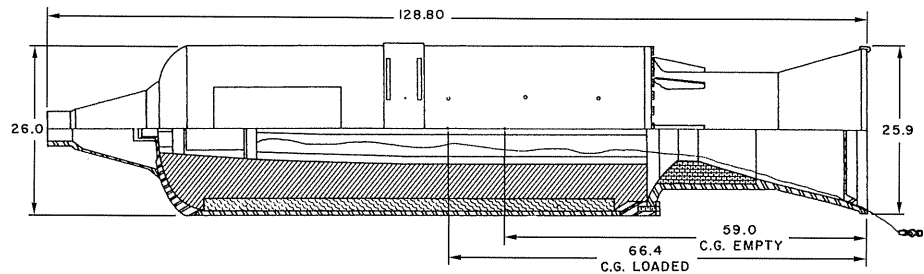


**TE-M-344 Cheyenne**

Length = 13.021 in  
 Prop Wt = 4.56 lb  
 $p_c$  (avg) = 1,230 psia  
 Composite AP/AL  
 16% AL  
 $\gamma$  (chamber) = 1.14  
 $\gamma$  (nozzle exit) = 1.18

Conical Divergent Section  
 Half Angle = 15.0 deg  
 Expansion Ratio = 18.0  
 Straight-Cut Throat  
 Throat L/D = 0.267  
 Rounded Entrance

Nozzle Performance (Vacuum):  
 Theoretical  $C_F$ :  $C_F^0 = 1.84$   
 Actual (Measured)  $C_F$ :  $C_{F,act} = 1.69$   
 Divergence Correction:  $\lambda = 0.98296$   
 Nozzle  $C_F$  Correction:  $\eta_F = 0.934$

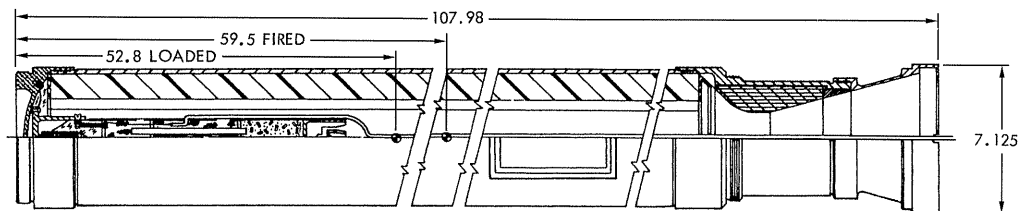


**TU-223 Mace Booster**

Length = 128.80 in  
 Prop Wt = 1,365 lb  
 $p_c$  (avg) = 725 psia (Note 6)  
 Polysulfide/AP  
 0% AL  
 $\gamma$  (chamber) = NA  
 $\gamma$  (nozzle exit) = 1.23

Conical Divergent Section  
 Half Angle = 15.0 deg  
 Expansion Ratio = 5.2  
 Straight-Cut Throat  
 Throat L/D = 0.303  
 Rounded Entrance

Nozzle Performance (Sea Level):  
 Theoretical  $C_F$ :  $C_F^0 = 1.54$   
 Actual (Measured)  $C_F$ :  $C_{F,act} = 1.48$   
 Divergence Correction:  $\lambda = 0.98296$   
 Nozzle  $C_F$  Correction:  $\eta_F = 0.978$



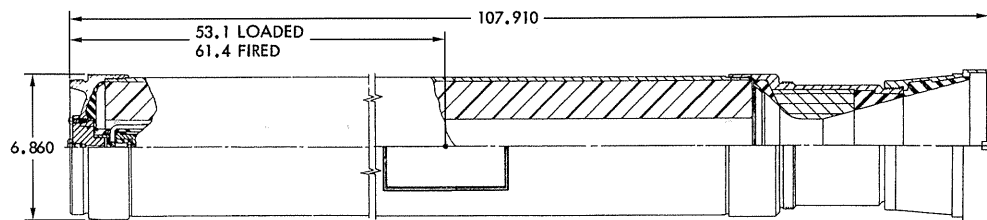
**TE-M-82-4 Cajun**

Length = 107.98 in  
 Prop Wt = 119 lb  
 $p_c$  (avg) = 1,077 psia  
 Polysulfide/AP  
 0% AL  
 $\gamma$  (chamber) = 1.25  
 $\gamma$  (nozzle exit) = NA

Conical Divergent Section  
 Half Angle = 15.0 deg  
 Expansion Ratio = 6.3  
 Straight-Cut Throat  
 Throat L/D = 0.423  
 Rounded Entrance

Nozzle Performance (100K ft):  
 Theoretical  $C_F$ :  $C_F^0 = 1.67$   
 Actual (Measured)  $C_F$ :  $C_{F,act} = 1.60$   
 Divergence Correction:  $\lambda = 0.98296$   
 Nozzle  $C_F$  Correction:  $\eta_F = 0.975$

**Figure 12 (continued)**

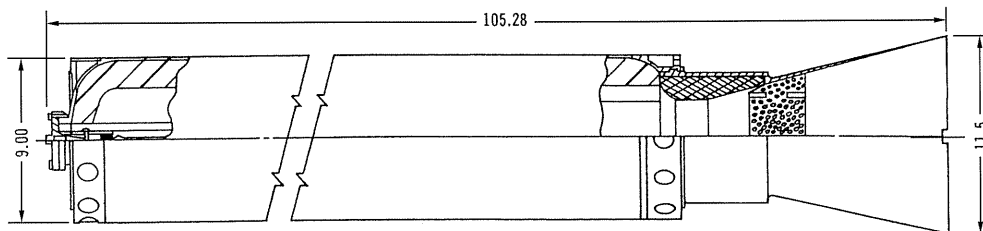


**TE-M-307-3 Apache**

Length = 107.910 in  
 Prop Wt = 132.9 lb  
 $p_c$  (avg) = 685 psia  
 Urethane/AP/AL  
 20% AL  
 $\gamma$  (chamber) = 1.16  
 $\gamma$  (nozzle exit) = NA

Conical Divergent Section  
 Half Angle = 15.0 deg  
 Expansion Ratio = 6.32  
 Straight-Cut Throat  
 Throat L/D = 0.431  
 Rounded Entrance

Nozzle Performance (70K ft):  
 Theoretical  $C_F$ :  $C_F^0 = 1.69$   
 Actual (Measured)  $C_F$ :  $C_{F,act} = 1.60$   
 Divergence Correction:  $\lambda = 0.98296$   
 Nozzle  $C_F$  Correction:  $\eta_F = 0.963$

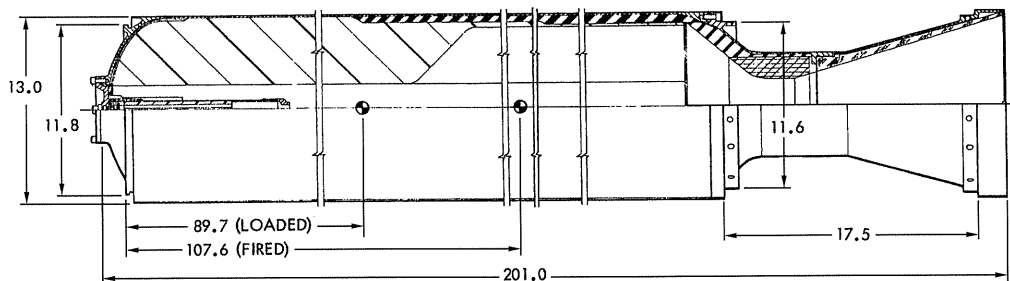


**TE-M-29-1 Recruit**

Length = 105.28 in  
 Prop Wt = 267 lb  
 $p_c$  (avg) = 1,710 psia  
 Polysulfide/AP  
 0% AL  
 $\gamma$  (chamber) = 1.19  
 $\gamma$  (nozzle exit) = NA

Conical Divergent Section  
 Half Angle = 15.0 deg  
 Expansion Ratio = 7.06  
 Straight-Cut Throat  
 Throat L/D = 0.44  
 Rounded Entrance

Nozzle Performance (Sea Level):  
 Theoretical  $C_F$ :  $C_F^0 = 1.60$   
 Actual (Measured)  $C_F$ :  $C_{F,act} = 1.42$   
 Divergence Correction:  $\lambda = 0.98296$   
 Nozzle  $C_F$  Correction:  $\eta_F = 0.903$



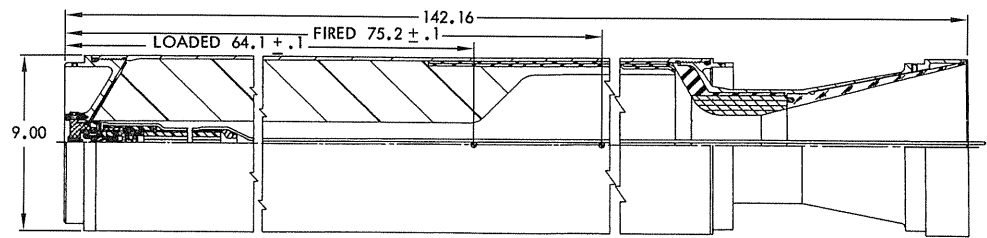
**TE-M-473 Sandhawk**

Length = 201.0 in  
 Prop Wt = 1,106 lb  
 $p_c$  (avg) = 1,168 psia  
 Composite AP/AL (Note 7)  
 18% AL  
 $\gamma$  (chamber) = 1.146  
 $\gamma$  (nozzle exit) = NA

Conical Divergent Section  
 Half Angle = 16.5 deg  
 Expansion Ratio = 10.9  
 Straight-Cut Throat  
 Throat L/D = 0.50  
 Rounded Entrance

Nozzle Performance (Sea Level):  
 Theoretical  $C_F$ :  $C_F^0 = 1.49$   
 Actual (Measured)  $C_F$ :  $C_{F,act} = 1.46$   
 Divergence Correction:  $\lambda = 0.97941$   
 Nozzle  $C_F$  Correction:  $\eta_F = 1.001$

**Figure 12 (continued)**

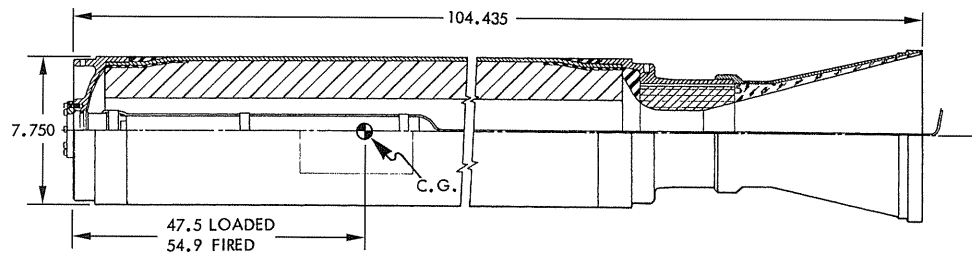


**TE-M-416 Tomahawk**

Length = 142.16 in  
 Prop Wt = 387.06 lb  
 $\rho_c$  (avg) = 920 psia  
 Composite AP/AL (Note 7)  
 20.6% AL  
 $\gamma$  (chamber) = 1.16  
 $\gamma$  (nozzle exit) = NA

Conical Divergent Section  
 Half Angle = 15.0 deg  
 Expansion Ratio = 6.66  
 Straight-Cut Throat  
 Throat L/D = 0.619  
 Rounded Entrance

Nozzle Performance (Sea Level):  
 Theoretical  $C_F$ :  $C_F^0 = 1.62$   
 Actual (Measured)  $C_F$ :  $C_{F,act} = 1.45$   
 Divergence Correction:  $\lambda = 0.98296$   
 Nozzle  $C_F$  Correction:  $\eta_F = 0.911$



**TE-M-388 Iroquois**

Length = 104.435 in  
 Prop Wt = 181 lb  
 $\rho_c$  (avg) = 615 psia  
 Composite AP/AL (Note 7)  
 18% AL  
 $\gamma$  (chamber) = 1.16  
 $\gamma$  (nozzle exit) = NA

Conical Divergent Section  
 Half Angle = 15.0 deg  
 Expansion Ratio = 9.0  
 Straight-Cut Throat  
 Throat L/D = 0.952  
 Rounded Entrance

Nozzle Performance (Sea Level):  
 Theoretical  $C_F$ :  $C_F^0 = 1.54$   
 Actual (Measured)  $C_F$ :  $C_{F,act} = 1.37$   
 Divergence Correction:  $\lambda = 0.98296$   
 Nozzle  $C_F$  Correction:  $\eta_F = 0.905$

**Notes for Figure 12:**

1) Theoretical  $C_F$  ( $C_F^0$ ) based on Eq. (9):

$$C_F^0 = \sqrt{\frac{2\gamma^2}{\gamma-1} \left(\frac{2}{\gamma+1}\right)^{\frac{\gamma+1}{\gamma-1}} \left[1 - \left(\frac{P_e}{P_c}\right)^{\frac{\gamma-1}{\gamma}}\right]} + \left(\frac{P_e - P_\infty}{P_c}\right) \epsilon$$

2) Actual (measured)  $C_F$  ( $C_{F,act}$ ) based on thrust and chamber pressure measurements from static test firings.

3) All nozzles in Figure 12 are conical nozzles. Nozzle divergence correction factor ( $\lambda$ ) based on Eq. (13):

$$\lambda = \frac{1}{2} (1 + \cos \alpha)$$

**Figure 12 (continued)**

4)  $C_F$  efficiency factor ( $\eta_F$ ) calculated based on Eq. (36):

$$\eta_F = \frac{C_{F,act}}{\lambda C_F^0}$$

- 5) Burn time average chamber pressure. Based on Thiokol burn time definition; starts when chamber pressure has risen to 10% of maximum value, ends when chamber pressure has dropped to 75% of maximum value.
- 6) Average chamber pressure for Mace Booster based on action time. Thiokol action time definition; starts when chamber pressure has risen to 10% of maximum value, ends when chamber pressure has dropped to 10% of maximum value.
- 7) Present author believes binder probably HTPB.

NA = Not Available

AL = aluminum

AP = ammonium perchlorate

PBAA = polybutadiene-acrylic acid polymer

HTPB = hydroxyl-terminated polybutadiene

MAPO = tris-[1- (2-methyl) aziridiny] phosphine oxide

### Figure 12 (concluded)

for high power and experimental/amateur solid rocket motor nozzles relative to the Thiokol data for professional solid rocket motors. A review of this experimental data is also useful for reviewing the measurement techniques and analysis techniques for the accurate measurement of thrust coefficient, chamber pressure, and  $C_F$  efficiency factor.

From Eq. (1) it's clear that to make an experimental measurement of thrust coefficient, the thrust needs to be measured (using a load cell, the basic requirement for any instrumented static test), and a measurement needs to be made of the chamber pressure.

Eq. (1): 
$$C_F \equiv \frac{F}{p_c A_{th}}$$

Figure 13 shows the typical location of the pressure tap used to measure chamber pressure in a solid rocket motor, the specific example shown being a high power rocket motor. Figures 14 and 15 show chamber pressure instrumentation mounted in an aerospike solid rocket motor (from Ref. 17) for inflight measurement of chamber pressure. Note in Figures 14 and 15 that the chamber pressure instrumentation is offset from the center of the motor (it reads pressure from a plenum area at the head end

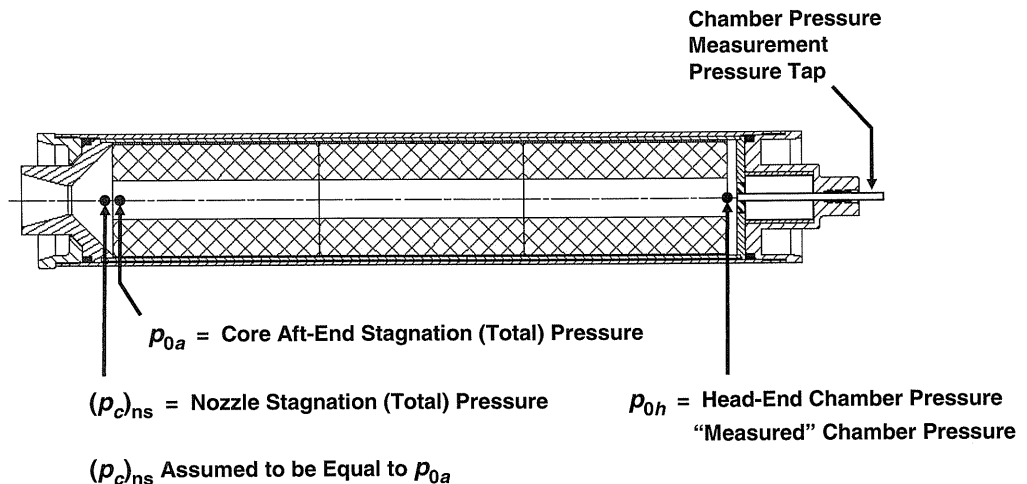


**Figure 13 — Typical Location for Pressure Tap for Measurement of Chamber Pressure, and Locations for Core Head-End Chamber Pressure ( $p_{0h}$ ), Core Aft-End Stagnation (Total) Pressure ( $p_{0a}$ ), and Nozzle Stagnation (Total) Pressure ( $(p_c)_{ns}$ ).**

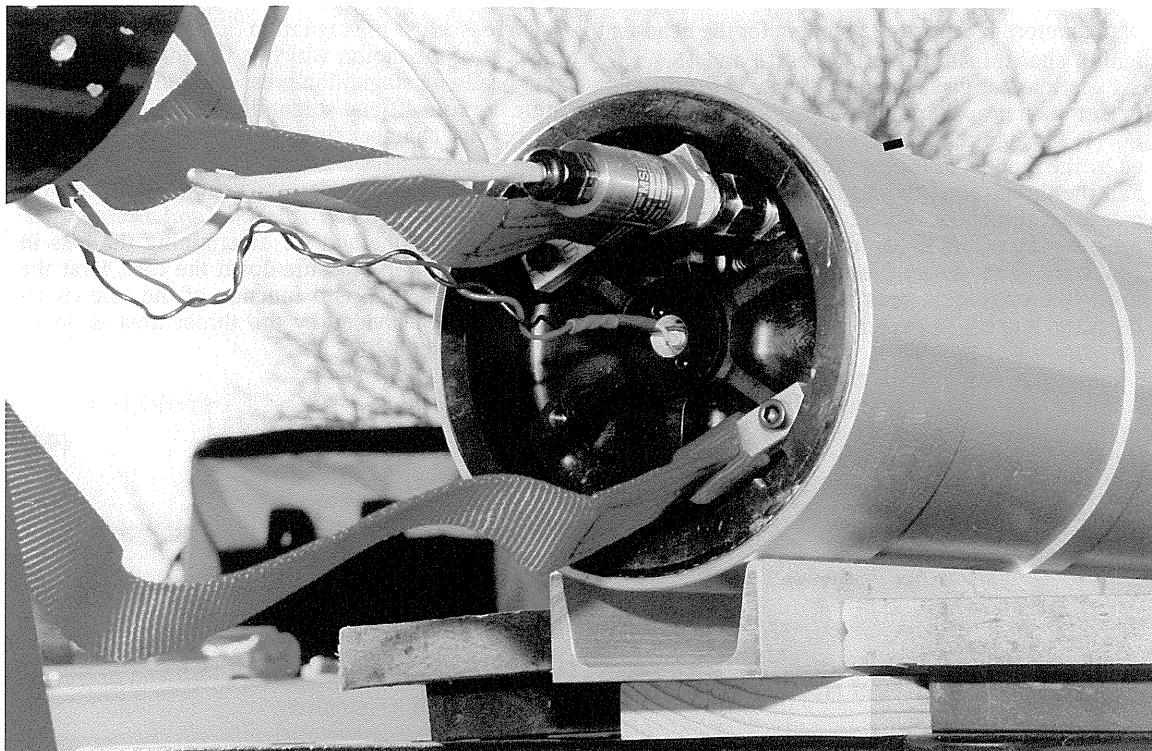


**Figure 14 — DART Aerospike Solid Rocket Motor Forward Bulkhead with Chamber Pressure Instrumentation and Head-End Ignitor.**

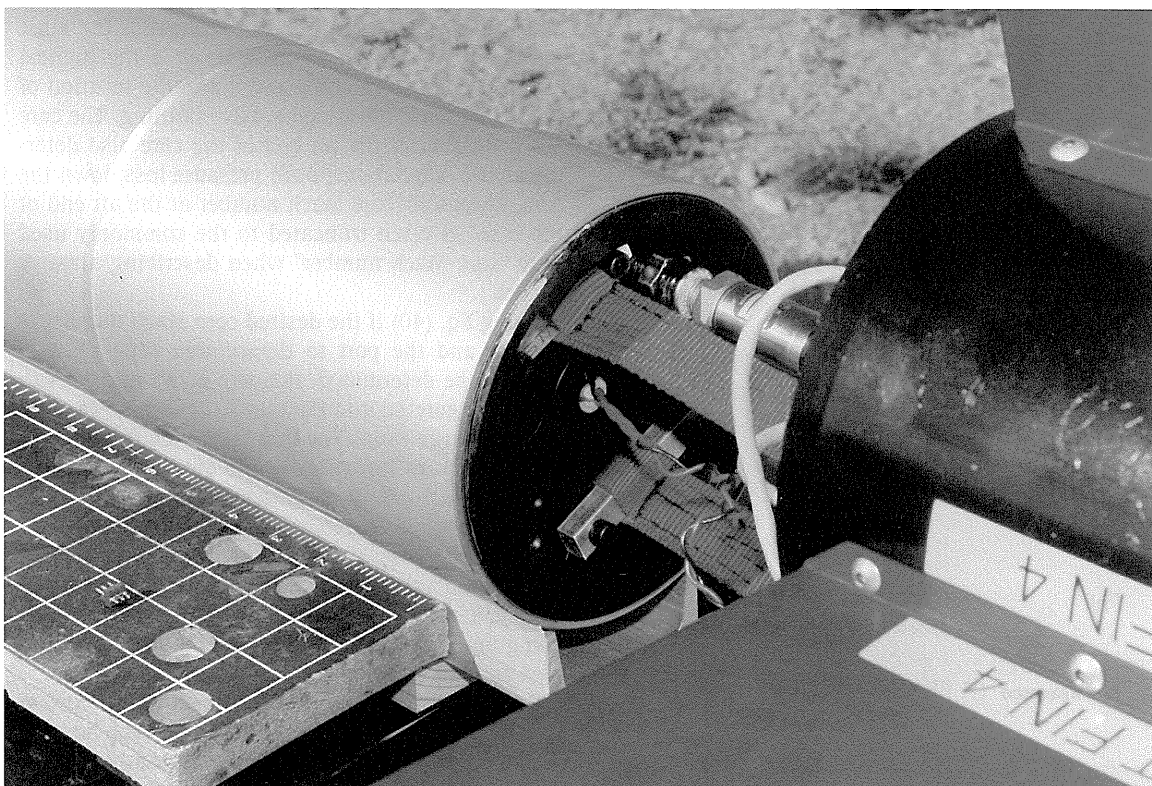


**Figure 15 — DART Aerospike Solid Rocket Motor with Chamber Pressure Instrumentation and Head-End Ignitor Ready for Installation into DART Aerospike Rocket.**

of the motor) in order to leave room for the head-end ignitor shown installed in Figures 14 and 15.

Experimental measurement of nozzle thrust coefficient at first appears to be straightforward. Using Eq. (1) the load cell measurement for thrust is divided by the product of the measured chamber pressure and the throat area; the result is an experimentally measured thrust coefficient. The problem is that the pressure tap shown in Figure 13 measures the head-end stagnation (total) pressure in the motor. The head-end stagnation pressure is not the chamber pressure, it needs to be corrected to become chamber pressure.

Just what precisely is chamber pressure? From NASA SP-125 (Ref. 18, portions reprinted in Ref. 19), the actual chamber pressure is the nozzle stagnation (total) pressure, the total (stagnation) pressure just prior to entering the convergent section of the nozzle (shown in Figure 13).

$$p_{c,act} = (p_c)_{ns} \quad (37)$$

Where:

$p_{c,act}$  = actual chamber pressure, Pa (lb/in<sup>2</sup>)

$(p_c)_{ns}$  = nozzle stagnation (total) pressure, Pa (lb/in<sup>2</sup>)

The assumption can be made that the stagnation (total) pressure at the end of the core ( $p_{0a}$ , shown in Figure 13) is equal to the nozzle stagnation pressure.

$$p_{c,act} = (p_c)_{ns} = p_{0a} \quad (38)$$

Where:

$p_{0a}$  = stagnation (total) pressure at aft end of core, Pa (lb/in<sup>2</sup>)

The measured chamber pressure is the stagnation (total) pressure at the head end of the core ( $p_{0h}$ , shown in Figure 13).

$$p_{c,measured} = p_{0h} \quad (39)$$

Where:

$p_{0h}$  = stagnation (total) pressure at head end of core, Pa (lb/in<sup>2</sup>)

$p_{c,measured}$  = measured chamber pressure, Pa (lb/in<sup>2</sup>)

Thus the measured chamber pressure ( $p_{0h}$ ) needs to be corrected to determine the core aft-end stagnation pressure ( $p_{0a}$ ), which is the actual chamber pressure of the motor.

There is a loss in stagnation (total) pressure down the core of the motor, which is the correction to the core head-end stagnation pressure required to determine the core aft-end stagnation pressure. (Of interest beyond chamber pressure measurement corrections, this stagnation pressure loss down the core is one of the performance losses from erosive burning.) *Space Propulsion Analysis and Design* (Ref. 10) presents a method for determining the loss in stagnation (total) pressure down the core. First the core Mach number as a function of the core cross-sectional area divided by the throat area is determined from Eq. (40).

$$\frac{A_p}{A_{th}} = \frac{1}{M_a} \left[ \frac{2 + (\gamma - 1)M_a^2}{1 + \gamma} \right]^{(\gamma + 1)/2(\gamma - 1)} \quad (40)$$

Where:

$A_p$  = port area (core cross-sectional area), m<sup>2</sup> (in<sup>2</sup>)

$M_a$  = core Mach number at aft end of core, dimensionless

Eq. (40) gives the core Mach number at the aft end of the core. The core Mach number is of course zero at the head end of the core (zero velocity). The core Mach number at the aft end of the core is the most important core Mach number, as it is the highest Mach number in the core and hence the location of the highest velocity-based erosive burning. The core Mach number at the aft end of the core also determines the stagnation (total) pressure loss down the core. The term "core Mach number at the aft end of the core" is often truncated to the commonly used term "core Mach number" when describing a motor design.

Using Eq. (40) if the desired core Mach number is known, and the port to throat area ratio ( $A_p/A_{th}$ ) needs to be determined, the core Mach number can simply be entered into Eq. (40) to determine the port to throat area ratio. The more common situation is that the port to throat area ratio is known, and it is the core Mach number that needs to be determined. Simple iterative methods can be used to solve Eq. (40) for the core Mach number given the port to throat area ratio, with the simplest method being simply iterating the core Mach number from zero using an increment of 0.01 until the port to throat area ratio is matched.

Once the core Mach number for a given port to throat area ratio is determined, Eq. (41) can be used to determine the ratio of the stagnation (total) pressure at the aft end of the core ( $p_{0a}$ ) divided by the stagnation (total) pressure at the head end of the core ( $p_{0h}$ ).

$$\frac{p_{0a}}{p_{0h}} = \frac{\{1 + [(\gamma - 1) / 2] M_a^2\}^{\gamma / (\gamma - 1)}}{1 + \gamma M_a^2} \quad (41)$$

Thus the measured chamber pressure from the pressure tap in Figure 13,  $p_{0h}$ , is converted to the core aft-end stagnation pressure ( $p_{0a}$ ) using Eq. (41), since the core aft-end stagnation pressure is assumed to be equal to the nozzle stagnation pressure (the actual chamber pressure), the core aft-end stagnation pressure is used as the chamber pressure in Eq. (1) to get the measured (actual) thrust coefficient.

$$C_{F,act} = \frac{F}{p_{0a} A_{th}} \quad (42)$$

Note that since Eqs. (40) and (41) are for the flow down the core inside the motor, if several values for the ratio of specific heats are available, the chamber value should be used, versus using the throat or nozzle exit values.

Note that the derivation of Eqs. (40) and (41) from Ref. 10 assumes a constant port area, i.e. a constant cross-sectional area of the core. A more complex

method for tapered cores is presented in Section 6.5.2 of Ref. 10. All cores that have erosive burning at ignition will have a tapered core later in the burn, but the present author recommends that Eqs. (40) and (41) be used for all solid rocket motors for chamber pressure corrections, with the caveat that the equations will be exact for constant cross-sectional area cores and non-erosive motors, and approximate for tapered cores and erosive motors.

Eqs. (40) and (41) are somewhat complex, although the equations can be built into the automated data reduction programs which are often used for recording, plotting, and manipulating data from static tests. Additionally, often times only a few hand calculations are required at select points along the thrust and chamber pressure time histories to determine the actual thrust coefficient for a few points along the thrust curve. Eqs. (40) and (41) can be used for hand calculations, but to simplify the process the present author has created Figure 16. Figure 16 is a plot of  $p_{0a} / p_{0h}$  as a function of  $A_p / A_{th}$  based on Eqs. (40) and (41) assuming a ratio of specific heats ( $\gamma$ ) equal to 1.2 (a good representative value for solid rocket motors). Experimental/amateur rocketeers can use Figure 16 for rapid

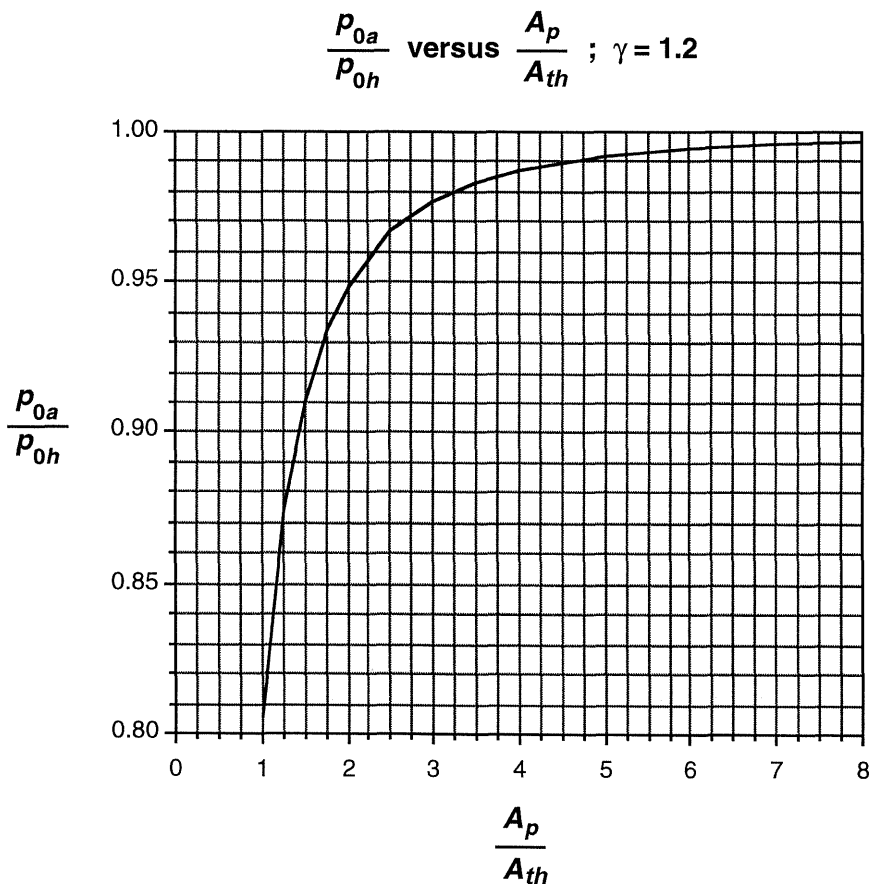
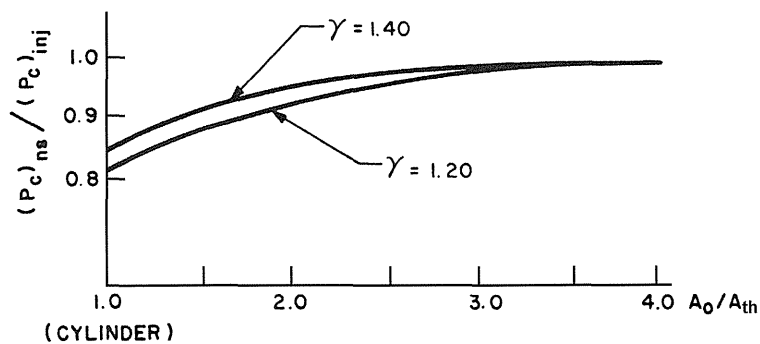


Figure 16 —  $p_{0a} / p_{0h}$  as a function of  $A_p / A_{th}$ ,  $\gamma = 1.2$ .



**Figure 17 —  $(p_c)_{ns}/(p_c)_{inj}$  as a function of  $A_0/A_{th}$ ,  $\gamma = 1.2$  and  $1.4$ .**

determination of  $p_{0a}/p_{0h}$  for a given  $A_p/A_{th}$  to correct measured chamber pressure to the actual chamber pressure for chamber pressure and thrust coefficient measurements.

Note from Figure 16 that it's probably a good idea for motors designed specifically for thrust coefficient measurement tests to have an initial port-to-throat area ratio ( $A_p/A_{th}$ ) of at least 3, and perhaps even as high as 5, to minimize the  $p_{0a}/p_{0h}$  correction to the measured chamber pressure to obtain higher quality chamber pressure and thrust coefficient data, and to allow for rapid reduction of chamber pressure/thrust coefficient data using Figure 16 with hand calculations.

Finally, to obtain  $C_F$  efficiency factor ( $\eta_F$ ) data from static test data, for either the entire thrust curve or selected points along the thrust curve, using the Standard Method the measured actual thrust coefficient ( $C_{F,act}$ ) based on the measured thrust and the corrected chamber pressure, is divided by the nozzle divergence correction factor ( $\lambda$ ) and the calculated ideal thrust coefficient ( $C_F^0$ ) to determine the experimentally measured  $C_F$  efficiency factor ( $\eta_F$ ).

Using the Standard Method (Eq. (28)):

$$\text{Eq. (28): } C_{F,act} = \lambda \eta_F C_F^0$$

Results in Eq. (43):

$$\eta_F = \frac{C_{F,act}}{\lambda C_F^0} \quad (43)$$

Note that since the actual thrust coefficient ( $C_{F,act}$ ) is based on the corrected chamber pressure ( $p_{0a}$ ), the ideal thrust coefficient ( $C_F^0$ ) used in Eq. (43) must also be based on the corrected chamber pressure. The ideal thrust coefficient is calculated using atmospheric pressure, so it is important to measure the atmospheric pressure (or obtain atmospheric pressure data from a nearby airfield or weather station) when performing static tests for

thrust coefficient measurements.

It's important to note that the chamber pressure correction method described above, for correcting the measured chamber pressure to the actual chamber pressure, is for chamber pressure measurements for solid rocket motors. Based on the derivation in Ref. 10 for the  $p_{0a}/p_{0h}$  correction, using a control volume analysis based on mass addition down the motor core, the present author proposes that Eqs. (37)-(43) can also be used for hybrid rocket motors.

For liquid rocket engines a different method for correcting the measured chamber pressure to the actual chamber pressure is used. The actual chamber pressure is the nozzle stagnation (total) pressure,  $(p_c)_{ns}$ , the total (stagnation) pressure just prior to entering the convergent section of the nozzle. For a pressure tap drilled through the injector face of a liquid rocket engine the measured chamber pressure is the injector stagnation (total) pressure,  $(p_c)_{inj}$ . Figure 17, from NASA SP-125 (Ref. 18, portions reprinted in Ref. 19), presents the correction to the injector stagnation (total) pressure to obtain the nozzle stagnation (total) pressure,  $(p_c)_{ns}/(p_c)_{inj}$ , as a function of the ratio of the combustion chamber cross-sectional area ( $A_0$ ) to the throat area ( $A_{th}$ ) for two ratios of specific heats.

Where:

$A_0$  = combustion chamber cross-sectional area, m<sup>2</sup> (in<sup>2</sup>)

$(p_c)_{inj}$  = injector stagnation (total) pressure, Pa (lb/in<sup>2</sup>)

Note that the data plotted in Figure 17 is for cylindrical combustion chambers, the combustion chamber shape used on almost all liquid rocket engines.

(This article will be continued in the next issue, Volume 35 Number 8, November 2004, and will include a glossary and references.)

# TECH SERIES

## The Solid Rocket Motor - Part 5 Departures from Ideal Performance for Conical Nozzles and Bell Nozzles, Straight-Cut Throats and Rounded Throats

by Charles E. Rogers

(Editor's note: Continued from the Volume 35, Number 7, October 2004 issue of *High Power Rocketry*.)

### Experimental Data for $C_F$ Efficiency Factor for Straight-Cut Throats

To verify the trends from the Thiokol solid rocket motor data from Ref. 16 presented in Figure 12, and to provide additional data from tests of high power solid rocket motors (versus professional motors from the Thiokol data), experimental data from static tests of two high power solid rocket motors was analyzed to obtain  $C_F$  efficiency factor ( $\eta_F$ ) data for high power solid rocket motors with straight-cut throats. The analysis of the experimental data from the two static tests also serve as examples of the application of the chamber pressure correction and the thrust coefficient and  $C_F$  efficiency factor measurement techniques/analysis methods presented in the previous section (Eqs. (37)-(43), Figures 13 and 16).

### EAC CSXT 75mm KN=484 Propellant Characterization Test Motor

As part of the motor development program undertaken by the Environmental Aerosciences Corporation (EAC) for the Civilian Space eXploration Team (CSXT) experimental/amateur rocket, the first non-professional/non-governmental rocket launched into space which reached an altitude of 379,900 feet (72 miles), a series of propellant characterization tests were performed by Derek Deville of EAC, with consultation by the present author, to characterize the propellant for the CSXT solid rocket motor. Erosive burning characterization tests were also performed,

but the tests of interest for determining nozzle thrust coefficient were the propellant  $K_n$  (propellant burning surface area divided by throat area) versus chamber pressure tests, due to the higher port-to-throat area ratio ( $A_p/A_{th}$ ) used on those tests (resulting in smaller corrections to the measured chamber pressure). One particular test was chosen for a thrust coefficient and  $C_F$  efficiency factor analysis, the 75mm diameter motor KN=484 propellant characterization test. Figure 18 shows the nozzle used on the 75mm KN=484 Propellant Characterization

### Journal of

## Pyrotechnics

FIREWORKS — PYROTECHNIC SPECIAL EFFECTS — PROPELLANTS & ROCKETRY — CIVILIAN PYROTECHNICS

The *Journal of Pyrotechnics* [ISSN 1082-3999] is a technical journal on pyrotechnics. Areas addressed include fireworks, pyrotechnic special effects, propellants & rocketry, and civilian pyrotechnics. The Journal is "dedicated to the advancement of pyrotechnics through the sharing of information". Table of Contents for the current issue are listed below. All previous issues are available as well as other Pyrotechnic Publications. Price is \$21 in the US and Canada (additional postage to all other countries is US \$1.50). Visit the Journal Web Site or contact us for more information.

- ◆ Simple Core Design for Neutral Burn Composite Rocket Motors
- ◆ Strobe Chemistry
- ◆ Maximizing the Number of Electric Matches That Can Be Fired in a Single Circuit
- ◆ Sparking Compositions for Garden Fireworks
- ◆ Principles of Solid Rocket Motor Design
- ◆ A Practical Performance Testing Protocol for Fireworks Mortar Tubes
- ◆ Fireworks Shells Subjected To a Modified Height-To-Detonation Test Communications:
- ◆ A Simplified Method for Determining the Strength of a Tube Subjected to Internal Pressure
- ◆ Review of: Amateur Rocket Motor Construction by David Sleeter
- ◆ Review of: Rocket Propulsion Elements by George P. Sutton and Oscar Biblarz

### Journal of Pyrotechnics, Inc.

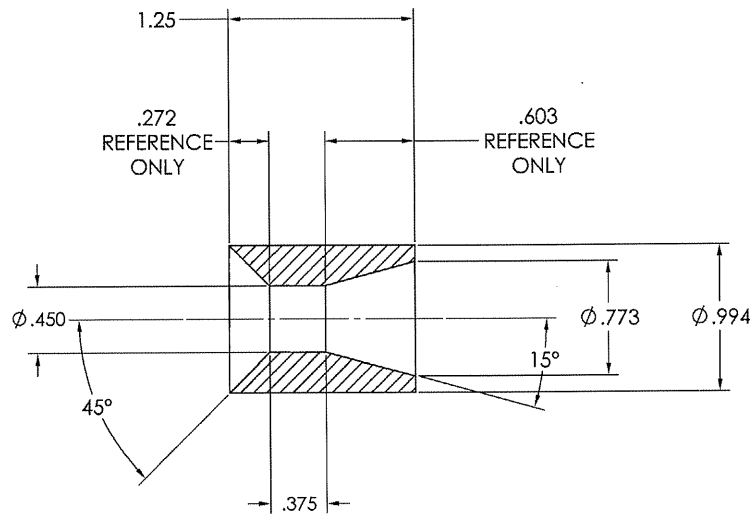
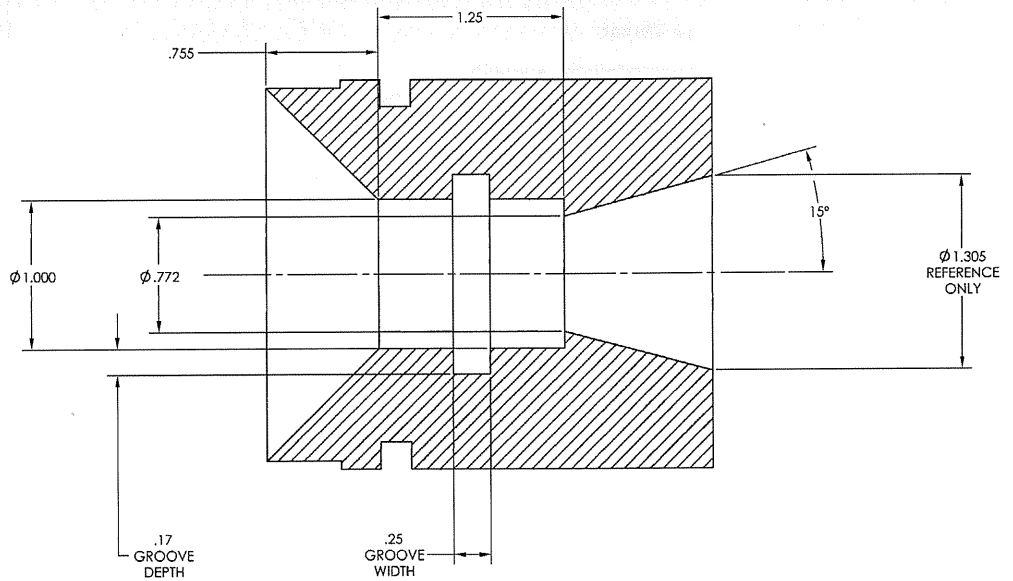
1775 Blair Rd., Whitewater, CO 81527 USA

Phone/FAX (970) 245-0692

email: bonnie@jpyro.com

Web Site: <http://www.jpyro.com>

Copyright ©2004 by Charles E. Rogers. All rights reserved. Published with permission.



### EAC CSXT 75mm KN=484 Propellant Characterization Test Motor Nozzle

Motor Data:  
 Length = 22.0 in  
 Prop Wt = 3.74 lb  
 HTPB/AP/MG/AL (Note 1)  
 8% MG/AL  
 $\gamma = 1.2363$

Conical Divergent Section  
 Half Angle = 15.0 deg  
 Expansion Ratio = 8.35  
 Straight-Cut Throat  
 Throat L/D = 0.833  
 Sharp Entrance  
 (non-rounded)

Nozzle Performance (30.09 in-Hg,  
 approximately Sea Level):  
 Divergence Correction:  $\lambda = 0.98296$   
 Nozzle  $C_F$  Correction:  $\eta_F = 0.90$   
 (measured)

Note:  
 1) MG = magnesium

**Figure 18 — EAC CSXT 75mm KN=484 Propellant Characterization Test Motor Nozzle.**

November 2004

EAC CSXT 75mm KN=484 Propellant Characterization Test Motor

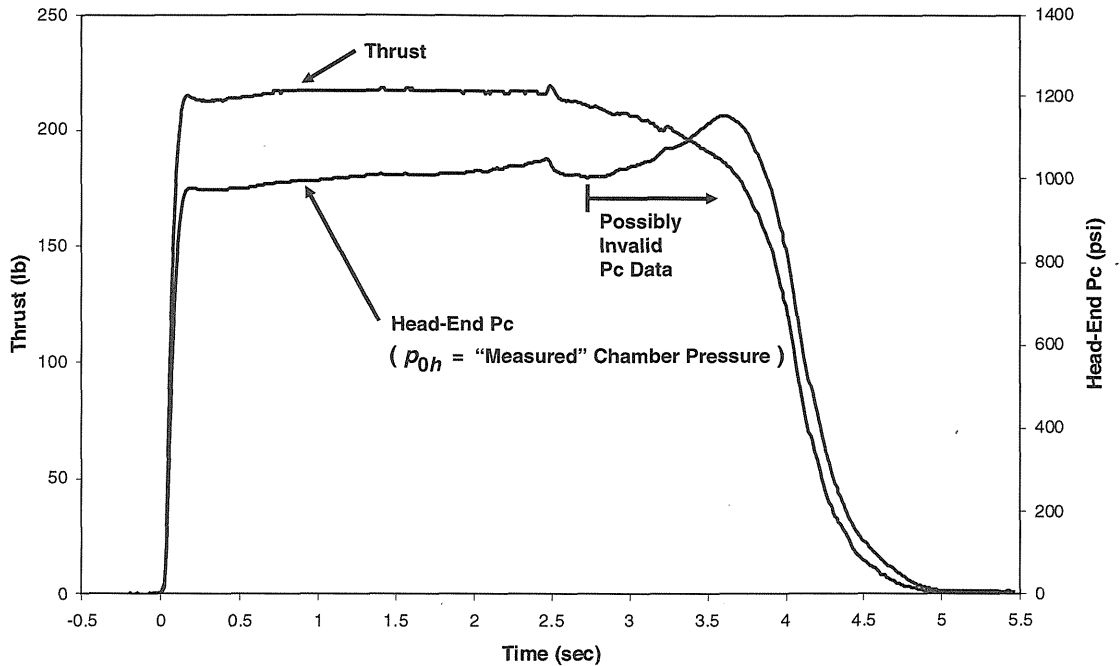


Figure 19 — Thrust and Chamber Pressure Time Histories for EAC CSXT 75mm KN=484 Propellant Characterization Test Motor.

**TOP FLIGHT RECOVERY, LLC**  
 Since 1991  
 www.topflightrecoveryllc.com  
 tfr@execpc.com

**PARACHUTES**  
**Crossfire- Heavy duty multi colored 6 panel chutes, flat braid nylon shroud lines.**

**Firewall - Nomex™ parachute & shock cord protectors.**

**Standard Chutes -Parachutes, X-type parachutes, streamers.**

**Fabric - Regular 1.7 oz. & 1.1oz. thin mill Ripstop nylon fabric in high visibility colors.**

**Swivels & Quick Links and other recovery supplies. Many sizes for model & high power rocketry.**

For catalog with complete product description & descent rate charts, send \$2.00 to:  
 TOP FLIGHT RECOVERY, LLC  
 S12621 Donald Road  
 Spring Green, WI 53588  
 (608) 588-7204

Test Motor. The nozzle drawing is in two parts, the main phenolic part of the nozzle, and the graphite throat insert. Also included in Figure 18 is data on the nozzle performance, including the results from the  $C_F$  efficiency factor analysis which follows.

Figure 19 presents the thrust and chamber pressure time histories for the EAC CSXT 75mm KN=484 Propellant Characterization Test Motor. The chamber pressure data shown in Figure 19 was measured using a pressure tap at the head end of the motor. Six points along the thrust and chamber pressure time histories during the first 2 seconds of the burn were analyzed using Eq. (28) (the Standard Method) and Eqs. (37)-(43) to (1) correct the measured head-end chamber pressure to the actual chamber pressure, (2) determine the actual thrust coefficient, (3) calculate the ideal thrust coefficient based on the actual chamber pressure and atmospheric pressure, and (4) calculate the measured  $C_F$  efficiency factor ( $\eta_F$ ). Table 2 presents the thrust coefficient and  $C_F$  efficiency factor analysis results for the EAC CSXT 75mm KN=484 Propellant Characterization Test Motor for the six points along the first 2 seconds of the thrust curve. Note for the results presented in Table 2 that a single ratio of specific heats was used for both the chamber pressure correction calculations and the nozzle ideal thrust coefficient calculations.

The analysis for the EAC CSXT 75mm KN=484 Propellant Characterization Test Motor presented in Table 2 is an example of doing hand calculations at selected points along the thrust and chamber pressure time histories to determine representative values for the thrust coefficient and  $C_F$  efficiency factor, without having to do the calculations for the entire

**EAC CSXT 75mm KN=484 Propellant Characterization  
Test Motor  $C_F$  Efficiency Factor Analysis Results**

$D_{th} = 0.45$  in  
 $A_{th} = 0.15904$  in<sup>2</sup>  
 $D_e = 1.3$  in  
 $A_e = 1.32732$  in<sup>2</sup>  
 Nozzle Expansion Area Ratio;  $\epsilon = 8.35$   
 Nozzle Divergence Half Angle;  $\alpha = 15.0$  deg  
 Ratio of Specific Heats;  $\gamma = 1.2363$   
 Atmospheric Pressure;  $p_\infty = 30.09$  in-Hg

Standard Method  
 $C_{F,act} = \lambda \eta_F C_F^0$

Time (sec)	Thrust (lb)	$p_{0h}$ (psia)	$A_p/A_{th}$	$M_\alpha$	$p_{0a}/p_{0h}$	$p_{0a}$ (psia)	$C_{F,act}$	$C_F^0$	$\lambda$	$\eta_F$
0.17	215.33	978.0	3.84	0.1556	0.9856	963.92	1.4046	1.5456	.98296	.9245
0.29	212.67	975.33	4.60	0.1293	0.9899	965.48	1.3850	1.5458	.98296	.9115
0.50	214.0	979.33	5.91	0.1003	0.9939	973.36	1.3824	1.5468	.98296	.9092
1.0	216.67	999.33	9.05	0.0653	0.9974	996.73	1.3824	1.5498	.98296	.9074
1.5	217.33	1013.33	12.18	0.0485	0.9986	1011.91	1.3504	1.5516	.98296	.8854
2.0	216.67	1020.67	15.32	0.0385	0.9991	1019.75	1.3360	1.5525	.98296	.8755

**Table 2 — EAC CSXT 75mm KN=484 Propellant Characterization Test Motor  $C_F$  Efficiency Factor Analysis Results.**

thrust curve.

The  $C_F$  efficiency factor results from Table 2 for the six points during the first 2 seconds of the thrust curve are plotted versus time in Figure 20. As can be seen from Table 2 and Figure 20, the  $C_F$  efficiency factor ( $\eta_F$ ) for the EAC CSXT 75mm KN=484 Propellant Characterization Test Motor Nozzle is approximately 0.90. A  $C_F$  efficiency factor of 0.90 represents a 10% loss in thrust coefficient, which is poor performance for a nozzle.

DART Project Conical Nozzle Control Motor

The NASA Dryden Aerospike Rocket Test (DART) aerospike rocket project, where an aerospike nozzle was retrofitted onto a high power solid rocket motor (documented in Ref. 17), had two solid rocket motor configurations that were static tested with thrust measurements and chamber pressure measurements; an aerospike motor, and a conical nozzle motor known as the "control" motor. The purpose of the conical nozzle control motor was to be identical in every way to the aerospike nozzle motor, (same propellant formulation, same propellant grain

geometry, same throat area), with the only difference being that a conventional conical nozzle was installed in place of the aerospike nozzle to allow the performance differences between the new aerospike nozzle and the conventional conical nozzle to be quantified. The aerospike nozzle motor and the conical nozzle control motor were both built by Cesaroni Technology Incorporated (CTI), and were based on the CTI O5100 reloadable high power rocket motor. Due to concerns about two-phase flow effects in the aerospike nozzle, the propellant used in the aerospike nozzle motor and the conical nozzle control motor had a reduced aluminum content (4% aluminum).

Figure 21 shows the nozzle used on the DART Project Conical Nozzle Control Motor, and includes additional data on the motor, and the results from the  $C_F$  efficiency factor analysis which follows.

In the thrust coefficient and  $C_F$  efficiency factor analysis for the DART Project Conical Nozzle Control Motor an automated approach was undertaken where Dr. Trong Bui from NASA-Dryden integrated Eq. (28) (the Standard Method) and Eqs. (37)-(43) into an automated MATLAB language program used for data reduction from motor static tests to (1) cor-

# CSXT 75mm KN = 484 Propellant Characterization Test Motor

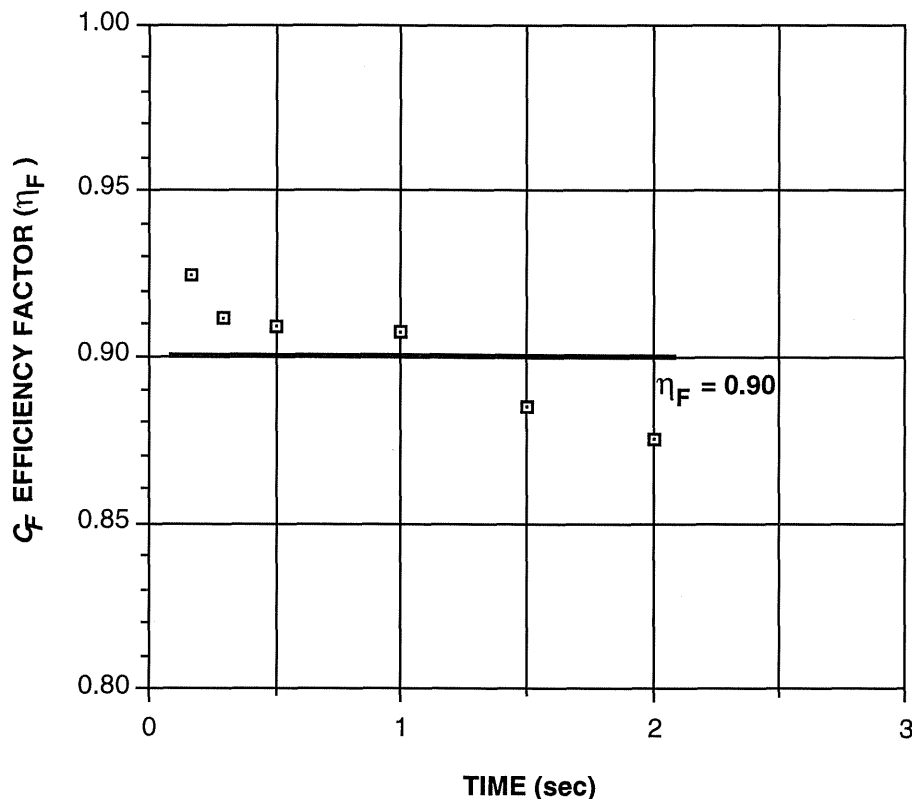


**Figure 20 —  $C_F$  Efficiency Factor ( $\eta_F$ ) versus Time for First 2 Seconds of Thrust Curve for EAC CSXT 75mm KN=484 Propellant Characterization Test Motor Nozzle.**

## FIBERGLASS ROCKET KITS BODY TUBES & FIN MATERIAL

Why build a toy rocket out of cardboard when you can build a "Real Rocket" out of Fiberglass? Send \$2.50 for our catalog on fiberglass kits and accessories. **Powdered Aluminum** also available, As low as \$ 4.00/pound.

### G-12 Filament Wound Glass-Epoxy Body Tubes.

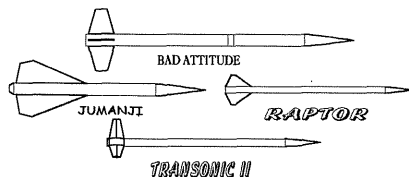
We carry popular sizes 29mm to 6".

### FR-4 Glass-Epoxy Sheets

FR-4 is the heat resistant version of G-10 and is better suited for fin material because of exhaust gases. These sheets are extremely strong with a tensile strength over 48,000 psi!

### Fiberglass Centering Rings

Aerospace grade Epoxy



HAWK MOUNTAIN ENTERPRISES

Rd 1 Box 231 New Ringgold, PA 17960

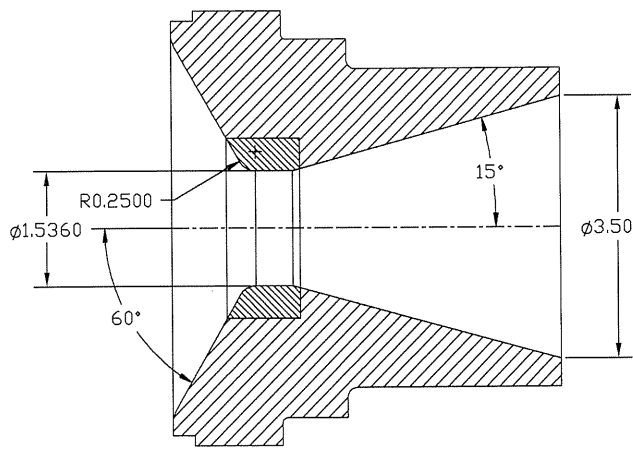
(570) 943-7644

<http://www.hawkmountain.ws>

rect the measured head-end chamber pressure to the actual chamber pressure, (2) determine the actual thrust coefficient, (3) calculate the ideal thrust coefficient based on the actual chamber pressure and atmospheric pressure, and (4) calculate the measured  $C_F$  efficiency factor. Note for the analysis results which will be presented for the DART Project Conical Nozzle Control Motor that a single ratio of specific heats was used for both the chamber pressure correction calculations and the nozzle ideal thrust coefficient calculations.

Figure 22 presents the thrust and chamber pressure time histories for the DART Project Conical Nozzle Control Motor. The chamber pressure data shown in Figure 22 was measured using chamber pressure instrumentation mounted in the forward bulkhead of the motor, in a configuration identical to the chamber pressure instrumentation used on the aerospike motor which was presented previously in Figures 14 and 15.

Figure 23 presents the port-to-throat area ratio ( $A_p/A_{th}$ ) versus time for the DART Project Conical Nozzle Control Motor. For the data plotted in Figure 23 the pre-firing prediction for the port-to-throat area ratio was adjusted based on the actual burn time and thrust curve of the motor (including tail-off effects) to open up the port all the way to the motor case propellant liner at



### Nozzle for DART Project Conical Nozzle Control Motor

Length = 29.315 in

Prop Wt = 28.525 lb

$p_c$  (avg) = 388.85 psia (Note 1)

HTPB/AP/AL

4% AL

$\gamma = 1.1941$

Conical Divergent Section

Half Angle = 15.0 deg

Expansion Ratio = 5.19

Straight-Cut Throat

Throat L/D = 0.30

Rounded Entrance

Nozzle Performance (30.388 in-Hg, approximately Sea Level):

Divergence Correction:  $\lambda = 0.98296$

Nozzle  $C_F$  Correction:  $\eta_F = 0.99$  (measured)

Note:

1) Burn time average chamber pressure. Burn time defined as initial thrust to final thrust.

**Figure 21 — Nozzle for DART Project Conical Nozzle Control Motor.**

# blacksky

Design, manufacture, and distribution of state-of-the-art rocketry products.

## **blacksky ELECTRONICS**

- *AltAcc2C* – Recovery, recording altimeter-accelerometer
- *Timer4* – PC programmed, multi-function, 4-channel timer
- *Timer2* – Field set, g-switch, 2-channel timer
- *Timer1* – Field set, g-switch, 1-channel timer

## **blacksky PYROTECHNICS**

- *ARRD* – Advanced Retention and Recovery Device
- *EJecter* – Re-useable recovery charge holder
- *HiRMI* – Electric matches, 1 amp and 0.4 amp
- *Head End Igniters* – 75mm and 98mm re-loadable motors

## **blacksky GROUND SUPPORT**

- *Standard, HPR and Ultimate Rails*
- *Rail Guides* – Plastic and aluminum
- *ProPad1* – For rockets up to 15 pounds
- *ProPad3C* – For rockets up to 250 pounds

## **Cesaroni PROPULSION**

- *Pro38, Pro54, Pro75, Pro98, Pro150* solid rocket motors
- *Hypertek* nitrous oxide hybrid rocket motors

**No Hype.**

**Simple.**

**Reliable.**

**Any Questions?**

**blacksky Corporation, 3179 Roosevelt St., Carlsbad, CA 92008-3018**  
**ORDERS & QUESTIONS (760)730 3701 or [www.blacksky.com](http://www.blacksky.com)**

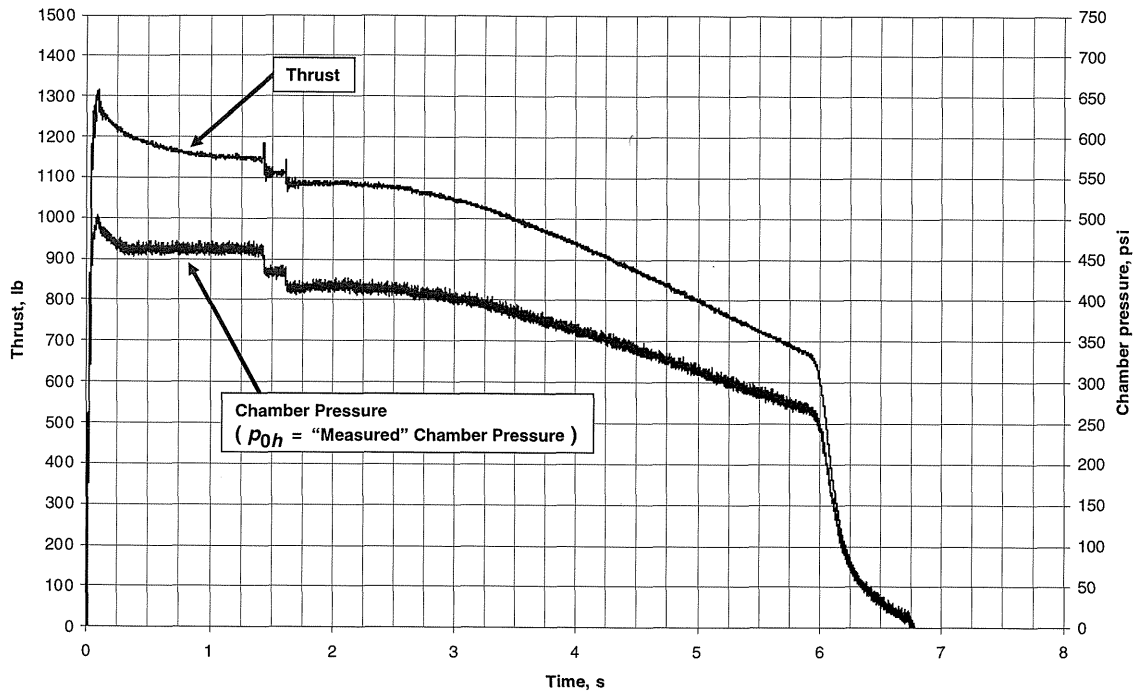


**Figure 22 — Thrust and Chamber Pressure Time Histories for DART Project Conical Nozzle Control Motor.**

burnout. Figure 24 presents the core Mach number ( $M_a$ ), the Mach number at the aft end of the core versus time (calculated using Eq. (40)). Figure 25 presents the head-end stagnation pressure ( $p_{0h}$ , the measured chamber pressure) and the core aft-end stagnation pressure ( $p_{0a}$ , the actual chamber pressure), showing the loss in stagnation pressure down the core of the motor (calculated using Eq. (41)). The difference between the  $p_{0h}$  and the  $p_{0a}$  curves in Figure 25 is the correction to the measured chamber pressure to get the actual chamber pressure. Note in Figures 23 and 25 how as the core opens up during

the burn (increased  $A_p/A_{th}$ ) the difference between  $p_{0h}$  and  $p_{0a}$  is decreased to the point where at 3 seconds into the burn ( $A_p/A_{th} = 6.9$ ) the correction to  $p_{0h}$  to get  $p_{0a}$  becomes negligible, and the head-end chamber pressure measurement can be used directly as the "actual" chamber pressure.

Figure 26 presents the actual (measured) thrust coefficient ( $C_{F,act}$ ) versus time, backed out from the measured thrust using Eq. (42) and the actual chamber pressure ( $p_{0a}$ ), for the DART Project Conical Nozzle Control Motor. Note the drop in thrust coefficient as the motor thrust curve begins to tail off. The thrust coefficient data at very low chamber pressures was considered to be invalid.

Finally, Figure 27 presents the  $C_F$  efficiency factor ( $\eta_F$ ) versus time, based on the Standard Method Eq. (28), calculated using Eq. (43), for the DART Project Conical Nozzle Control Motor. While there was some variation in the  $C_F$  efficiency factor during the first 1.75 seconds of the burn, for most of the burn the  $C_F$  efficiency factor was approximately 0.99, which is a high value and indicates excellent performance for the nozzle. Theoretically the  $C_F$  efficiency factor cannot exceed 1.0, since it is applied to the ideal thrust coefficient, which theoretically is the highest possible thrust coefficient. Therefore the  $C_F$  efficiency factor data over 1.0 during the low chamber pressure phase and tail-off phase of the burn was discarded as invalid data.



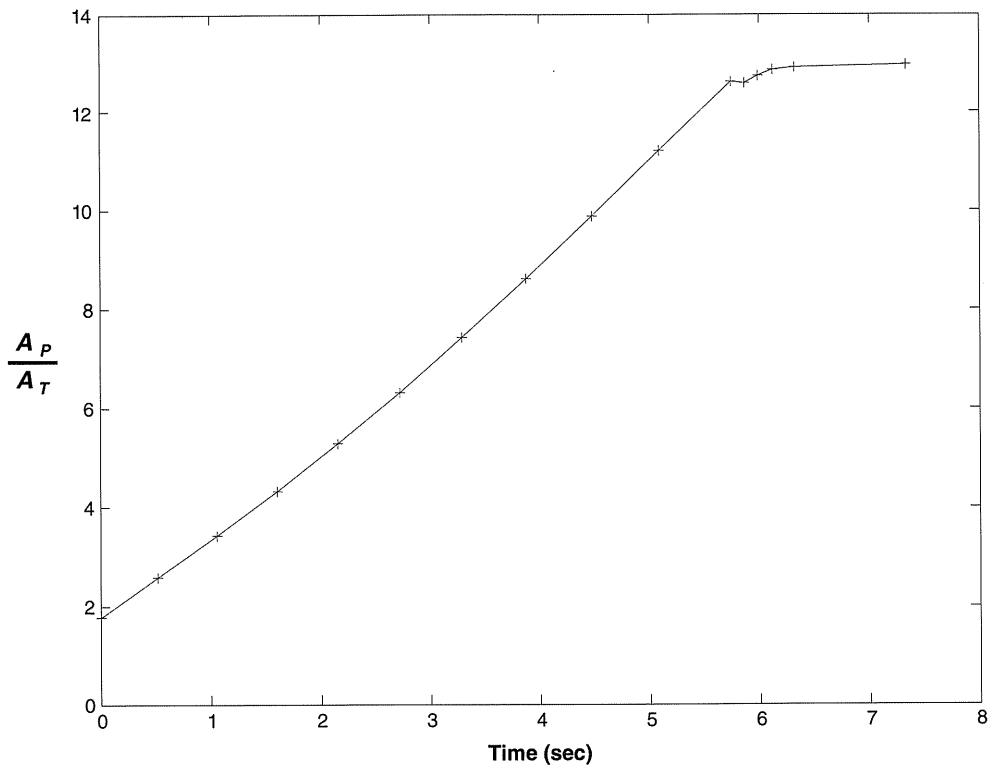


**Figure 23 — Port-to-Throat Area Ratio ( $A_p/A_{th}$ ) versus Time for DART Project Conical Nozzle Control Motor.**

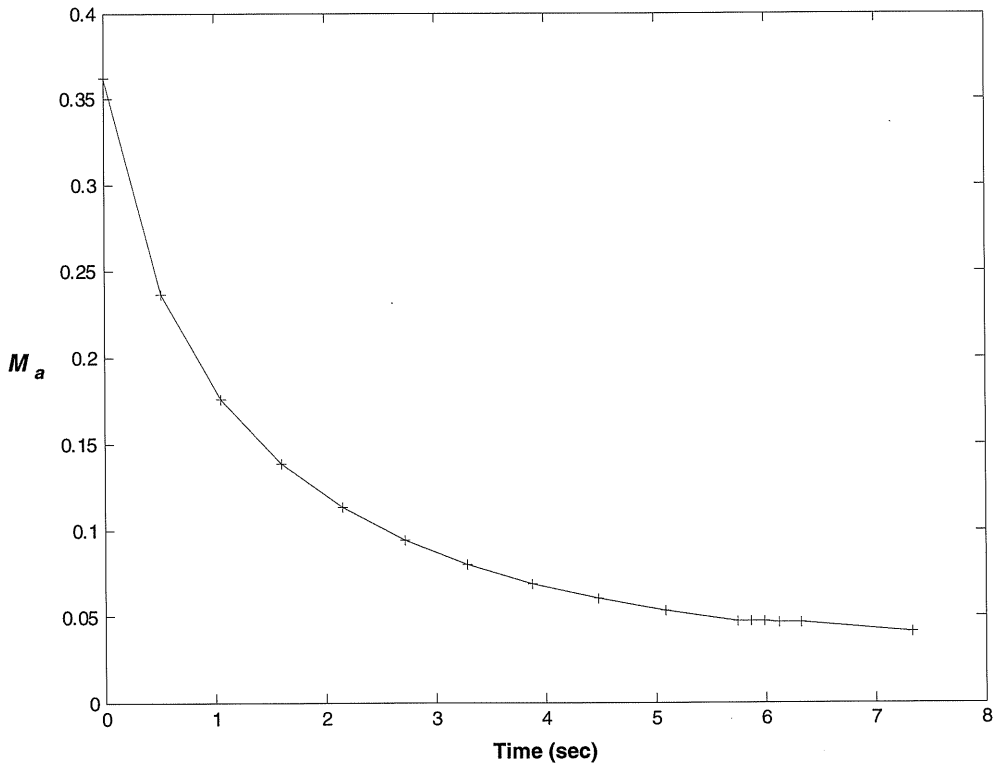


**Figure 24 — Core Mach Number ( $M_a$ ) versus Time for DART Project Conical Nozzle Control Motor.**

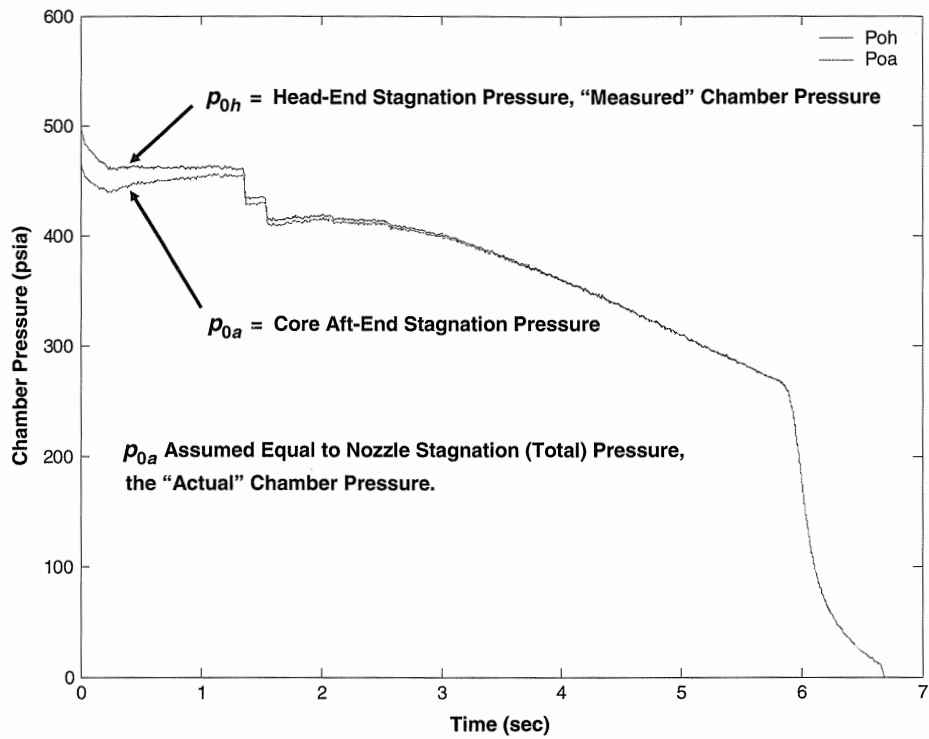


Figure 25 —  $p_{0h}$  and  $p_{0a}$  versus Time for DART Project Conical Nozzle Control Motor.

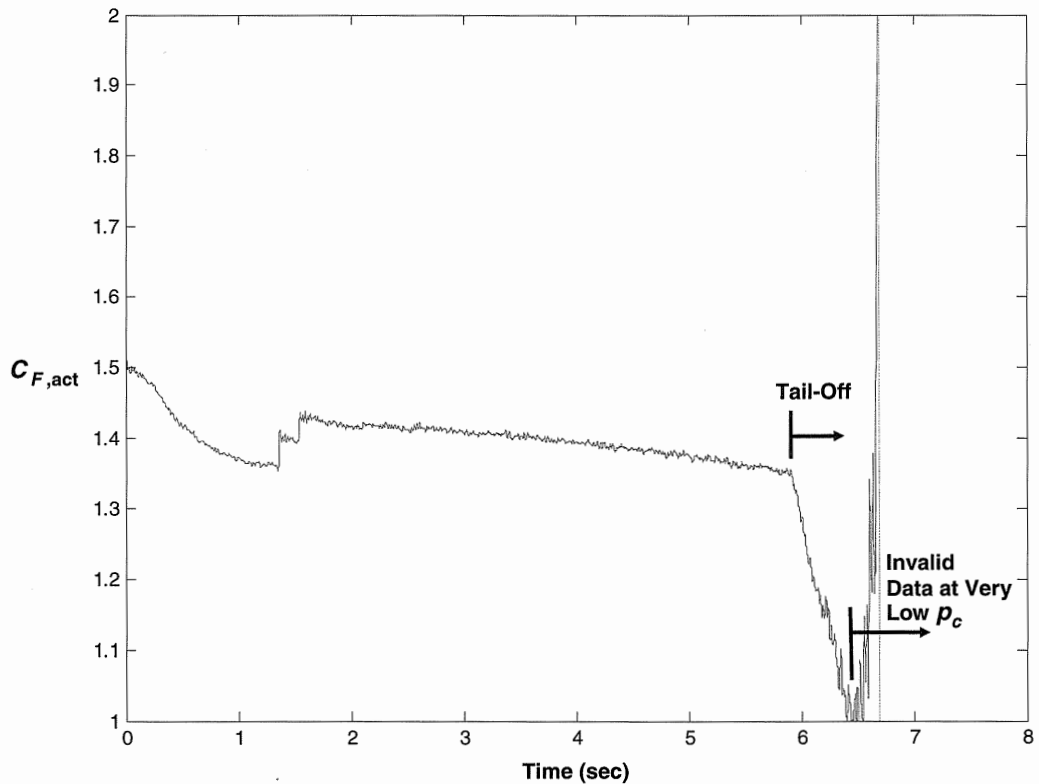
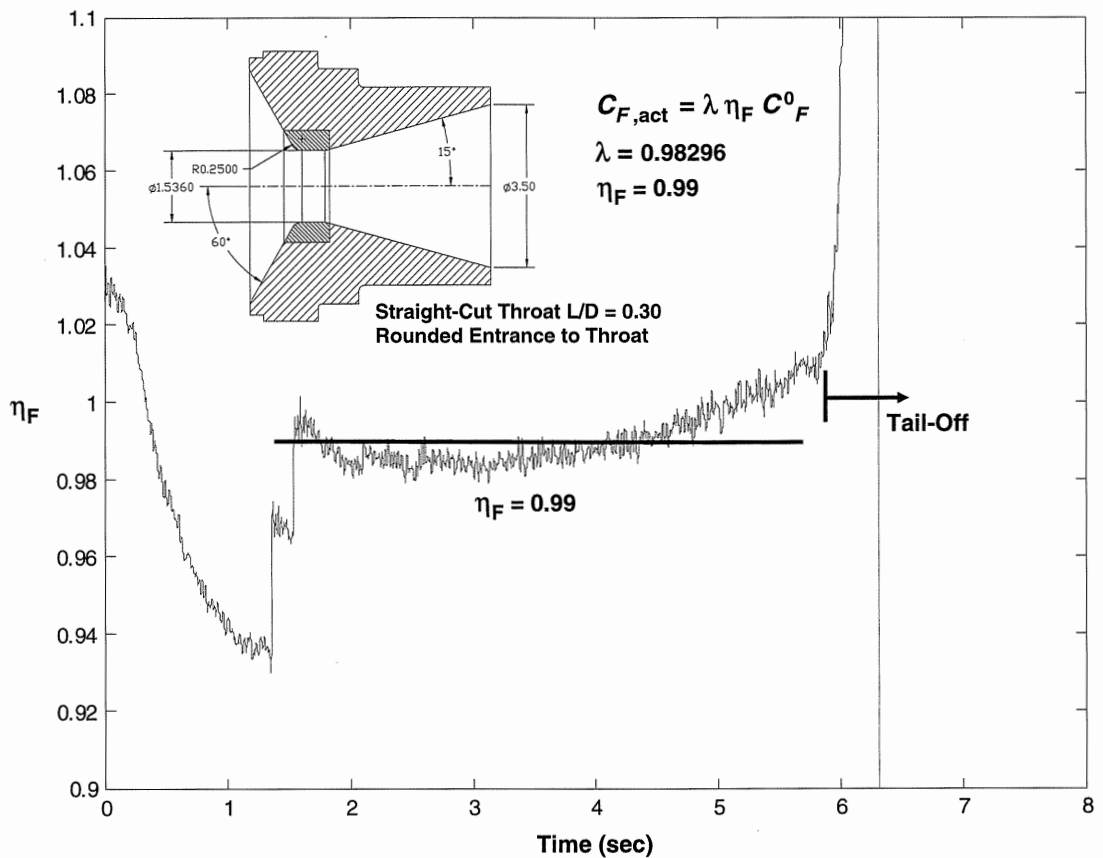


Figure 26 — Actual (Measured) Thrust Coefficient ( $C_{F,act}$ ) versus Time for DART Project Conical Nozzle Control Motor.



**Figure 27 —  $C_F$  Efficiency Factor ( $\eta_F$ ) versus Time for DART Project Conical Nozzle Control Motor.**

**Summary of  $C_F$  Efficiency Factor Results for Conical Nozzles with Straight-Cut Throats**

Figure 28 presents the results of the  $C_F$  efficiency factor ( $\eta_F$ ) study performed for this article. Both the historical Thiokol data from Ref. 16 presented in Figure 12, and the  $C_F$  efficiency factor experimental data from the EAC CSXT 75mm KN=484 Propellant Characterization Test Motor and the DART Project Conical Nozzle Control Motor (labeled as CTI DART Modified O5100) are included in Figure 28.

When the present author was reviewing the historical Thiokol data and the experimental data from the CSXT and DART motors, some interesting trends in terms of the variation of the  $C_F$  efficiency factor with the Length-to-Diameter (L/D) ratio of the straight section of the straight-cut throats became apparent.

Figure 28 plots the  $C_F$  efficiency factor ( $\eta_F$ ) for the nozzles presented in this article versus throat L/D. Both straight-cut and rounded throats are presented, the rounded throats have a throat L/D of zero. All of the nozzles have rounded throat entrances, with the exception of the CSXT Propellant Characterization Test Motor which has a sharp throat entrance.

Most of the data is the historical Thiokol data from Figure 12, the two experimental data points for high power rocket motors are indicated by the solid symbols (CSXT and DART motors). Included in the Figure 28 plot is a dashed line marking the maximum theoretical value for the  $C_F$  efficiency factor ( $\eta_F = 1.0$ , ideal performance). It's apparent from the data presented in Figure 28 that straight-cut throats with throat L/D's greater than 0.45 have very low performance, the  $C_F$  efficiency factors are approximately 0.905, resulting in an approximately 9.5% loss in thrust coefficient, thrust, total impulse, and specific impulse. Nozzles with lower throat L/D's (shorter straight-cut throat lengths) have higher performance, as expected. But what is most interesting is the jump in nozzle performance (increased  $C_F$  efficiency factor) for throat L/D's less than 0.45. For throat L/D's less than 0.45 the data groups into two groups, a low performance group and a high performance group. In both cases as the throat L/D approaches zero the straight-cut throat data merges into the rounded throat data (throat L/D = 0). In either case there is a substantial increase in performance when the throat L/D is reduced below 0.45.

### CF EFFICIENCY FACTOR VERSUS THROAT L/D STRAIGHT-CUT THROATS ON CONICAL NOZZLES

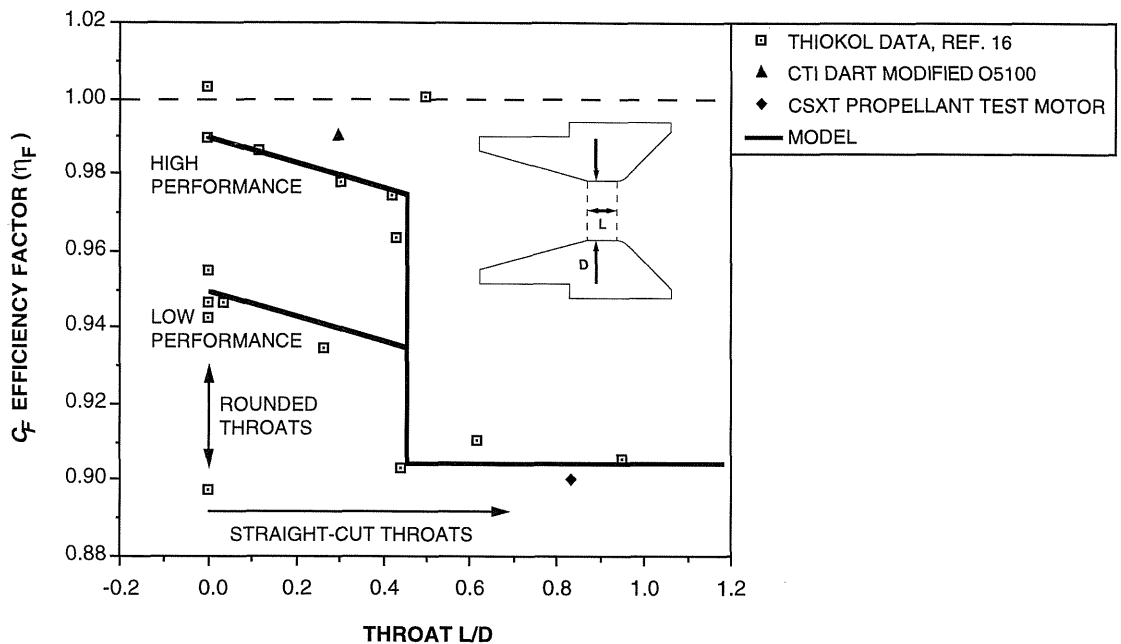


**Figure 28 —  $C_F$  Efficiency Factor ( $\eta_F$ ) versus Throat L/D for Straight-Cut Throats on Conical Nozzles.**

Based on the data presented in Figure 28, and using the Standard Method, the present author proposes the following  $C_F$  efficiency factor ( $\eta_F$ ) models:

For Conical Nozzles with Straight-Cut Throats:

$$C_{F,act} = \lambda \eta_F C_F^0$$

For Throat L/D < 0.45

High Performance:

$$\eta_F = 0.99 - (0.0333 * L/D)$$

Low Performance:

$$\eta_F = 0.95 - (0.0333 * L/D)$$

For Throat L/D ≥ 0.45

$$\eta_F = 0.905$$

For Conical Nozzles with Rounded Throats:

$$C_{F,act} = \lambda \eta_F C_F^0$$

$$\eta_F = 0.99 \text{ (high performance) to } 0.95 \text{ (low performance)}$$

The above models can be used in solid rocket motor simulations, hybrid rocket motor simulations, solid and hybrid rocket motor nozzle design studies, and are most likely also applicable to liquid rocket engines with straight-cut throats. The present author recommends that for liquid rocket engines with rounded throats, and in particular bell nozzles with rounded throats, that more sophisticated analyses tailored to liquid rocket engine nozzles should be used.

There are several important results from the  $C_F$  efficiency factor data presented in Figure 28:

(1) To the present author's knowledge, for the first time for high power and experimental/amateur solid rocket motors the thrust coefficient losses from using straight-cut throats have been quantified. The general theory amongst high power and experimental/amateur rocketeers was that shorter straight-cut throat sections delivered higher performance, but that there wasn't much of a penalty for using straight-cut throats, and not much additional penalty from having longer straight-cut throats. One of the surprises was that for the throat L/D's typically used by high power and experimental/amateur rocketeers (throat L/D's greater than 0.45) there are very high losses from using straight-cut throats, losses in thrust, total impulse, and specific impulse of approximately 9.5%.

(2) Many high power and experimental/amateur rocketeers when calculating a predicted thrust coefficient simply apply the nozzle divergence correction factor to the ideal thrust coefficient.

$$C_F = \lambda C_F^0$$

This is equivalent to using the Standard Method,

$$C_{F,act} = \lambda \eta_F C_F^0$$

and assuming that the  $C_F$  efficiency factor ( $\eta_F$ ) is equal to 1.0. If the nozzle uses a straight-cut throat with a throat  $L/D \geq 0.45$ , the actual  $C_F$  efficiency factor will be approximately 0.905, thus the predicted thrust coefficient, and therefore the predicted thrust will be off by 9.5%, a large misprediction in thrust coefficient and thrust.

(3) From Figure 28 it is clear that if the nozzle designer can reduce the throat  $L/D$  of the straight-cut throat to just under 0.45, there will be a large jump in performance. Previously high power and experimental/amateur rocketeers thought that there was only a gradual increase in nozzle performance with reduced straight-cut throat length. The data presented in Figure 28 show a discrete jump in performance when the throat  $L/D$  is less than 0.45. Clearly the nozzle designer now has the incentive that if there is any possible way to reduce the throat

$L/D$  to below 0.45, it should be pursued as there will be a large increase in nozzle performance.

(4) Based on the data presented in Figure 28, the present author recommends the following throat design criteria for conical nozzles using a straight-cut throat:

Throat Design Criteria for Conical Nozzles using a Straight-Cut Throat:

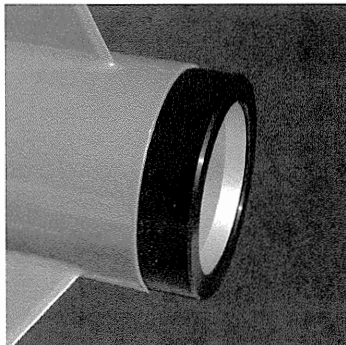
$$\text{Throat } L/D \leq 0.40$$

Using a throat design criteria of a throat  $L/D \leq 0.40$  provides margin on the indicated break in the data at a throat  $L/D = 0.45$ , to make sure that the large jump in nozzle performance indicated by the data in Figure 28 will occur.

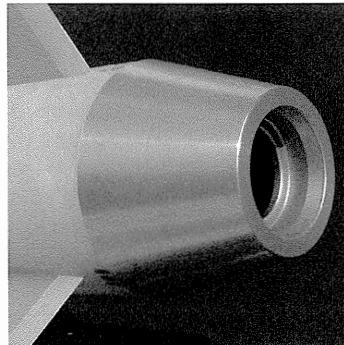
(5) The experimental data for the CSXT Propellant Characterization Test Motor and the DART Project Conical Nozzle Control Motor follow, and thus confirm the trends in the Thiokol historical data which is the majority of the data plotted in Figure 28. The DART Project Conical Nozzle Control Motor with a throat  $L/D = 0.30$  delivered a  $\eta_F = 0.99$ , following the throat  $L/D < 0.45$  High Performance trend line in Figure 28. The CSXT Propellant Characterization Test Motor with a throat  $L/D = 0.833$  delivered a  $\eta_F = 0.90$ , grouping with the Thiokol nozzles with throat  $L/D$ 's greater than 0.45 that delivered low performance (average  $\eta_F$  of 0.905).

## AERO PACK INTERNATIONAL

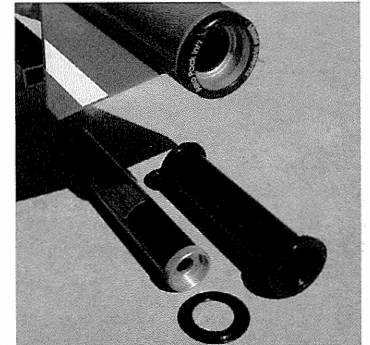
- |   |  |
|---|--|
| <ul style="list-style-type: none"> <li>&gt;&gt; Quick-Change Motor Retainers</li> <li>&gt;&gt; Quick-Change Tailcone Retainers</li> <li>&gt;&gt; Quick-Change Motor Adapters</li> <li>&gt;&gt; Stainless Ball Bearing Swivels</li> <li>&gt;&gt; Laser Engraving Service</li> <li>&gt;&gt; Ultimate Rocketry Hats</li> </ul> | <ul style="list-style-type: none"> <li>29 thru 98mm precision machined and anodized 6061-T6 &lt;&lt;</li> <li>38mm to 3.0", 54mm to 3.0", 54mm to 3.9", 75 mm to 3.9" &lt;&lt;</li> <li>29-38mm, 38-54mm, 54-75mm, 64-75mm, 75-98mm &lt;&lt;</li> <li>Stainless steel, 500lb rating, 3/4" welded stainless rings &lt;&lt;</li> <li>Personalized identification, TRA / NAR no, phone no. &lt;&lt;</li> <li>Cotton duck, embroidered, large flap for neck &amp; ears &lt;&lt;</li> </ul> |
|---|--|



RA54 Retainer w/AeroTech motor



TRA5439 Tailcone Retainer w/AeroTech motor



A3854 Adapter w/AeroTech motors

sales@aeropack.net

<http://aeropack.net>

phone: 858.566.2900

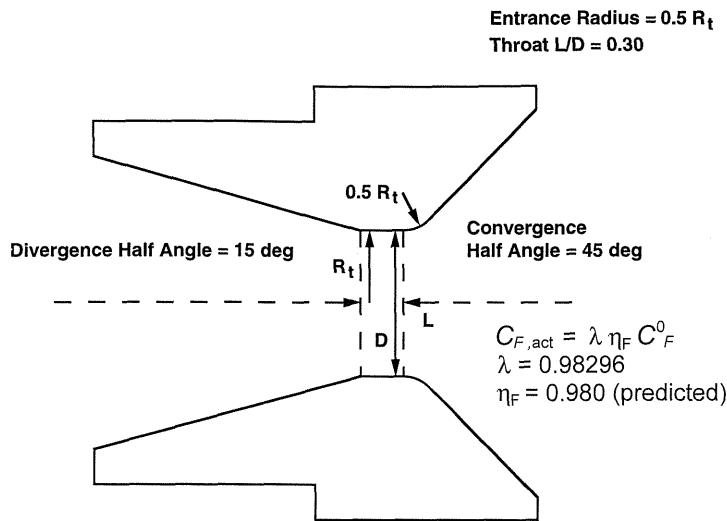


**Figure 29 — Optimal Nozzle Design.**

(6) Many experimental/amateur rocketeers when performing propellant characterization tests for  $K_n$  (propellant burning surface area divided by throat area) versus chamber pressure and burn rate versus chamber pressure do not directly measure chamber pressure. The chamber pressure is instead estimated from the measured thrust by using a prediction or estimate for the thrust coefficient. As noted previously, by basing this estimate for the thrust coefficient on simply applying the divergence correction factor to the ideal thrust coefficient, equivalent to  $\eta_F = 1.0$ , if the nozzle has a throat  $L/D \geq 0.45$  all of the estimated chamber pressures for the propellant characterization data will be off by 9.5% ( $\eta_F$  actually approximately equal to 0.905). This brings up the interesting possibility that much experimental/amateur propellant characterization data is actually in error by approximately 9.5%. Why haven't experimental/amateur rocketeers noticed this effect, noticed that their propellant data is in error? If based on Eq. (1) and Eq. (28), the chamber pressure is backed out from the measured thrust

$$p_c = F / (\lambda \eta_F C_F^0 A_{th})$$

assuming that  $\eta_F = 1.0$ , the propellant characterization data will be off by 9.5% in chamber pressure. For a given  $K_n$ , the chamber pressure will be 9.5% low. But when in motor simulation programs the 9.5% low chamber pressure is used with the Standard Method thrust equation (Eq. (28)) and Eq. (1),

$$C_{F,act} = \lambda \eta_F C_F^0$$

$$F = C_{F,act} A_{th} p_c$$

again assuming that  $\eta_F = 1.0$ , the predicted thrust coefficient and predicted thrust will be exactly correct. As long as the same method used to back out the chamber pressure from the thrust is used to predict the thrust from a given a chamber pressure, then the resultant predicted thrust will be correct.

### Optimum and Universal Nozzle Designs

Based on the  $C_F$  efficiency factor ( $\eta_F$ ) study results presented in Figure 28, the present author has proposed a straight-cut throat design criteria, and proposes two generic nozzle designs; an "optimal" very high performance nozzle, and a "universal" nozzle capable of being drilled with straight-cut throats of varying diameter yet still having high performance.

As presented previously; based on the  $C_F$  efficiency factor ( $\eta_F$ ) study results presented in Figure 28, the present author recommends a throat design criteria, throat  $L/D \leq 0.40$ , for conical nozzles with straight-cut throats.

Figure 29 presents a generic Optimal Nozzle design proposed by the present author for an "optimal" nozzle for very high performance. For very high performance the straight-cut throat  $L/D$  is reduced to 0.30, and the radius of the rounding of the throat entrance is increased to 0.5 times the throat radius, for a well rounded entrance to the throat. (This is the rounding radius for fully rounded throats on conical nozzles recommended by NASA SP-125 [Ref. 18].) Using a 15° divergence half angle, the divergence correction factor ( $\lambda$ ) is 0.98296. Based on the High Performance model, the predicted  $C_F$  efficiency factor ( $\eta_F$ ) is 0.980. Note that the nozzle on the DART Project Conical Nozzle Control Motor, which had the same throat  $L/D$  (0.30) and a rounded throat

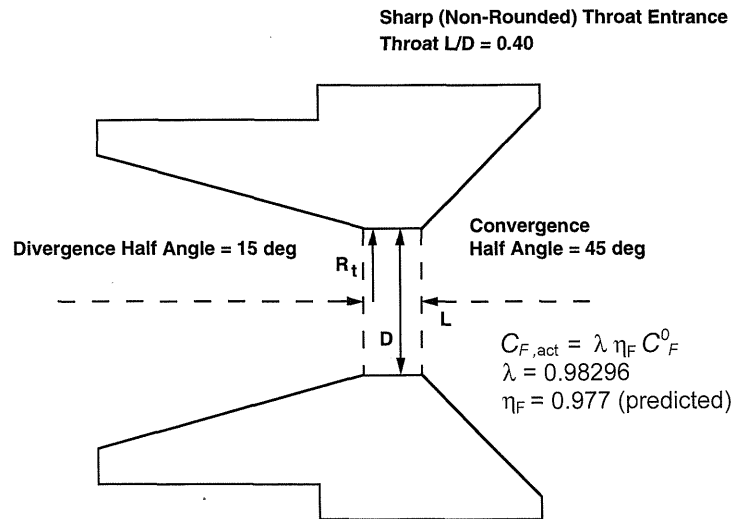


**Figure 30 — Universal Nozzle Design.**

entrance, although not nearly as well rounded, delivered a nozzle performance ( $\eta_F = 0.99$ ) similar to that predicted for the Optimal Nozzle design.

The disadvantage of the Optimal Nozzle design presented in Figure 29 is that while the throat can be drilled to a certain extent to different throat areas, if the throat is drilled too much the rounding of the throat entrance will be compromised by a sharp "lip" on the throat entrance. Thus the Optimal Nozzle design is somewhat fixed in throat area; beyond a certain variation in throat area the nozzle must be sized up or down, requiring a new nozzle machined "blank" or a new mold for an injection-molded phenolic nozzle.

To solve the throat area variation problem on the Optimal Nozzle design, the present author proposes the Universal Nozzle design presented in Figure 30. The Universal Nozzle design trades slightly lower performance, being still a high performance nozzle, for an increased capability for variation in the throat area. For high performance a straight-cut throat  $L/D = 0.40$  is used, making sure (with margin) that the big jump in performance for throat  $L/D$ 's less than 0.45 shown in Figure 28 is achieved. A shorter throat  $L/D$  less than 0.40 is not used, to provide extra margin for the throat in terms of heating and ablation/recession (depending on throat material), and to allow extra variation in the throat area when different straight-cut throats are drilled into the nozzle. There is no rounding of the throat entrance, a sharp throat entrance is used so the convergent and divergent nozzle profiles are maintained with sharp transitions as the nozzle throat is drilled over a wide range of throat areas. Using a  $15^\circ$  divergence half angle, the divergence correction factor ( $\lambda$ ) for this nozzle is 0.98296. Based on the

High Performance model, the predicted  $C_F$  efficiency factor ( $\eta_F$ ) for this nozzle is 0.977.

Note that with the exception of the CSXT Propellant Characterization Test Motor, all of the  $C_F$  efficiency factor ( $\eta_F$ ) data presented in Figure 28 is for nozzles with rounded throat entrances. Thus the predicted  $C_F$  efficiency factor for the Universal Nozzle design is somewhat speculative; it's based on the assumption that throat  $L/D$  is the major driver for  $C_F$  efficiency factor, not rounding or non-rounding or the radius of the rounding of the throat entrance. Hence, unlike the Optimal Nozzle design where a similar nozzle has been tested and has delivered performance similar to predicted performance, test data is required for the Universal Nozzle to validate the predicted  $C_F$  efficiency factor ( $\eta_F$ ) listed above and in Figure 30.

### **Nozzle Thrust Coefficient Measurement Tests - The Key to Understanding the Actual Performance of Existing Nozzles, and Optimizing Nozzle Design for Increased Performance**

As the data and analysis results presented in the previous sections show, much can be learned from performing thrust coefficient measurement tests for high power rocket motor nozzles and experimental/amateur rocket motor nozzles. An experimental/amateur rocketeer should measure, and thus understand, just what level of performance in terms of thrust coefficient and  $C_F$  efficiency factor that his or her nozzles are actually delivering. With experimental data, and a better understanding through additional tests how changes in nozzle design affect

nozzle performance, the experimental/amateur rocketeer can optimize their nozzle designs for increased performance.

### Performing Nozzle Design Optimization Tests Without Chamber Pressure Measurements

Can nozzle design optimization tests and studies be performed without chamber pressure instrumentation? Can nozzle designs be optimized without chamber pressure measurements?

First, based on Eqs. (1), (2), (28) and (43), to quantify the thrust coefficient and the  $C_F$  efficiency factor ( $\eta_F$ ) you have to measure chamber pressure. Second, a major point of the detailed analysis in the previous sections was to quantify just how well the nozzles were performing, and to accurately measure nozzle performance an accurate measurement of chamber pressure is required. Theoretically the maximum value for  $\eta_F$  is 1.0. Just how well have high power and experimental/amateur nozzles been performing? It turns out for many of the nozzles  $\eta_F = 0.905$ , a 9.5% loss in thrust that most high power and experimental/amateur rocketeers weren't even aware of.

An experimental/amateur rocketeer can optimize nozzle designs without chamber pressure instrumentation. The technique which can be used is to test a series of identical motors with different nozzles. The motors must be identical in propellant formulation (for the same  $K_n$  versus chamber pressure for the propellant), and have identical grain geometry and throat areas (for the same  $K_n$ , and thus the same chamber pressure). Operating at the same chamber pressure, and with the same throat area, different variations in straight-cut throat L/D, amount of rounding on the throat entrance, testing a fully-rounded throat for comparison with straight-cut throats, can all be tested. The thrust curve and the total impulse for each of the motors, from load cell data from static test firings, can be compared. While the actual values of the thrust coefficient and the  $C_F$  efficiency factor will not be measured or quantified, if a given nozzle is actually producing, as an example a 3% to 5% higher thrust coefficient, then the thrust and total impulse of the motor will be higher by 3% to 5%. For two motors operating at the same chamber pressure with the same throat area, the 9% difference in performance between the nozzle on the DART Conical Nozzle Control Motor ( $\eta_F = 0.99$ ) and the nozzle on the CSXT Propellant Characterization Test Motor ( $\eta_F = 0.90$ ) would certainly have been noticed. While the experimental/amateur rocketeer will not know exactly what level of thrust coefficient performance his or her nozzle is

delivering, for a motor with a fixed  $K_n$  and thus a fixed chamber pressure, the more efficient nozzle will deliver a higher thrust and a higher total impulse.

### Potential for Across-the-Board Improvements in Thrust, Total Impulse, and Specific Impulse for High Power and Experimental/Amateur Solid Rocket Motors

The thrust coefficient and  $C_F$  efficiency factor results presented in this article indicate that there is a considerable opportunity to improve the thrust coefficient performance of high power and experimental/amateur solid rocket motors by the design optimization of the straight-cut throats used on the motors. As an example, if a high power or experimental/amateur solid rocket motor uses a conical nozzle with a straight-cut throat, and if the straight-cut throat has a throat L/D > 0.45, then based on the  $C_F$  efficiency factor study results presented in Figure 28, the motor nozzle will have a  $C_F$  efficiency factor ( $\eta_F$ ) equal to 0.905. If the recommended design criteria for straight-cut throats is followed, and a throat L/D = 0.40 is used, the  $C_F$  efficiency factor ( $\eta_F$ ) for the nozzle will be between 0.937 (the Low Performance model) and 0.977 (the High Performance model). Based on the Standard Method (Eq. (28)),

$$\text{Eq. (28): } C_{F,act} = \lambda \eta_F C_F^0$$

this would result in an increase in thrust and total impulse of 3.5% ( $\eta_F$  increased from 0.905 to 0.937) to 8% ( $\eta_F$  increased from 0.905 to 0.977). Based on the Standard Method (Eq. (31)),

$$\text{Eq. (31): } I_{spd} = \lambda \eta_F \eta_\theta I_{sp}^0$$

the increase in the  $C_F$  efficiency factor ( $\eta_F$ ) from 0.905 to between 0.937 and 0.977, would result in a similar percentage increase in the delivered specific impulse of 3.5% to 8%.

To assess how widespread the potential improvement in nozzle thrust coefficient may be for high power solid rocket motors, the present author performed a survey of throat L/D for nozzles used on AeroTech production reloadable solid rocket motors. The throat geometry data was obtained from AeroTech Reloadable Motor System (RMS) assembly drawings and AeroTech nozzle drawings from the RCS Resource Library Compact Disk (CD) (Ref. 4). (Many of the RMS assembly drawings and nozzle drawings are also available on the RCS website listed in Ref. 4.) All AeroTech RMS reloadable motors

Throat L/D Survey Data for Nozzles Used on AeroTech Reloadable Motor System (RMS) Production Motors

All Nozzles Conical Nozzles with Straight-Cut Throats

Some Nozzle Throat Entrances Rounded  
Some Sharp (Non-Rounded)

	Throat L/D $\leq$ 0.40	Throat L/D $>$ 0.40
Model Rocket Motors E - G	0 (0%)	25 (100%)
High Power Rocket Motors H - I	10 (40%)	15 (60%)
High Power Rocket Motors J - K	3 (13%)	20 (87%)
High Power Rocket Motors L	1 (12.5%)	7 (87.5%)
High Power Rocket Motors M - N	8 (80%)	2 (20%)
<b>Totals</b>		
Model and High Power Rocket Motors E - N	22 (24%)	69 (76%)
High Power Rocket Motors H - N	22 (33%)	44 (67%)

**Table 3 — Throat L/D Survey Data for Nozzles Used on AeroTech Reloadable Motor System (RMS) Production Motors.**

use conical nozzles with straight-cut throats. The throat L/D survey data in terms of comparing the throat L/D's to the recommended design criteria of a throat L/D  $\leq$  0.40, is presented in Table 3.

Some observations can be made from the results of the nozzle survey data presented in Table 3.

(1) Model rocket motors (E-G) appear to be penalized in terms of throat L/D due to their relatively small size. For the smaller motors it may not be possible to shorten up the throat L/D due to ablation and erosion/recession effects on the nozzle throats.

(2) Some excellent nozzles with low throat L/D's are available in the H-I high power range, although 60% of the H-I high power rocket motors still have throat L/D's greater than 0.40.

(3) Some excellent nozzles with low throat L/D's are available for the large high power rocket motors in the M-N range, which also take advantage of the large size of the motor where a given straight-cut throat length gives a lower throat L/D due to the increased throat diameter for motors in this class. In the high power M-N range 80% of the motors have throat L/D's less than 0.40.

(4) For many of the nozzles in Table 3 which had throat L/D's greater than 0.40, while their throat L/D's were over 0.40, their throat L/D's were close to 1.0. If the many nozzles with throat L/D's close to 1.0 could have their throats shortened-up only a small amount to a throat L/D of 0.40, the nozzles would have a substantial increase in performance.

Summarizing Table 3, based on a comparison with the recommended throat design criteria, 76% of the AeroTech production RMS model rocket and high power rocket motors (E-N power range), and 67% of the AeroTech production RMS high power rocket motors (H-N power range) could have increases in thrust, total impulse, and specific impulse of 3.5% to 8% by retrofitting the motors with nozzles with straight-cut throats with a throat  $L/D = 0.40$ .

From the present author's experience most solid rocket motors built by experimental/amateur rocketeers use conical nozzles with straight-cut throats, with sharp (non-rounded) throat entrances, and with no particular concern about the length of the straight-cut throat. In the present author's opinion almost all experimental/amateur solid rocket motors have throat  $L/D$ 's greater than 0.40, the recommended throat design criteria. Thus almost all experimental/amateur solid rocket motors could have increases in thrust, total impulse, and specific impulse of 3.5% to 8% by using straight-cut throats with a throat  $L/D = 0.40$ .

### Conclusions and Recommendations

The present author presents the following conclusions and recommendations from the research and experimental work undertaken in the development of the material presented in this article:

1) The present author recommends that the Standard Method be used for correcting the ideal thrust coefficient and the theoretical specific impulse to the actual thrust coefficient and the delivered specific impulse. The key summary equations for the Standard Method are Eqs. (28) and (31).

$$\text{Eq. (28):} \quad C_{F, \text{act}} = \lambda \eta_F C_F^0$$

$$\text{Eq. (31):} \quad I_{spd} = \lambda \eta_F \eta_\theta I_{sp}^0$$

2) To the present author's knowledge at the time of the writing of this article, with the exception of some internal-use computer programs by the present author, every solid rocket motor, hybrid rocket motor, and liquid rocket engine computer program, software, spreadsheet, performance charts, etc., for predicting performance and calculating thrust from chamber pressure used by model, high power, and experimental/amateur rocketeers is based on simply multiplying the ideal thrust coefficient by the nozzle divergence correction factor ( $\lambda$ ) to obtain the actual thrust coefficient.

$$C_{F, \text{act}} = \lambda C_F^0$$

This is equivalent to assuming that the  $C_F$  efficiency factor ( $\eta_F$ ) is equal to 1.0. All of these computer programs, software packages, spreadsheets, performance charts, etc., can be easily updated to the Standard Method by simply multiplying the ideal thrust coefficient and the divergence correction factor with the  $C_F$  efficiency factor ( $\eta_F$ ) (i.e., using Eq. (28)).

$$C_{F, \text{act}} = \lambda \eta_F C_F^0$$

Models for  $C_F$  efficiency factor ( $\eta_F$ ) for straight-cut throats (both high performance and low performance) and for rounded throats were presented in a previous section. These  $C_F$  efficiency factor models can be retrofitted into computer programs, software packages, spreadsheets, etc., using Eq. (28).

3) Many high power and experimental/amateur rocketeers run programs such as PROPER, or the USAF ISP code, and assume that the theoretical specific impulse ( $I_{sp}^0$ ) predicted by the programs for their propellant will be the delivered specific impulse for their rocket motors using the propellant. Based on the Standard Method delivered specific impulse ( $I_{spd}$ ) equation (Eq. (31)),

$$I_{spd} = \lambda \eta_F \eta_\theta I_{sp}^0$$

this is equivalent to assuming that the divergence correction factor,  $\lambda = 1.0$ , the  $C_F$  efficiency factor,  $\eta_F = 1.0$ , and the  $c^*$  efficiency factor,  $\eta_\theta = 1.0$ . Even if correct values for the divergence correction factor and the  $C_F$  efficiency factor are used, representative values for the  $c^*$  efficiency factor are still required.

Smaller, shorter motors using aluminized or metallized propellants will have lower residence times in the motor, thus reduced combustion efficiency, resulting in a lower  $c^*$  efficiency factor. Larger motors are more efficient than smaller motors, due to increased residence times, proportionally less heat transfer into the motor case and nozzle, and proportionally smaller boundary layers for lower boundary layer losses. Thus for any given propellant it is important to track the variation of the  $c^*$  efficiency factor ( $\eta_\theta$ ) with motor size.

The present author recommends that in addition to the normal propellant characterization tests for  $K_n$  (propellant burning surface area divided by throat area) versus chamber pressure, burn rate versus chamber pressure, and erosive burning characteristics, that an additional "characterization" of the propellant should be performed where the experimental/amateur rocketeer will track delivered specific impulse as a percentage (0-100%) of the theoretical specific impulse, and  $c^*$  efficiency factor ( $\eta_\theta$ ), both as a function of motor size. Based on represen-

tative data that was presented, as the motor size is increased from 1 lb propellant weight the delivered specific impulse can be increased by 5% for 50 lb propellant weight motors, and 7.5% for 350 lb propellant weight motors.

4) For the first time to the present author's knowledge, thrust coefficient losses from using straight-cut throats for high power and experimental/amateur solid rocket motors have been quantified. The thrust coefficient losses were much higher than most high power and experimental/amateur rocketeers probably would have expected. While most high power and experimental/amateur rocketeers have performed thrust coefficient calculations assuming no losses beyond divergence losses (equivalent to a  $C_F$  efficiency factor,  $\eta_F = 1.0$ ), the actual thrust coefficient loss from using a straight-cut throat was found to be approximately 9.5% ( $\eta_F = 0.905$ ) for the straight-cut throat lengths used on most high power and experimental/amateur rocket motors. While the results presented in Figure 28 were primarily based on historical Thiokol data from Ref. 16, static firings with chamber pressure measurements for determining experimental thrust coefficient values were also performed for two large high power rocket motors, the test results from which confirm the trends from the historical Thiokol data.

5) Most high power and experimental/amateur rocketeers, beyond expecting thrust coefficient losses from straight-cut throats to be small, probably expected a somewhat linear variation of thrust coefficient loss with straight-cut throat length. A surprise finding from the  $C_F$  efficiency factor data presented in Figure 28 was the definite jump in nozzle thrust coefficient performance for straight-cut throat L/D's less than 0.45.

6) From the data presented in Figure 28 it is clear that if the nozzle designer can get the throat L/D of the straight-cut throat under 0.45, there will be a large jump in performance. Based on this result from the data plotted in Figure 28, the present author recommends the following throat design criteria for conical nozzles with straight-cut throats:

Throat Design Criteria for Conical Nozzles using a Straight-Cut Throat:

$$\text{Throat } L/D \leq 0.40$$

As noted in a previous section, a throat L/D of  $\leq 0.40$  is used in place of an  $L/D < 0.45$ , to provide extra margin to be sure that the jump in performance indicated by the data plotted in Figure 28 is achieved.

If there is a single conclusion that the reader should come away with from reading this article, it is that on straight-cut throats to make sure that the throat L/D is  $\leq 0.40$ .

7) Based on the  $C_F$  efficiency factor study results presented in Figure 28, the present author has proposed two high-performance nozzle designs using straight-cut throats. The first nozzle is an "optimal" very high performance design using a shorter length straight-cut throat and a well-rounded throat entrance, but which can only be drilled for throat area adjustments to a limited degree. The second nozzle is a "universal" nozzle design with the straight-cut throat length short enough to meet the throat L/D design criteria and get the jump in performance indicated by the data in Figure 28, with no throat entrance rounding, but with the ability to be drilled to a wide range of throat areas while still maintaining the same throat entrance profile (a sharp throat entrance).

8) Techniques, methods and equations for making corrections to the head-end chamber pressure to determine the actual chamber pressure were presented, including one example done using hand calculations, and one example done using an automated computer program, where thrust and head-end chamber pressure measurements were used to determine the actual chamber pressure, the nozzle thrust coefficient, and the  $C_F$  efficiency factor. Head-end chamber pressure must be corrected to the actual chamber pressure (the nozzle stagnation [total] pressure, the stagnation pressure just prior to entering the convergent section of the nozzle) in order to make accurate chamber pressure, thrust coefficient, and  $C_F$  efficiency factor measurements. A method for correcting head-end chamber pressure was presented based on determining the aft-end stagnation (total) pressure for the motor core, and then assuming that the core aft-end stagnation pressure is equal to the nozzle stagnation pressure, the actual chamber pressure.

9) The present author highly recommends that experimental/amateur rocketeers perform thrust coefficient measurement tests to understand the actual performance that their nozzles are delivering, and to perform additional tests with modified nozzles to test nozzle design changes for increased performance.

10) While the present author highly recommends that thrust coefficient measurement tests be performed using chamber pressure instrumentation, nozzle designs can be optimized using static test data even if no chamber pressure instrumentation is

installed. Experimental/amateur rocketeers who wish to optimize their nozzle designs can build a series of identical test motors, but using different nozzles. The key is to make all of the motors identical in size, propellant type, grain geometry, propellant surface area and throat area, so all of the motors will have the same propellant weight, chamber pressure and burn time. The thrust curves from each of the motors can then be compared. While it will not be possible to quantify the actual performance of each of the nozzles, the nozzle delivering a higher thrust coefficient when installed in the motor will produce a higher thrust, a higher total impulse, and a higher specific impulse. Using this technique, with no chamber pressure instrumentation and only a thrust stand with a load cell, experimental/amateur rocketeers can optimize their nozzle designs by comparing the thrust curves produced by the different nozzles.

11) From a survey performed by the present author of straight-cut throats used on AeroTech production RMS model rocket and high power rocket reloadable solid rocket motors, 76% of the motors in the E-N

power range (67% if the power range is H-N) could have increases in thrust, total impulse, and specific impulse of 3.5% to 8% by retrofitting the motors with nozzles with straight-cut throats with a throat  $L/D = 0.40$ . Many of the AeroTech straight-cut throat nozzles had throat  $L/D$ 's approximately equal to 1.0, so only a moderate reduction in throat length would be required to get the throat  $L/D$  down to 0.40, to get the jump in performance indicated by the data in Figure 28. In the present author's opinion almost all experimental/amateur solid rocket motors have throat  $L/D$ 's greater than 0.40, and thus would also see increases in thrust, total impulse, and specific impulse of 3.5% to 8% by using straight-cut throats with a throat  $L/D = 0.40$ .

Summarizing; a significant across-the-board increase in performance of 3.5% to 8% for most high power rocket motors, and probably almost all experimental/amateur rocket motors can be achieved by optimizing the design of straight-cut throat nozzles by using straight-cut throats with a throat  $L/D = 0.40$ . □

### Glossary

$A_0$	combustion chamber cross-sectional area, $m^2$ ( $in^2$ )
$A_e$	nozzle exit area, $m^2$ ( $in^2$ )
$A'_e$	nozzle spherical exit area, $m^2$ ( $in^2$ )
$A_p$	port area (core cross-sectional area), $m^2$ ( $in^2$ )
$A_{th}$	nozzle throat area, $m^2$ ( $in^2$ )
$c^*$	characteristic velocity, $m/sec$ ( $ft/sec$ )
$C_F$	thrust coefficient, dimensionless
$C_F^0$	ideal thrust coefficient, dimensionless
$C_{F,act}$	actual thrust coefficient, including all nozzle losses, dimensionless
$C_{F,vac}^0$	ideal thrust coefficient (Eq. (9)), with $p_\infty = 0$ (vacuum), dimensionless
$D$	nozzle straight-cut throat section diameter, $m$ ( $in$ )
$D_e$	nozzle exit diameter, $m$ ( $in$ )
$D_{th}$	nozzle throat diameter, $m$ ( $in$ )
$F$	thrust, $N$ ( $lb$ )
$F_a$	actual thrust, $N$ ( $lb$ )

$F_i$	ideal thrust, N (lb)
$g_0$	acceleration due to gravity at sea level, 9.8066 m/sec <sup>2</sup> (32.174 ft/sec <sup>2</sup> )
$I_{sp}$	specific impulse, N-sec/kg (sec), lbf-sec/lbm (sec)
$I_{sp}^0$	theoretical specific impulse, N-sec/kg (sec), lbf-sec/lbm (sec)
$I_{spd}^0$	theoretical delivered specific impulse, N-sec/kg (sec), lbf-sec/lbm (sec)
$I_{spd}$	delivered specific impulse, N-sec/kg (sec), lbf-sec/lbm (sec)
$I_{tot}$	total impulse (total integral of thrust-time), N-sec (lb-sec)
$K_n$	propellant burning surface area divided by throat area, dimensionless
L	nozzle straight-cut throat section length, m (in)
$L_n$	nozzle length, throat to exit plane, m (in)
$\dot{m}$	mass flow rate of propellant, kg/sec (slugs/sec)
$\bar{M}$	average molecular weight of combustion gases, kg/mol (lb/mole)
$\dot{m}_a$	actual mass flow rate through nozzle, kg/sec (lbm/sec)
$M_a$	core Mach number at aft end of core, dimensionless
$\dot{m}_i$	ideal mass flow rate through nozzle, kg/sec (lbm/sec)
$p_{0a}$	stagnation (total) pressure at aft end of core, Pa (lb/in <sup>2</sup> )
$p_{0h}$	stagnation (total) pressure at head end of core, Pa (lb/in <sup>2</sup> )
$p_c$	chamber pressure, Pa (lb/in <sup>2</sup> )
$\bar{p}_c$	average chamber pressure, Pa (lb/in <sup>2</sup> )
$p_{c,act}$	actual chamber pressure, Pa (lb/in <sup>2</sup> )
$(p_c)_{inj}$	injector stagnation (total) pressure, Pa (lb/in <sup>2</sup> )
$p_{c,measured}$	measured chamber pressure, Pa (lb/in <sup>2</sup> )
$(p_c)_{ns}$	nozzle stagnation (total) pressure, Pa (lb/in <sup>2</sup> )
$p_e$	nozzle exit pressure, Pa (lb/in <sup>2</sup> )
$p_\infty$	atmospheric pressure, Pa (lb/in <sup>2</sup> )
R	radius of rounding of throat or throat entrance, m (in)
R	universal gas constant, 8314.3 J/mole - °K (1545 ft-lb/mole - °R)
$R_e$	nozzle exit radius, m (in)

$R_t$	nozzle throat radius, m (in)
$T_c$	adiabatic equilibrium flame temperature, °K ( °R)
$u_e$	nozzle exhaust velocity, m/sec (ft/sec)
$V_e$	nozzle exhaust velocity, m/sec (ft/sec)
$\dot{w}$	propellant flow rate, lb/sec
$\alpha$	nozzle divergence half angle, deg
$\epsilon$	nozzle expansion area ratio, dimensionless
$\gamma$	ratio of specific heats, dimensionless
$\eta_F$	$C_F$ efficiency factor, dimensionless
$\eta_\mu$	deliverable motor efficiency, dimensionless
$\eta_\theta$	$c^*$ efficiency factor, dimensionless
$\lambda$	nozzle divergence correction factor, dimensionless
$\theta_{ex}$	nozzle exit plane lip angle, deg
$\phi$	angle between local velocity vector and nozzle centerline, deg
$\zeta_d$	discharge correction factor, dimensionless
$\zeta_F$	thrust correction factor, dimensionless
$\zeta_v$	velocity correction factor, dimensionless

## References

1. Summerfield, Martin, forward by Rogers, Charles E., "Performance Analysis of the Ideal Rocket Motor," *High Power Rocketry Magazine*, Vol. 12, No. 1, January 1997, pages 12-24.
2. "Solid Propellant Selection and Characterization," excerpts from NASA SP-8064 with additional material, forward by Rogers, Charles E., *High Power Rocketry Magazine*, Vol. 15, No. 6, February (A) 2001, pages 42-64, and Vol. 15, No. 7, February (B) 2001, pages 45-72.
3. "Solid Propellant Grain Design and Internal Ballistics," excerpts from NASA SP-8076 with additional material, forward by Rogers, Charles E., *High Power Rocketry Magazine*, Vol. 33, No. 5-6, October/November 2002, pages 14-71.
4. RCS Resource Library CD-ROM, available from RCS Rocket Motor Components, Inc., <http://www.rocketmotorparts.com>.
5. Sutton, George P., and Biblarz, Oscar, *Rocket Propulsion Elements*, 7th Edition, John Wiley and Sons, Inc., 2001.
6. *Solid Propellant Grain Design and Internal Ballistics*, NASA Space Vehicle Design Criteria (Chemical Propulsion), NASA SP-8076, March 1972.
7. *Solid Rocket Motor Performance Analysis and Prediction*, NASA Space Vehicle Design Criteria (Chemical Propulsion), NASA SP-8039, May 1971.
8. *Solid Propellant Selection and Characterization*, NASA Space Vehicle Design Criteria (Chemical Propulsion), NASA SP-8064, June 1971.

9. Cruise, D.R., *Theoretical Computations of Equilibrium Compositions, Thermodynamic Properties, and Performance Characteristics of Propellant Systems*, NWC-TP-6037, Naval Weapons Center, China Lake, California, 1991.
10. Humble, Ronald W., Henry, Gary N., and Larson, Wiley J., *Space Propulsion Analysis and Design*, The McGraw-Hill Companies, Inc., 1995.
11. Hill, Philip G., and Peterson, Carl R., *Mechanics and Thermodynamics of Propulsion*, Addison-Wesley Publishing Company, Inc., 1965.
12. *Recommended Procedure for the Measurement of Specific Impulse of Solid Propellants*, ICRPG Solid Propellant Rocket Static Test Working Group, CPIA Publ. 174, August 1968.
13. Brown, B., *Oxide Particles in Solid Rocket Exhausts-Their Formation and Growth*, Paper P334, Institute for Defense Analysis Research, November 1967.
14. Scortia, T. N., *Demonstration of an Advanced Solid Propellant*, Rep. UTC 2068-FR, United Technology Center, July 15, 1965.
15. *ICRPG Liquid Propellant Thrust Chamber Performance Evaluation Manual*, CPIA Publ. 178, Performance Standardization Working Group, Chemical Propulsion Information Agency, September 1968.
16. *Rocket Propulsion Data*, Thiokol Chemical Corporation, January 1968.
17. Bartel, Scott, and Rogers, Charles E., "The Dryden Aerospike Rocket Test (DART) Project - Launch Report for Aerospike Rocket Flights," *High Power Rocketry Magazine*, Vol. 35, No. 5, August 2004, pages 6-46.
18. Huzel, Dieter K., and Huang, David H., *Design of Liquid Propellant Rocket Engines*, NASA SP-125, Rocketdyne Division, North American Aviation, Inc., 1967.
19. Huzel, Dieter K., and Huang, David H., forward by Rogers, Charles E., "Introduction to Liquid Propellant Rocket Engines," excerpts from Chapter 1 of NASA SP-125, *High Power Rocketry Magazine*, Vol. 34, No. 5, June 2003, pages 17-23, and Vol. 34, No. 7, August 2003, pages 5-19 and 42-44.

Please Note this Correction to The Solid Rocket Motor, Part 4, Vol. 35, No. 7, October 2004 *High Power Rocketry*;

Errata:

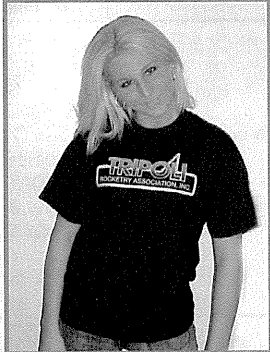
On Page 27; Eq. (7) should read

$$I_{sp} = (c^* C_F) / g_0 \quad (7)$$

**Note: Has been corrected in this pdf file.**



THE SOURCE  
FOR OFFICIAL  
**TRIPOLI**  
T-SHIRTS, CAPS  
& SWEAT SHIRTS



**ROCKETEES**  
HIGH POWER SPORTSWEAR  
visit our website at  
[www.rocketees.com](http://www.rocketees.com)

H  
I  
G  
H  
  
P  
O  
W  
E  
R  
  
R  
O  
C  
K  
E  
T  
R  
Y

# HIGH POWER ROCKETRY



\$5.95 CANADA \$8.50  
UK £4.25



FEATURES

**INCREASING PERFORMANCE OF SOLID ROCKET MOTORS** | **RRS 50 MILE BOOSTED DART**

HIGH POWER ROCKETRY

# HIGH POWER ROCKETRY



\$5.95 CANADA \$8.50  
UK £4.25



CTRA 10TH INVITATIONAL | THE MYTHBUSTERS | THE SOLID ROCKET | BOOK REVIEW:  
INVITATIONAL | EXPOSE WAN HOO | MOTOR PART 5 | ROCKET SCIENCE